Post Combustion Capture of Carbon Dioxide through Hydrate Formation in Silica Gel Column

by

ADEBOLA ADEYEMO

B.Sc., The University of Lagos, 2004

A THESIS SUBMITTED IN PARTIAL FULFILLMENT OF THE
REQUIREMENTS FOR THE DEGREE OF

MASTER OF APPLIED SCIENCE

in

THE FACULTY OF GRADUATE STUDIES

(Chemical and Biological Engineering)

THE UNIVERSITY OF BRITISH COLUMBIA
(Vancouver)

February 2008

Abstract

Carbon dioxide (CO_2) capture through hydrate formation is a novel technology under consideration as an efficient means of separating CO_2 from flue/fuel gas mixtures for sequestration and enhanced oil recovery operations. This thesis examines post-combustion capture of CO_2 from fossil-fuel power plant flue-gas streams through hydrate formation in a silica gel column. Power plant flue-gas contains essentially CO_2 and nitrogen (N_2) after suitable pre-treatment steps, thus a model flue-gas comprising 17% CO_2 and 83% N_2 was used in the study. Previous studies employed a stirred-tank reactor to achieve water-gas contact for formation of hydrates; recent microscopic studies involved using water dispersed in silica gel to react with gas, showing potential for improved hydrate formation rates without the need for agitation. This study focuses on macroscopic kinetics of hydrate formation in silica gel to evaluate hydrate formation rates, CO_2 separation efficiency and determining optimal silica gel properties as a basis for a CO_2 capture process.

Spherical silica gels with 30.0 and 100.0 nm pore sizes and 40-75 and 75-200 μm particle sizes were studied to determine pore size and particle size effects on hydrate formation. 100.0 nm pores achieved higher gas uptake and CO_2 recovery over the 30.0 nm case. Improved CO_2 separation was obtained when 75-200 μm particles with 100.0 nm pores were used. The two effects observed are due to improved gas diffusion occurring with larger pore and particle size, favouring increased hydrate formation. Compared to stirred-tank experiments, results in this study show a near four-fold increase in moles of gas incorporated in the hydrate per mole of water, showing that improved water-to-hydrate conversion is obtained with pore-dispersed water. At similar experimental conditions, CO_2 recovery improved from 42% for stirred-tank studies to

51% for the optimum silica (100.0 nm 75-200 μm) determined in this study. Finally, effects of tetrahydrofuran (THF) - an additive that reduces operating pressure were evaluated. Experiments with 1 mol% THF, the optimum determined from previous stirred tank studies, showed improved gas consumption in silica but reduced CO_2 recovery, indicating that the optimum concentration for use in silica is different from that in stirred-tank experiments.

TABLE OF CONTENTS

Abstract ..... **ii**

Table of Contents ..... **iv**

List of Tables ..... **vi**

List of Figures ..... **vii**

Acknowledgements ..... **x**

Co-Authorship Statement ..... **xi**

CHAPTER-1: INTRODUCTION

1.1 Carbon dioxide capture and sequestration 1

1.2 Introduction to gas hydrates 2

1.3 Structure of gas hydrates 3

1.4 Importance of gas hydrates 5

1.5 Energy consumption and climate change 9

1.6 Gas hydrates and CO_2 capture 11

CHAPTER-2: LITERATURE REVIEW & RESEARCH OBJECTIVES

2.1 Thermodynamic studies of clathrate hydrates 13

2.2 Hydrate formation in porous media 14

2.2.1 Effect of porous media on hydrate formation 15

2.2.2 Kinetic studies of hydrate formation in porous media 17

2.2.3 Phase equilibrium studies of hydrate formation in porous media 19

2.2.4 Prediction of hydrate equilibrium in porous media 23

2.5.3 Diameter range of pore effects on gas hydrate equilibrium 29

2.3 Gas hydrate formation as a novel CO_2 capture technology 33

2.3.1 Thermodynamics and kinetics of CO_2 and N_2 hydrates 34

2.3.2 Pre and Post-Combustion CO_2 capture via gas hydrates 35

2.3.3 Effect of additives on CO_2 and N_2 hydrate formation 38

2.3.4 Significance of gas-water contact mode 39

2.4 CO_2 capture via hydrate formation in silica gel pores 43

2.4.1 Silica gel properties 43

2.4.2 Experimental studies for CO_2 capture 47

2.5 Motivation for research and research objectives 49

CHAPTER-3: MATERIALS AND METHODS

3.1 Apparatus 51
3.2 Materials 54
3.3 Silica gel preparation and analysis 55
3.3.1 Determination of free water content of water sorbed silica gel 56
3.3.2 Freezing point determination for water confined in silica gel pores 56
3.4 Experimental procedure 57
3.4.1 Hydrate formation 57
3.4.2 Operating conditions 58
3.4.3 Hydrate dissociation 59
3.5 Hydrate analysis 59
3.5.1 Structure determination 60
3.5.2 Raman spectroscopy 60
3.6 Gas phase analysis 61
3.7 Material balance calculations 61
3.8 CO_2 recovery and efficiency 62

CHAPTER-4: RESULTS AND DISCUSSION

4.1 Freezing point depression and free water content of silica gel pores 64
4.2 Gas uptake measurements 67
4.3 Pore size effect on hydrate formation kinetics and CO_2 recovery efficiency 69
4.4 Particle size effect on hydrate formation kinetics and CO_2 recovery efficiency 79
4.5 PXRD and Raman analysis 84
4.6 CO_2/N_2/THF hydrate formation in silica gel pores 87
4.7 Comparison between hydrate formation kinetics in bulk water systems and water dispersed in silica gel pores 90

CHAPTER-5: CONCLUSIONS AND RECOMMENDATIONS

5.1 Conclusions 95
5.2 Recommendations 97
REFERENCES 100
APPENDIX 107

LIST OF TABLES

Table 1.1. 4
Hydrate structural properties
Table 3.1. 54
Location of thermocouples within hydrate reactor
Table 3.2. 62
Silica Gel Properties.
Table 4.1. 76
CO_2 Recovery, Separation Factor and Hydrate Formation Rates for gel 1 and 2
Table 4.2. 82
CO_2 Recovery, Separation Factor and Hydrate Formation Rates for gel 1, 2 and 3

LIST OF FIGURES

Figure 1.1. 4
Structure and geometry of clathrate hydrate cages
Figure 1.2. 10
Global distribution of large stationary sources of CO_2 emissions
Figure 1.3. 11
CO_2 capture processes and systems.
Figure 2.1. 21
Hydrate equilibrium for bulk and porous media propane hydrates.
Figure 2.2. 27
Schematic of fluid in a capillary.
Figure 2.3. 33
500MWe ultra-super critical pulverized coal unit stack emissions.
Figure 2.4. 34
Equilibrium hydrate formation conditions for the CO_2-H_2O system
Figure 2.5. 35
Equilibrium hydrate formation conditions for the N_2-H_2O system
Figure 2.6. 40
Fugacity gradients in the diffusion and adsorption "reaction" film around a growing hydrate particle.
Figure 2.7. 42
Single stage of hydrate formation/decomposition of a hydrate based process for post combustion CO_2 capture.
Figure 2.8. 44
Scanning electron microscope (SEM) image of porous silica gel
Figure 2.9. 46
Different forms of hydroxyl group that can occur on the surface of silica gel.
Figure 2.10. 47
Pressure-composition diagram of the ternary N_2-CO_2-water system measured at 272.1 K

Figure 3.1. 52
Experimental apparatus for investigating hydrate formation kinetics in a silica gel column.
Figure 3.2. 53
Rates Hydrate Reactor (HR) cross section and dimensions.
Figure 4.1. 66
DSC spectra of water adsorbed in 30nm pore size silica gel.
Figure 4.2. 66
Thermo-gravimetric analysis results for water adsorbed in 30 nm silica gel
Figure 4.3. 68
Gas uptake measurement curve for CO_2/N_2 hydrate in 30.0nm silica gel pores at 272.15 K and 8.0 MPa.
Figure 4.4. 68
Temperature profiles for CO_2/N_2 hydrate formation in 30.0nm silica gel pores at 272.15 K and 8.0 MPa.
Figure 4.5. 70
Gas uptake measurement curves for hydrate formation in 30.0 nm and 100nm silica gel pores at 272.15 K and 8.0 MPa (a) and 9.0 MPa (b).
Figure 4.6. 74
Gas phase CO_2 measurements during hydrate formation at 272.15 K and 9.0 MPa in 30.0 nm (a) and 100.0 nm (b) silica gel.
Figure 4.7. 75
CO_2 content in the gas phase (initial composition), hydrate phase and residual gas phase (final composition) for CO_2/N_2 hydrate formation at 272.15 K and 8.0 MPa (a) and 9.0 MPa (b).
Figure 4.8. 81
Gas uptake measurement curves for hydrate formation in two 100.0 nm silica gels with varying particle size at 272.15 K and 8.0 MPa (a) and 9.0 MPa (b).
Figure 4.9. 83
CO_2 content in the gas phase (initial composition), hydrate phase and residual gas phase (final composition) for CO_2/N_2 hydrate formation at 272.15 K and 8.0 MPa (a) and 9.0 MPa (b).
Figure 4.10. 85
PXRD Pattern of CO_2/N_2/Water hydrate in 30.0nm silica gel forming sI hydrate

Figure 4.11. 86

Raman spectra of 17% CO_2/N_2/1.0 mol% THF (sI) hydrate in 100.0 nm silica gel.

Figure 4.12. 88

Gas uptake curves for CO_2/N_2 and CO_2/N_2/THF hydrate formation in 100.0 nm, 75-200 μm silica gel.

Figure 4.13. 89

Comparison of CO_2 phase compositions from hydrate formation in THF solution and pure water systems.

Figure 4.14. 92

Comparison between gas uptake data of bulk water systems with pore confined water in silica gel for hydrate formation from 17% CO_2/N_2 mixture.

Figure 4.15. 93

Comparison between gas uptake data of bulk systems with pore confined water in silica gel in the presence of 1mol% THF for hydrate formation from 17% CO_2/N_2 mixture

ACKNOWLEDGEMENTS

I would like to appreciate Dr. Peter Englezos and Dr. John Ripmeester for their immense guidance and assistance in the course of producing this thesis; I greatly appreciate the support of Dr. Steven Lang for his expertise and help in setting up experiments and performing the various analyses required during the course of this work.

My heartfelt thanks go to my colleagues in the hydrates research group at UBC – Rajnish Kumar, Praveen Linga, Robin Susilo, Jeffry Yoslim and Cef Haligva. Thank you for your invaluable inputs and for allowing me to see things from your perspective.

Finally I want to appreciate my parents Mr. and Mrs. Bola Adeyemo, and my best friend Moyo Makanjuola for their immeasurable support and encouragement throughout the course of this work. Thank you so much for being there when I needed you the most.

CO-AUTHORSHIP STATEMENT

This thesis was written wholly by A. Adeyemo under the supervision of Professor P. Englezos (Chemical and Biological Engineering UBC) and Dr. J. A. Ripmeester (National Research Council Canada). Dr. S. Lang – a technical officer at the National Research Council Canada provided technical training and helpful discussions to complete this project

CHAPTER 1

INTRODUCTION

1.1 Carbon dioxide capture and sequestration

Human activity through increasing industrialization, improvement of standards of living and rapid economic growth has led to increases in fossil fuel use with the attendant increase in emissions of carbon dioxide (CO_2) and to a lesser extent, nitrous oxide and methane, all of which are known greenhouse gases (GHGs). This designation arises because of their ability to absorb infrared radiation that leads to a rise in atmospheric temperature (global warming). The bulk of the global warming effect is attributed to CO_2 because of its dominant position in terms of atmospheric concentration and quantity emitted compared to the other GHGs. Global warming is likely to induce large climatic changes with many consequences and as a result is receiving increasing global attention.

In order to prevent detrimental changes in the earth's climate, it is of utmost importance that actions are taken to reduce or eliminate the rate of emission of the GHGs into the atmosphere. The major thrust of these efforts is termed CO_2 Capture and Sequestration (CCS), defined as application of technology aimed at reducing greenhouse gas emissions from burning fossil fuels during industrial and energy-related processes involving the capture, transport and long-term storage of carbon dioxide. It is envisaged that alongside other actions such as improving energy efficiency, switching to less carbon intensive fuels, and making better use of renewable energy resources, CCS will lead to a reduction in CO_2 emissions and prevent untoward effects of climate change. [1]

1.2 Introduction to gas hydrates

Gas hydrates are crystalline water compounds that belong to a group of solids called clathrates. Clathrate hydrates are a class of solids in which gas molecules occupy "cages" made up of hydrogen-bonded water molecules. They are formed from water and small molecules at suitably high pressures and low temperatures. These hydrates form when water molecules (host) develop linkages by hydrogen bonding to form crystal lattices (cages) with cavities, which then enclose the small non-polar molecule (guest) forming a stable structure. In these clathrate hydrates, there is no chemical bonding between the host water molecules and the enclosed guest molecule, which is why they are referred to as solid solutions.

Gas hydrates are stable only under specific pressure-temperature conditions. Under the appropriate pressure, they can exist at temperatures significantly above the freezing point of water. The maximum temperature at which gas hydrate can exist depends on pressure and gas composition. Hydrate stability can also be influenced by other factors, such as salinity. The discovery of gas hydrates is attributed to Davy [2] who discovered that a solid could be formed when an aqueous solution of chlorine was cooled below 9^{o}C. Gas hydrates are known to occur in vast amounts in nature, mainly methane-hydrate in the sea bed and below permafrost [3]. The rise to prominence of gas hydrates was tied to the discovery by Hammerschmidt [4] that plug formation in oil and gas pipelines was as a result of gas hydrate formation and not ice as previously thought, leading to a period of intense research. The research efforts led to the development of measures to prevent or delay the formation of gas hydrates in pipelines.

1.3 Structure of Gas Hydrates

The structure of gas hydrates have become known through the application of x-ray diffraction [5] with various studies after these resulting in the elucidation of three common structures sI, sII and sH [6-9]. Water molecules are linked through hydrogen bonding and form lattice-like structures with cavities. The cavities have diameters in the range 780 to 920pm. The guest molecules which do not disrupt the hydrogen bonding of water and possess a diameter less than that of the cavity render the structure stable thus producing the gas hydrate.

The cage sizes, geometries, and packing configurations are different among the three structures but they have a common basic cage - the small cage with 12-pentagonal faces (5^{12}). A larger cage is present in the hydrate structures, each with 12-pentagonal faces, plus 2-hexagonal faces ($5^{12}6^2$) for sI, plus 4-hexagonal faces ($5^{12}6^4$) for sII and plus 8-hexagonal faces ($5^{12}6^8$) for sH hydrate. A cage with 3-square faces, 6-pentagonal faces, and 3-hexagonal faces ($4^3 5^6 6^3$) is also formed for sH hydrate, which has similar size to the small cage (5^{12}). The size of the large cage increases from sI, sII to sH. As a result, the stable hydrate structure formed from a given water-guest(s) mixture is controlled by the size and geometry of the guest molecules that occupy these cavities.

Table 1.1: Hydrate structural properties

Structure	I	II	H
Crystal system	Cubic	Cubic	Hexagonal
Space group	Pm3n	Fd3m	P6/mmm
Lattice parameters	a = 12A	a = 17.3A	a = 12.2 A c = 10A
Number of cage	2	2	3
Cage identification	Small/S (5^{12}) Large/L ($5^{12}6^2$)	Small/S (5^{12}) Large/L ($5^{12}6^4$)	Small/S (5^{12}) Medium/M ($4^3 5^6 6^3$) Large/L ($5^{12}6^8$)
Ideal unit cell formula	$2S.6L.46H_2O$	$16S.8L.136H_2O$	$3S.2M.1L.34H_2O$
Cage radius	r_S = 3.95A r_L = 4.33A	r_S = 3.91A r_L = 4.73A	r_S = 3.91A r_M = 4.06A r_L = 5.71A
Coordination number	S = 20 L = 24	S = 20 L = 28	S = 20 M = 20 L = 36

Small (S)	Medium (M)	Large (L)	Structure/Formula
	-	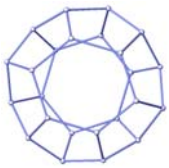	Structure I (sI)
5^{12}		$5^{12}6^2$	$2S.6L.46H_2O$
	-	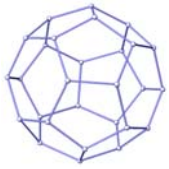	Structure II (sII)
5^{12}		$5^{12}6^4$	$16S.8L.136H_2O$
		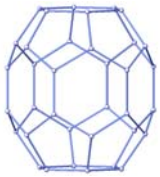	Structure H (sH)
5^{12}	$4^3 5^6 6^3$	$5^{12}6^8$	$3S.2M.1L.34H_2O$

Figure 1.1: Structure and geometry of clathrate hydrate cages

1.4 Importance of Gas Hydrates

Oil and Gas Industry

The major concern of the oil and gas industry is the formation of gas hydrates in pipelines, causing blockages and delays in operations, and possibly explosions due to pressure build up within pipelines. Other concerns include hydrate formation in drilling mud, plugging of blow out preventers by hydrates, and safety issues related to drilling through a hydrate containing region during deep sea exploration. These problems arise primarily due to the physical nature of hydrates – they are non-flowing crystalline solids, and hold large quantities of gas trapped in the crystal lattices [10]. To mitigate these problems, efforts must be made to maintain pipelines and other processing equipment outside the hydrate stability region, with attendant financial costs. These efforts are usually classified as 'flow assurance' activities [11] involving drying of the natural gas, heating gas to temperature above equilibrium hydrate formation temperature, reducing pressure of gas to one below the equilibrium hydrate formation pressure at a given temperature or injecting inhibitors to compete with the hydrate for water, or to delay the formation of hydrates or to prevent agglomeration once formed. These activities are not without their attendant financial implications, with cost of use for one of the typical inhibitors - methanol estimated at over US$220 million annually [10].

Environmental Hazards

The main environmental threat posed primarily by methane hydrates in the earth stems from its possible role in climate change. Methane has a global warming potential 21 times greater than that of carbon dioxide, thus massive releases caused by hydrate composition could lead to a 'runaway' green-house effect with very negative implications for the environment [14-15]. Specifically, as the earth warms, increasing bottom water temperatures could cause gas hydrate disassociation in many marine shelf locations. This gas hydrate disassociation would cause further warming due to the greenhouse effects of the gas which is released. Previous climatic changes have been attributed to the release of large quantities of methane from hydrates [16]. There is however no uniform agreement on the veracity of the so called 'hydrate gun hypothesis' [17], nevertheless, a significant risk to the environment from decomposition of the oceanic and permafrost hydrates exists.

Certain slumps in the sea floor have been found to be linked to gas hydrate decomposition leading to release of methane and instability in the sea floor [8]. In addition, the stability of offshore platforms and drilling rigs may also be affected by this phenomenon. The Blake-Bahama ridge off the south-western U.S. coast contains a good example of such a slump [10].

Potential Energy Source

Methane hydrates occurring in nature are estimated to contain 2.1 x 10^{16} SCM and 7.4 x 10^{14} SCM respectively in the oceans and permafrost respectively. These quantities amount to twice the energy sum of all other fossil fuels on earth [11] albeit with some margin of error, thus making them a huge potential source for meeting future energy needs. Significant challenges still exist however, but advances are being made which could lead to gas production from these sources in the next two decades [10]. As mentioned earlier methane trapped in hydrates have been found to occur extensively beneath permafrost and below the ocean floor. Even the most conservative current estimates suggest that the amount of energy in hydrates is equivalent to twice that of all other fossil fuels combined.

Most of the natural-gas-containing hydrates are in the ocean bottom, and although production of gas from such deep-lying hydrates is now too expensive, improvements in technology and growing energy demands will likely lead to production of gas from these sources in the near future. Estimation of the quantity of hydrates in the oceans is done primarily through indirect seismic evidence using what is known as a bottom simulating reflector (BSR) which indicates reflections of gas from the base of the hydrate. BSR indications are not totally reliable, and other more accurate methods are needed. In addition to indirect methods, drilling programs such as the ocean drilling program (ODP) have been carried out to increase the knowledge base on hydrate occurrences. Permafrost regions tend to contain hydrates in higher concentrations, compared with the oceanic hydrates which generally occur in more dispersed form. As a result pilot drilling

programs in permafrost regions such as the 1998 Mallik 2L-38 well and the Mallik 5L international field experiment concluded in March 2002 on Richards island in the McKenzie delta of Canada at a cost of US$17 million have been used to learn how to produce from these concentrated hydrate formation with the view to eventually developing technology to develop the larger and more dispersed oceanic hydrates [13].

Technological Applications

Gas hydrates are currently being studied with regard to developing economically feasible applications for their use. A number of such applications include carbon dioxide (CO_2) sequestration, natural gas transport, and wastewater minimization, amongst others [10]. A number of technologies have already been developed, but with limited applications, either due to cost factors or non desirable effects on the final product quality. A number of applications have been proposed to exploit hydrate formation in order to fulfill specific purposes. Applying hydrate formation as a separation technology is a major focus, employing particular features of gas hydrates - gas hydrates contain only water and the hydrate-forming substances and the composition of hydrate forming substances in the crystal hydrate is different from that in the originating phases. A number of possible applications include concentrating organic solutions, producing sugar from sugar beet among others have been attempted [10].

Methane hydrates have received considerable attention as an alternative natural gas storage medium. In comparison with the conventional Liquefied Natural Gas (LNG) which is produced and stored at extremely low temperature of -162°C, the production cost for methane hydrates is much lower. Although the transportation amount per unit energy of methane hydrates is more than that of LNG, the facilities for production, storage, transport and gasification can be simplified because natural gas hydrate (NGH) requires a milder condition i.e. -20°C under atmospheric pressure. Eventually, the total cost of NGH system including production, storage, transportation and gasification could be much cheaper than that of LNG [18]. This technology is also receiving attention because it could allow for production from gas fields too small for liquefaction plants or pipeline developments, estimated at 40% of total conventional gas reserves.

1.5 Energy consumption and climate change

The growth of developing economies and the drive to bring significant portions of the world population out of poverty implies that energy consumption especially in the form of fossil fuels like coal, oil and gas are set to keep increasing, thereby further increasing CO_2 emissions. It is estimated that eighty percent of energy growth from 2000 through 2020 will be devoted to improving living standards in the developing world, where about 85% of the world's population will live in 20 years, with world energy increasing by 55% over 2005 levels [19]. There is concerted effort being applied to develop alternative sources of energy without the attendant impact on the environment, and some progress has been achieved in this area, but with issues such as high cost, reliability and widespread availability [19].

Figure 1.2 Global distribution of large stationary sources of CO_2 emissions

As a result, fossil fuels will continue to play a central role in the energy equation for the foreseeable future, during the period when these alternative energies can be fully developed to technological and economical viability [21]. These trends lead to continued growth in global energy-related emissions of CO_2, from 27 Gt in 2005 to an estimated 42 Gt in 2030 – a rise of 57% [19].

It is therefore of utmost importance to devise mechanisms to control the increase of CO_2 in the atmosphere while still maintaining the quality of life and sustaining economic growth. Urgent action is needed if greenhouse-gas concentrations are to be stabilised at a level that would prevent dangerous interference with the climate system. Responding to these needs will involve an iterative risk management process that includes both adaptation and mitigation and takes into account climate change damages, co-benefits, equity, and the associated risks while ensuring that reliable technologies are implemented while promoting improved energy efficiency without undermining economic and social development [21]

1.6 Gas Hydrates and CO_2 Capture

Numerous existing technologies and novel concepts being considered for CO_2 capture can be found in the literature encompassing a wide range of approaches including absorption, cryogenic distillation, use of solid adsorbents, ammonium carbonation amongst others , as well as efforts aimed at storage and sequestration of the captured CO_2 [23-25]. While absorption with amine solutions is currently the best method for CO_2 separation, there still exists a strong motivation for research into other alternative technologies in order to achieve improved efficiency, lower operating costs and better process performance.

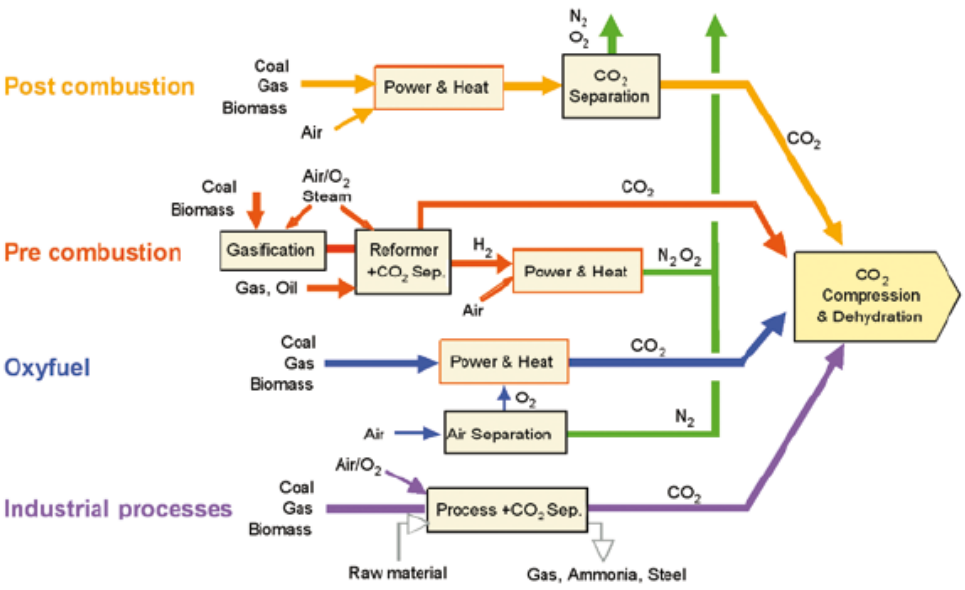

Figure 1.3 CO_2 capture processes and systems

Recent reports indicate that most of the existing CCS technologies are yet to be optimized. It is thus recommended that research and development on the science and technology underlying each capture and storage option is continued in order to improve existing technologies and enable development of critical new components that can

optimize capture and storage systems. In addition, it is recommended that efforts should be directed towards reducing costs and developing effective, safe and environmentally sound storage options. [26]. CO_2 capture, storage and sequestration via gas hydrate formation is a subject of active research, with various groups applying a number of approaches to gain insight into the processes involved. A concept for recovering CO_2 from the flue gases is based on the formation of gas hydrates [27] with recovery of a high purity CO_2 stream (99mol %) from flue gas via a hydrate formation process. A conceptual process involving three stages of hydrate formation/decomposition coupled with a membrane process has been proposed [28, 29]. The latter work [29] presents a process involving the use of an additive which allows for lower operating pressure with attendant energy savings. It was concluded that better modes of gas-water contact need to be investigated to achieve higher process efficiency and conversion. Recent work [30] indicates that capture of CO_2 from flue gases through hydrate formation in porous silica gel can be achieved due to faster reaction rates without the need for stirring and an excess water phase. This new approach improves reaction rates by increasing the contact area for gas-water contact by dispersing the water in the pores of silica gel. More studies are however required to investigate macroscopic conditions of the process such as kinetics as well as heat and mass transfer characteristics of the process. Such information is essential for detailed engineering design and feasibility study of the technology.

CHAPTER 2

LITERATURE REVIEW & RESEARCH OBJECTIVES

2.1 Thermodynamic studies of clathrate hydrates

The initial focus of clathrate hydrate studies was on the gathering of incipient equilibrium hydrate formation data. The incipient equilibrium refers to a condition in which an infinitesimal amount of the hydrate phase is present in equilibrium with fluid phases. This type of data is essential for the accurate and economic design of processes and apparatus in which gas hydrate formation could be encountered. This initial stage was then followed by the development of predictive methods for the calculation of phase equilibria in order to be able to obtain reproducible results without resorting to experimentation for each case or situation encountered. The latter has been primarily achieved through development of computational methods employing thermodynamic models to describe the hydrate and fluid phases.

Most of the work on natural gas hydrate formation has concentrated on making macroscopic time-independent measurements to determine the equilibrium properties of gas hydrates. Sloan has reviewed much of this work [31]. These studies have also focused on the gathering of incipient hydrate equilibrium data, as well as the composition of the phases in equilibrium. Such experimental studies have led to the development of phase diagrams showing the possible equilibrium conditions as well as the phases present in each case.

Experimental studies have focused primarily on natural gas components and other hydrocarbons, with a few exceptions mainly because of the importance of hydrate formation in pipelines and process equipment to the oil and gas industry. All such phase diagrams are based on experimental data for phase boundaries and quadruple points, along with the application of the Gibbs Phase Rule. On these diagrams, quadruple points (co-existence of 4 phases –ice, solid hydrate, aqueous liquid and vapour) are defined by the intersection of four three-phase lines for sI and sII hydrates. Numerous workers [3, 32-33] have published detailed phase diagrams of the type described. The literature on sH hydrates is not as abundant as for the other two common structures, and current pressure-temperature (P-T) diagrams have quintuple points joined by two four-phase lines [34]. Both sI and sII hydrate formers (except N_2 and methane) exhibit two quadruple points, and these points are unique for each hydrate former [31].

The phase behaviour of hydrocarbon + water mixtures differs significantly from that of normal hydrocarbon mixtures, due to two main effects. In clathrate hydrates the main difference is due to the presence of the hydrate phase as a significant part of all phase hydrocarbon + water phase diagrams for hydrocarbons with a molecular size of less than 0.9nm. In addition, water and hydrocarbon molecules exhibit such different behaviours that two distinct phases are formed in the condensed phase, with very low mutual solubilities.

2.2 Hydrate Formation in Porous Media

The worldwide occurrences of natural gas hydrates, both onshore buried under the permafrost as well as offshore buried in the oceanic sediments, are estimated to be the largest reserve of natural gas, thus creating the possibility of its use as an energy source on one hand, as well as the possibility of increasing the atmospheric methane content if they become unstable and release the trapped gas. These hydrates are often found dispersed in pores of coarse grained sediments or fractures in the earth's crust, or as 'massive hydrates' containing less than 6% sediment [31]. In addition, studies are underway to deploy gas hydrates in a separation process using porous materials as a support [30]. In view of the foregoing, it is of obvious importance that we understand the thermodynamics and kinetics of hydrates in porous media. Typical natural materials known as hydrate bearing sediments include silica sand, sandstone and clays [31]; laboratory studies are also often performed using uniformly sized glass beads in order to better understand results.

2.2.1 Effect of porous media on hydrate formation

There has been a lot of discussion on the formation and growth habit of gas hydrates in porous media [38, 39] with the main talking point being whether hydrate formation is preferentially on grain surfaces or in the center of the pore space. A second important question is the degree to which pore size and surface properties of the host sediment grain influence hydrate growth and distribution. Clennell et al. [37] and Henry et al. [10] proposed a capillary-thermodynamic model that can explain some of the

observations concerning hydrate distribution in relation to pore size and sediment type. Inside the porous media the thermodynamic potential of chemical components can change with respect to bulk conditions as a result of two factors:

- Molecular interactions at the pore walls, usually attraction of the fluid molecules by hydrophilic mineral surfaces
- The energy required to maintain capillary equilibrium.

The consequence is that reactions involving water are inhibited in fine grained sediments.

Heterogeneous nucleation occurs when clusters form on a third surface such as gas bubbles or mineral surfaces. The level of super-saturation required for heterogeneous nucleation in porous media is normally much smaller than that required for homogeneous nucleation under bulk aqueous conditions. Experimental observations of short induction times [40] suggest that heterogeneous nucleation in pore spaces is the norm when gas hydrates form in porous sediments and rocks. From these observations, it was concluded that water activity is depressed by the partial ordering and bonding of water molecules with hydrophilic pore surfaces. This decrease leads to the shift of hydrate formation condition to a much higher pressure at a specified temperature, or to a much lower temperature at a specific pressure. Handa and Stupin [36] previously observed this phenomenon in mixtures containing electrolytes and alcohols, thus leading to the conclusion that water activity reduction caused by the geometrical constraints in porous media can be considered equivalent to a change in activity as caused by the inhibitors. The pore size effect will be discussed in detail subsequently.

Genov et al. [41] analyzed the peculiarities of methane hydrate formation and the effect of sediment properties. They found that only a part of the pore water was transformed to hydrate in methane saturated sediments. The portion of water transformed to hydrate was found to be maximum (about 80%) in sandy sediments. The minimum transformation (about 15%) was observed in montmorillonite clay. So, the hydrate ratio decreased in accordance with the rise of bonding energy of pore water and mineral surface in presence of clay. The fraction of water transformed to hydrate also decreased with increase of salinity.

2.2.2 Kinetic studies of hydrate formation in porous media

Yousif and co workers [42] studied the dissociation of methane hydrate in Berea Sandstone by the depressurization of a hydrate-containing core at constant temperature. The hydrates were formed in a cylindrical Berea Sandstone core enclosed in a heat shrunk plastic tube which was in turn encased in a stainless steel pressure bomb, placed in a temperature controlled bath. The sample was first evacuated after which a 1.5 wt% sodium chloride solution was injected into the sample till saturation was achieved, after which methane was supplied to the core at a pressure higher than the equilibrium hydrate formation pressure, thereby resulting in some water production/displacement. The sample was then isolated for hydrate formation and allowed to proceed till there was no further pressure reduction, indicating hydrate formation had ceased. The outlet pressure was then reduced to a value below the equilibrium pressure (2.84MPa) to allow dissociation to begin. Throughout the process the temperature was kept constant at 273.7 K.

Pressure measurements at the gas inlet and outlet points as well as the volume of gas produced were measured as a function of time during dissociation. Two core samples with permeability values of 8.388 x 10^{-14} and 40 x 10^{-14} m^2 respectively were used. They observed that the lower permeability core required a longer span of time for hydrate formation to be complete (20-30 hours) than the higher permeability core (4-5 hours). There was a significant pressure drop noticed between the gas inlet point and outlet on the core after hydrate formation, caused by greater hydrate being formed at the inlet which reduced the core permeability and thus the transmission of pressure to the outlet point.

Yousif et al [40] and Yousif and Sloan [43] improved on this work using the same apparatus; this time they carried out annealing processes- cycled heating dissociation and reforming of the hydrates in the core, so as to achieve more uniform hydrate distribution along the core. Electrical resistance measurements were also taken at four locations along the core length in order to provide an additional method to check for hydrate formation besides the pressure drop in the core samples. The experimental data showed that an appreciable amount of water is also produced simultaneously with gas production as a result of hydrate dissociation. In both works a 1D numerical model was developed to simulate the isothermal hydrate dissociation, with the model providing a satisfactory match to the experimental data.

Kumar [44] studied CO_2 hydrate dissociation using a high pressure vessel capable of withstanding a maximum pressure of 9.0 MPa and glass beads with diameters ranging between 0.0889-0.14986 mm of density 2620 kg/m^3 which served as the porous medium. A brine solution was injected into the pressure cell, prior to pressurization with the gas after which hydrate formation was allowed to proceed. Temperature profiles along the core during hydrate dissociation were measured by four thermocouples installed along the cell length. Permeability measurements were performed before and after hydrate formation, indicating that there is reduced permeability due to hydrate formation in the pore spaces. Gas production during the dissociation experiments was measured and collected in a graduated displacement column. Different water saturations were employed to determine the effects of water saturation on the formation of hydrates. The work indicated that at water saturations of less than 35%, hydrate formation occurred on the grain/particle surfaces, while at water saturations greater than 35% hydrate formation occurred in the pore spaces.

2.2.3 Phase equilibrium studies of hydrates in porous media

Handa and Stupin [36] studied phase equilibrium of methane and propane hydrates in 70 Å silica gels. Based on their previous work, they concluded that the thermodynamic properties of hydrates change the same way as those of ice confined in small pores. They reported equilibrium pressures 20-100% higher than those for bulk hydrates. Uchida et al [45] studied equilibria of methane hydrate confined in small pores of porous glass. Their measurements were made under conditions similar to those of

Handa and Stupin [36] and this work showed that the smaller the pore diameter, the larger the temperature-shift of the equilibrium line.

Seshadri et al [46] studied propane hydrate formation in silica gels with nominal pore sizes of 2.0, 3.0 5.0 and 7.5 nm. Their method for forming the hydrates was similar to that employed previously [36]. Two silica gel samples of 7.5nm nominal pore radius were used in this study with particle size distributions of 33-74 μm and 74-250 μm for comparison with previous studies by Handa and Stupin [36]. The equilibrium pressure-temperature dissociation experiments carried out on these two silica gels were in good agreement, indicating that dissociation of the hydrates is controlled primarily by the pore radius, not the particle size, and thus support the conclusion that hydrate formation occurs in the silica gel pores, and not in the inter-particle spaces. The results also showed excellent agreement with the results of Handa and Stupin [36]. The equilibrium P-T profiles of the silica gel hydrates for all four pore sizes studied were compared with those obtained for bulk propane hydrates as shown in Figure 2.2. The figure shows that the equilibrium pressures increased with decreasing pore radius at a given temperature. The increase obtained was 53-87% for the nominal 7.5nm pores, 79-110% for the nominal 5nm pores, 78-131% for the nominal 3.0nm pores, and 200-300% for the nominal 2.0nm pores. The lower quadruple points (*H-I-*L_w*-V*) were also determined for each sample using an empirical correlation for the second virial coefficient given by Pitzer [47]. The values obtained were found to be consistent with both theoretical and experimental melting temperatures of ice in small pores based on the use of nominal pore sizes to represent the samples.

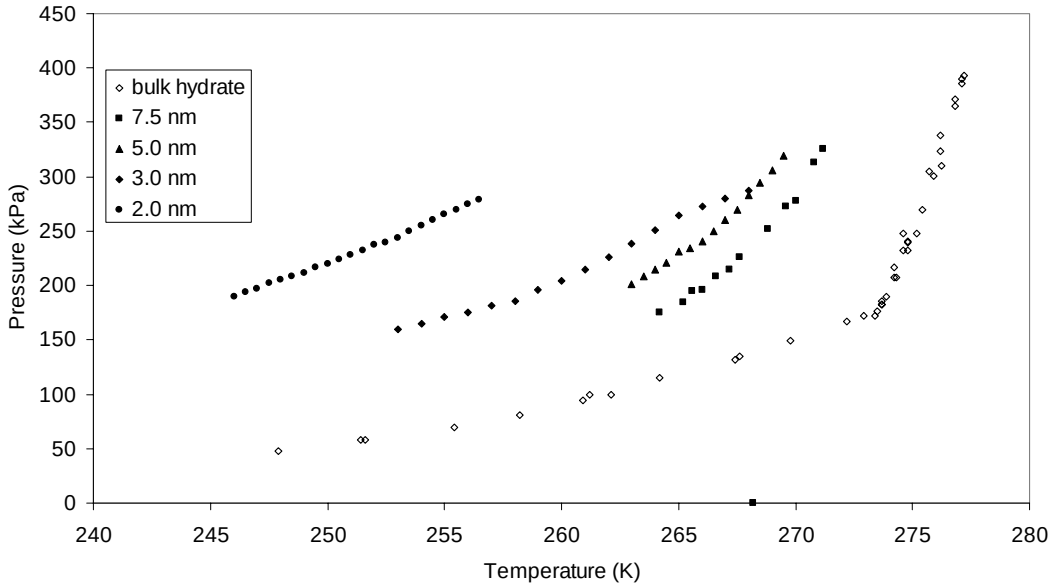

Figure 2.1 Hydrate equilibrium for bulk and porous media propane hydrates

Seo et al [48] studied hydrate phase behaviour of the CO_2+CH_4 system in silica gels of three different nominal diameters, and compared their data with those of previous workers as well as a modified van der Waals Platteeuw model. The correction term added to the model accounts for the capillary effect and activity decrease effect of porous media on water activity. The improved model gave a better agreement with the experimental data. Their experimental data was in good agreement with those of Uchida et al [49], but largely deviated from those of Handa and Stupin [36] and Smith et al [50]. Their results indicate that the decrease of pore diameter led to increasing shift of the equilibrium L_w-H-V line shifted toward lower temperature at a given pressure, compared to bulk hydrates.

Seo and Lee [51] have studied hydrate phase equilibria in silica gel pores for single hydrate (CO_2, CH_4) and mixed hydrate (CO_2+CH_4) formation in the presence of sodium chloride (NaCl) electrolyte. The aim was to investigate fundamental electrolyte role on hydrate formation processes occurring in pores, in connection with hydrate formation on the sea floor. In addition, various pore diameters were used in the study alongside varying CO_2 composition for the mixed hydrate study in order to meet changeable surroundings of sea floor sediments. At a specified temperature, three phase L_w-H-V equilibrium curves of pore hydrates were shifted to a higher pressure region depending on NaCl concentrations and pore sizes.

Uchida and co workers [49] studied the effect of pore sizes on the dissociation temperatures and pressures of methane, propane and carbon dioxide hydrates in several kinds of porous media. They reported dissociation temperature shifts to a lower temperature at a given pressure compared with bulk hydrates.

2.2.4 Prediction of hydrate equilibrium in porous media

Prediction of hydrate equilibria is based mainly on the application of the statistical thermodynamic model of van der Waals and Platteeuw [35], in conjunction with the basic phase equilibria conditions. The major difference in the prediction of hydrate formation in porous media and bulk hydrates lies in modifications made to this model to account for the different conditions encountered in porous media.

For vapour-liquid-hydrate equilibria, the basic equations for the equilibrium are

$$\mu_i^V = \mu_i^L \qquad (2.1)$$

$$\mu_i^H = \mu_i^V \qquad (2.2)$$

(i =1,…, N) For all the N components, and by

(j =1,…, c)

For all the c hydrate forming components including water

In terms of fugacities,

$$f_i^L = f_i^V \qquad f_j^H = f_j^V \qquad (2.3)$$

Because the gas phase fugacity is implicit in the hydrate phase fugacity expression, the equilibrium relationship for water can be represented by

$$f_W^H = f_W^L \qquad (2.4)$$

The expressions for equation (2.4) for bulk hydrates are

$$f_W^H = f_W^{MT} \exp\left(-\frac{\Delta\mu_W^{MT-H}}{RT}\right) \tag{2.5}$$

$$\frac{\Delta\mu_W^{MT-H}}{RT} = \sum_1^2 \upsilon_m \ln(1+\sum_1^{nc} C_{mj} f_j) \tag{2.6}$$

where

$$C_{mj} = \frac{4\pi}{kT}\int_0^{Rm} \exp(\frac{-W_{mj}(r)}{kT}) r^2 dr \tag{2.7}$$

and

$$f_W^{MT} = f_W^{Lo} \exp\left(\frac{\Delta\mu_W^{MT-Lo}}{RT}\right) \tag{2.8}$$

$$\frac{\Delta\mu_W^{MT-Lo}}{RT} = \frac{\Delta\mu_W^0}{RT} - \int_{To}^{T} \frac{\Delta h_W^{MT-Lo}}{RT^2} dT + \int_0^P \frac{\Delta v_w^{MT-Lo}}{RT} dP \tag{2.9}$$

The equilibrium relationship in equation (2.4) can thus be represented by

$$f_W^H = f_W^{Lo} \exp\left(\frac{\Delta\mu_W^{MT-Lo}}{RT}\right)\exp\left(-\frac{\Delta\mu_W^{MT-H}}{RT}\right) = f_W^L \tag{2.10}$$

or

$$\ln\left(\frac{f_W^L}{f_W^{Lo}}\right) = \frac{\Delta\mu_W^{MT-Lo}}{RT} - \frac{\Delta\mu_W^{MT-H}}{RT} \tag{2.11}$$

$$a_w = \frac{f_W^L}{f_W^{Lo}} \tag{2.12}$$

However, in the case of hydrate formation in porous media, the situation encountered above is now different. The surface effects neglected in the case of bulk

hydrate formation cannot be neglected in the case of porous media. This is because the hydrates form in the small capillaries or pores present in the latter. As a result the Gibbs free energy for the system changes, leading to a situation that at equilibrium, the pressure in the liquid phase will not be equal to that in the gas phase. In a capillary system, the pressure will be greater on the side that of the interface that contains the center of curvature of the curved surface (i.e. the vapour phase). This pressure difference between the vapour and liquid phase can be expressed as a function of the surface tension between the vapour and the liquid. [38]

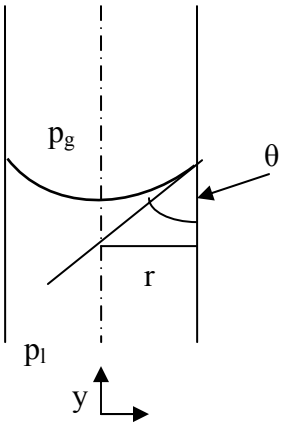

Figure 2.2 Schematic of fluid in a capillary

$$\Delta p = p_g - p_l = \frac{2\sigma \cos\theta}{r} \tag{2.14}$$

where r =radius of the capillary,

θ = wetting angle (angle between wall and meniscus)

σ = interfacial tension between hydrate and water

When the wetting angle is 90°, the pressures will be equal, corresponding to bulk hydrate formation. The effect of this pressure reduction is primarily on the activity of the water, due to the capillary effect and geometrical constraints. The activity of water can thus be written as

$$\ln a_w = \frac{v_l}{RT}(p_l - p_g) \tag{2.15}$$

Substituting (2.14) into (2.15) gives

$$\ln a_w = \frac{-2\sigma v_l \cos\theta}{rRT} \tag{2.16}$$

v_l = molar volume of liquid water

The effect of the pressure differential between the vapour and liquid phases results in two other changes – firstly the integration of P in (2.9) above must now be done at the liquid pressure, p_l, while the vapour phase fugacities, f_i must be computed using the vapour phase pressure, p_g .

In earlier modeling attempts, the interfacial tension between hydrate and liquid water was assumed to be the same as that between ice and liquid water (0.027J/m^2). The use of this value led to large discrepancies between experimental and calculated values. Uchida et al. [45] have calculated values of σ by fitting their data to the Gibbs-Thompson equation which describes the pore size dependence of the hydrate equilibrium temperature compared to the bulk hydrate phase. They reported a value of 0.039J/m^2 as interfacial tension for CH_4 hydrate.

$$\Delta T = T_d^{pore} - T_d^{bulk} \tag{2.17}$$

$$\Delta T / T_d^{bulk} = -4\sigma_{HW} / \rho_H L_H d \tag{2.18}$$

Equation (2.18) is the Gibbs Thompson Equation

where

T_d^{pore} = pore hydrate dissociation temperature

T_d^{bulk} = bulk hydrate dissociation temperature

ρ_H = density of the hydrate

L_H = dissociation heat for the hydrate

d = pore diameter

The value of the interfacial tension between the hydrate and water can be estimated from the slope of the plot of $\Delta T_d/T_d^{bulk}$ against *1/d.*

Uchida et al [49] determined the value of σ_{HW} with a wider range of pore sizes used compared to their previous work. They reported values for CH_4 hydrate ($0.017 J/m^2$) and CO_2 hydrate ($0.014 J/m^2$) that were lower than those previously obtained. The higher accuracy of these new values is attributed to the wider pore size range used. Seo et al [48] used these values in their model and reported a better agreement with experimental data.

Seo et al [51] studied hydrate phase equilibria of methane and CO_2 mixtures with aqueous solutions of sodium chloride in porous media. In describing the water activity, decrease due to the capillary effect and geometrical constraints as well as the effect of the presence of electrolytes were considered. The fugacity coefficient of water in aqueous electrolyte liquid is given by the model of Aasberg-Peterson et al [52]:

$$\ln \varphi_w = \ln \varphi_w^{EOS} + \ln \gamma_w^{EL} \tag{2.19}$$

The first term is the normal contribution that can be obtained from a cubic equation of state, while the second term for the electrolyte contribution can be calculated from the Pitzer model [53, 54]

$$\gamma_W^{EL} = \frac{a_W^{EL}}{x_W} \tag{2.20}$$

$$\ln a_W^{EL} = -\frac{M_w vm}{1000}\phi \tag{2.21}$$

a_W^{EL} is the activity of water in the electrolyte solution, M_w is the molecular weight of water, m represents the molality of the electrolyte, v stands for the number of ions the electrolyte dissociates into, while Φ is the osmotic coefficient. The osmotic coefficient can be obtained from expressions available in the literature.

The decrease in water activity is thus expressed as

$$\ln a_W = \ln a_W^{EL} - \frac{V_L 2\cos\theta\sigma_{HW}}{rRT} \tag{2.22}$$

The pore hydrate model developed by Seo et al [51] using the activity term in the above equation gave both quantitative and qualitative agreement, with values of percent absolute average deviations (%AAD) reported in the range of 1.73 to 11.86.

2.2.5 **Diameter range of pore effects on gas hydrate equilibrium**.

Uchida et al [49] determined the diameter range in which hydrates formed in porous media have physical properties similar to the bulk hydrate phase. They determined this range by means of the Gibbs-Thomson equation.

For the largest pore size studied in this work, 100 nm, the shift in the dissociation temperature obtained was approximately -0.5 K at a given pressure. If the pore space is much larger however, the pore effect will not be measurable. In determining the upper limit for which no pore effects occur, the maximum pore size, d_{max}, is estimated such that the value of ΔT is less than the accuracy of the temperature measurements, i.e. the ΔT is so small that it is not measurable by current measurement apparatus. In their experiment, the accuracy of temperature measurement was approximately $\pm$0.15 K, whereas the accuracy for equilibrium temperature in a field measurement is 0.5 K. This field value was used in the Gibbs-Thomson equation along with a T_{bulk}= 293.2 K chosen as the temperature of the hydrate stability zone at approximately 3200m below sea level of the Blake Ridge [56]. The calculations yield a value of d_{max}=101nm. According to Henry et al [39] pore size distributions cannot be obtained for pore diameters of less than 100nm, thus the pore size measurements in the field will yield values of ΔT less than 0.5 K. IF smaller pore sizes can be measured, however, then the temperature shifts would be greater.

In determining the minimum pore size that would cause a temperature shift, experimental data could not be used due to the increasing difficulty in forming hydrates as lower pore diameters were used. Consequently the minimum pore diameter, d_{min}, was obtained from a combination of the Gibbs-Thomson equation and the homogeneous nucleation theory. The application of the Gibbs-Thomson equation is predicated on the bulk hydrate and the hydrate in the pores possessing the same structure. Since bulk properties of materials depend on the unit cell, the pore should therefore have a size larger than the unit cell for the G-T equation to be applicable.

Therefore, the maximum shift of the dissociation temperatures at a given pressure caused by the Gibbs-Thomson effect is when the critical radius r_c for nucleation of a spherical hydrate crystal has decreased to the point where it equals the unit cell radius.

From homogeneous nucleation theory, this critical radius is

$$r_c = 2v\gamma / \Delta\mu \tag{2.23}$$

where v is the specific volume of water molecules in the hydrate structure (either 3.8 x $10^{-29}m^3$ for type I or 3.6 x10^{-29} m^3 for type II) and $\Delta\mu$ is the chemical potential difference of water between the solution and the hydrate phase (1263 J/mol for sI or 884 J/mol for sII).15 By using the obtained interfacial tension γ_{HW}, they obtained the critical size to be 0.6, 0.5, and 1.1 nm for CH_4, CO_2, and C_3H_8 hydrates, respectively. The lattice constant of the unit cell for each crystal structure is approximately 1.2 nm for sI hydrates and 1.7 nm for sII. So the size of the critical nucleus is considered to be equivalent to that of the unit cell. The lower limit of the effective pore diameter d_{min} for a given hydrate structure must exceed the unit cell size of the bulk hydrate structure. By assuming that the bound

water is independent of the gas molecule and of the formation of solid structures, as suggested by Handa and Stupin [36], the thickness of the bound water layer around the hydrate is also estimated to be approximately two molecular layers or approximately 0.5 nm in the present study. The value of d_{min} is, therefore, approximately 3 nm.

According to equation (2.18) for gas hydrates with d_{min} = 3 nm, the value of ΔT is approximately 16, 13, and 20 K at T_d = 273.2 K for CH_4 hydrate, CO_2 hydrate, and C_3H_8 hydrate, respectively. These are considered to be the maximum shift of the dissociation temperatures at a given pressure caused by the Gibbs-Thomson effect. This pore diameter range is valid only for porous media with similar properties to the silica gels and vycor glass used in this study, since it has been observed by Uchida [45] that shifts in P-T diagrams for CH_4 hydrates were different in various porous media.

Wilder et al [57] has suggested that the equilibrium temperatures for hydrates in silica gel pores below the H-V-L_w-I quadruple point should be the same as that of the bulk hydrate phase. This arose from the experimental data from methane hydrate formation in 7.5nm silica gels, showing that the H-V-I line for the porous hydrates coincided with the bulk hydrate H-V-I line. Their work involved development of a conceptual model based on hydrate formation in porous media comprised of a bundle of tubes of different radii. From their modeling work, prediction of the exact dissociation pressure was obtained using a specific pore size corresponding to the equilibrium point, not the nominal pore size used by Clarke et al [58]. This was later confirmed by workers in the same group [59] using ethane hydrate and a wide pore size range, indicating there

are no detectable effects of pressure due to the restricted geometries of the porous media. From these results it was suggested that the interface relevant to the formation of hydrate in silica gel pores is that between the hydrate and the appropriate aqueous phase, and that the surface energy γ_{IH} between hydrate and ice phases is equal to zero. Uchida et al. [49] however considered γ_{IH} not equal to zero and report a value of 4.1×10^{-2} J/m^2.

2.3 Gas hydrate formation as a novel CO_2 capture technology

There are a variety of technologies for CO_2 capture and the largest portion of the cost of a capture and storage sequestration scheme is due to CO_2 separation and compression [60-62]. Aaron and Tsouris [24] have extensively reviewed the existing and proposed technologies available and it is noted that absorption with amine based solutions is the best developed and cost effective method currently available. The fact that most fossil fuel power plants use air instead of oxygen results in flue gases with relatively low CO_2 concentrations of 15-19 mol% and large quantities of N_2. This necessitates that a difficult and expensive separation process be deployed to capture CO_2 as a concentrated stream, as is required in most storage, conversion and reuse applications [63]. Approximately 80% of world energy needs are met using fossil fuels, with coal being the dominant fuel for power generation. When this is coupled with increased coal use under any foreseeable energy scenario due to its cheapness and widespread abundance, it is of great necessity that new technologies are investigated to provide alternative methods of capture and sequestration of CO_2. [64]

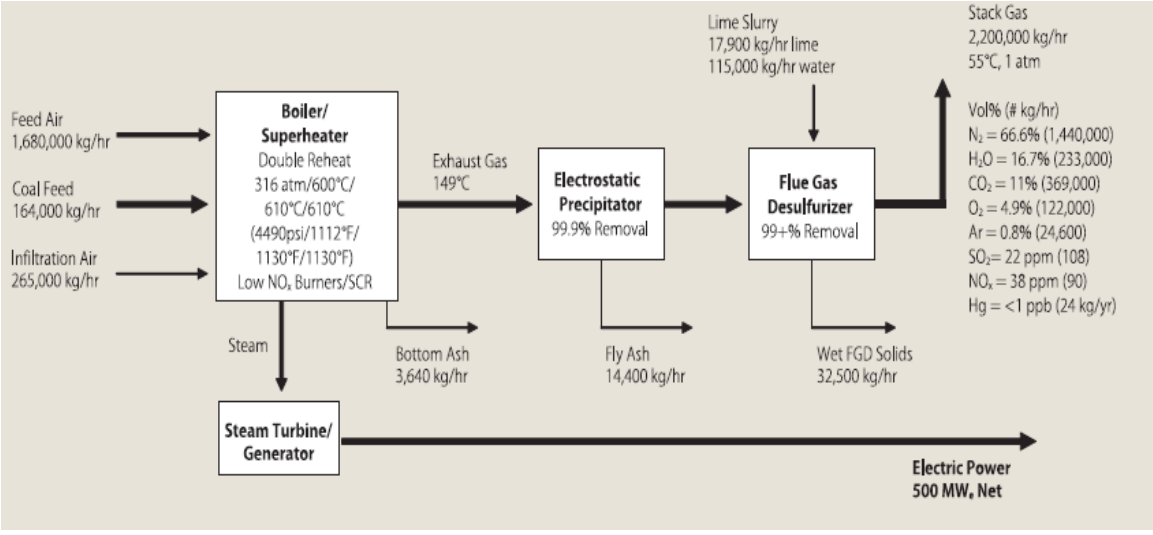

Figure 2.3 500MWe ultra-super critical pulverized coal unit stack emissions

2.3.1 Thermodynamics and kinetics of CO_2 and N_2 hydrates

CO_2 forms structure I hydrate as a single guest. The CO_2 molecules occupy primarily the large cavities and some small ones [38, 39]. Incipient hydrate equilibrium conditions for CO_2 were investigated and reported by numerous workers in the literature [67-70]. The equilibrium hydrate formation conditions for CO_2 in water are shown in Figure 2.4. Dholabhai et al. [71] measured the formation conditions of CO_2 hydrates in aqueous electrolyte solutions. Englezos and Hall [72] investigated the equilibrium hydrate formation conditions of carbon dioxide in the presence of aqueous electrolyte solutions, water soluble polymers and montmorillonite. Breland and Englezos [73] investigated the equilibrium hydrate formation conditions of carbon dioxide in the presence of glycerol. Fan et al. [74] studied the hydrate formation conditions for carbon dioxide and carbon dioxide rich gas mixtures in the presence of ethylene glycol.

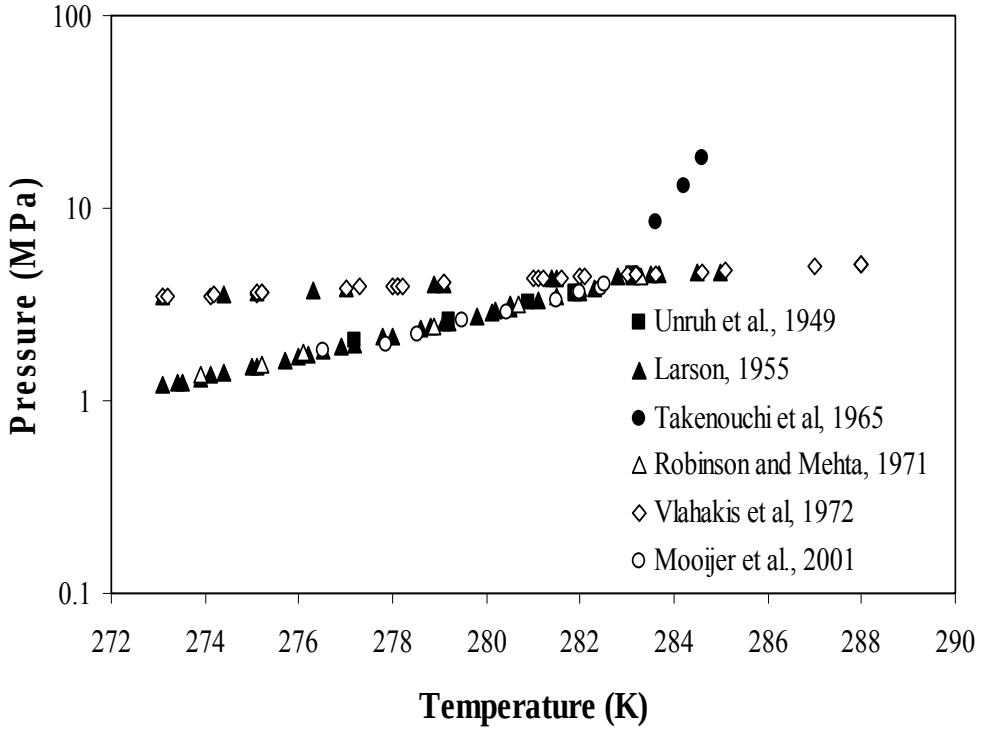

Figure 2.4 Equilibrium hydrate formation conditions for the CO_2-H_2O system

N_2 is known to form structure II hydrate as a single guest with the N_2 molecules occupying both cages [75]. The equilibrium hydrate formation conditions for nitrogen were observed by van Cleef et al [76]. Marshall et al. also [77] investigated and reported equilibrium hydrate formation conditions for nitrogen. Reported equilibrium hydrate formation conditions for N_2 in water from various workers are shown in Figure 2.5. Sugahara et al [78] studied the equilibrium hydrate conditions of nitrogen for higher temperatures.

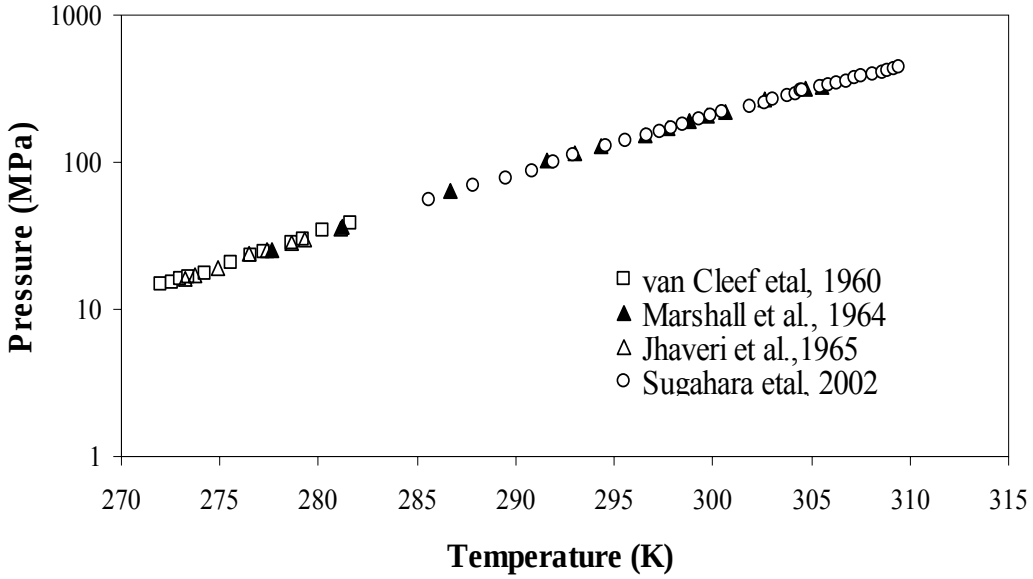

Figure 2.5 Equilibrium hydrate formation conditions for the N_2-H_2O system

2.3.2 Pre and Post-Combustion CO_2 capture via gas hydrates

It has been proposed that gas hydrates can be applied as a separation method to achieve CO_2 capture from flue and fuel gas streams, CO_2 sequestration, as well as hydrogen storage, with significant research efforts being undertaken by various groups to assess the feasibility and efficiency of such processes [79].

Kang and Lee [80] proposed a hydrate-based crystallization process that can recover 99mol% of CO_2 from the flue gas. The flue gas from a power plant is fed to a commercial desulphurization plant for removal of sulphur oxides $\{SO_x\}$. The pre-treated flue gas is passed through the first hydrator I in which carbon dioxide is separated from nitrogen. The hydrate slurry is then decomposed in a dissociator. The gas from the dissociator is compressed and sent to second hydrator and dissociator and then finally through the third hydrator and dissociator. Kang et al. [81] reported equilibrium hydrate formation data for a mixture of carbon dioxide and nitrogen with varying ratios of each. Such data are needed for the design of hydrate-based separation processes. Their work involved incipient hydrate phase equilibrium measurements in the range 272-295K with different CO_2/N_2 mixture compositions to determine operating conditions for the proposed process. This work also included statistical thermodynamic modeling to predict phase equilibrium, and good agreement was reported between the experimental and model results.

Kang et al. [82] reported the enthalpy of dissociation for carbon dioxide and nitrogen hydrates. They employed a calorimetric technique to measure the enthalpy of dissociation of hydrates. The enthalpies of dissociation reported were for CO_2 (65.2±1.0 kJ/mol of CO_2 hydrate) and for N_2 (65.8±1.0 kJ/mol of N_2 hydrate) at 273.7K and 0.1MPa. Seo and Lee [83] studied the structure and guest distribution of mixed (CO_2+N_2) hydrates of carbon dioxide and nitrogen using X-ray diffraction and C NMR spectroscopy. X-ray diffraction results showed that for mixed (CO_2+N_2) hydrates with 3-20mol% CO_2, the unit cell parameter was ~11.8Å and the structure formed is structure I.

For 1mol% CO_2, the unit cell parameter was found to be 17.26Å and the structure formed was identified as Structure II. They also found that the NMR spectra results revealed that carbon dioxide molecules mainly occupied the large $5^{12}6^2$ cages of structure one when the mixed hydrate (CO_2+N_2) was formed at a vapour phase composition range of 10-20mol% CO_2. They also reported that with a small increase of carbon dioxide in the vapour phase the amount of carbon dioxide in the mixed (CO_2+N_2) hydrates increased greatly. Finally, Seo and Lee reported that CO_2 molecules may occupy both large and small cavities of structure I when the CO_2 content in the gas phase exceeds 33%.

Linga et al [28] studied hydrate formation from CO_2+N_2 and CO_2+H_2 gas mixtures using a semi-batch stirred vessel operating at isothermal and isobaric conditions. Incipient equilibrium hydrate compositions were reported for both gas mixtures as well as with gas uptake measurements and phase composition determination during kinetic experiments. It was concluded that the rate of hydrate growth was faster from the CO_2+H_2 mixture, with CO_2 preferentially incorporated into the hydrate phase. It is also noted that higher operating pressures lead to increased incorporation of N_2 for the flue gas experiments. Linga et al [84] provided basic thermodynamic and kinetic data for conceptual process design of hydrate based separation processes from CO_2+N_2 and CO_2+H_2 gas mixtures. Hybrid conceptual processes for both pre and post-combustion capture based on hydrate formation coupled with membrane separation were developed. In addition, two metrics called the *split fraction* and *separation factor* were defined to quantify the separation achieved by the process. CO_2 recovery was found to be 42.1% in one stage at 10.0 MPa and 0.6^oC for CO_2/N_2 and 42.5% at 8.5 MPa and 0.6^oC for the

CO_2/H_2 mixture. The hybrid hydrate-membrane processes developed involved the use of three hydrate stages coupled with a membrane process and two hydrate stages coupled with a membrane process for CO_2/N_2 and CO_2/H_2 mixtures respectively, each producing a 98-99% CO_2 stream suitable for disposal. It is noted that high pressures are required for the process and additives need to be investigated which can lower pressures without compromising separation efficiency and CO_2 recovery.

2.3.3 Effects of additives on CO_2 and N_2 hydrate formation

Mooijer-van-der Heuvel et al. [85] investigated the effect of additives on carbon dioxide hydrate formation conditions. The additives used were organic substances like tetrahydropyran, cyclobutanone, cyclohexane and methylcycohexane. Cyclic organic compounds as additives are attractive to use if the reduction of hydrate equilibrium pressure is desired. Kang and Lee [80] presented thermodynamic data showing that the addition of THF in the water results in a reduced hydrate formation pressure at a given temperature compared to a system in which THF is absent. A 1mol% addition of THF lowers the incipient hydrate formation pressure from 8.4 to 0.5 MPa for a 17%CO_2/83% N_2 mixture at 2^{o}C. Linga et al [28] studied the effect of THF on CO_2/N_2 hydrate formation and reported incipient hydrate equilibrium data that was in agreement with the previous work of Kang and Lee [80]. In addition, kinetic gas uptake measurements were presented which indicated a shorter induction time for hydrate formation in the presence of THF as well as lower operating pressure. It is also noted that the rate and overall gas consumption over time are significantly lower compared to the experiments in the absence of THF.

Linga et al. [29] presented thermodynamic, kinetic and separation efficiency data for a medium-pressure process for post-combustion CO_2 capture from conventional power plant flue gases. The conceptual process consists of three hydrate formation/decomposition stages operating at 0.6^oC and a reduced pressure of 2.5 MPa due to the presence of 1mol% THF, coupled with a membrane separation state to tackle a CO_2-lean stream. The proposed process was the culmination of their study based on the preliminary work of Kang and Lee [82] aimed investigating the effect of THF as an additive on the hydrate formation kinetics of flue gas (CO_2/N_2) mixtures with a view of determining an optimal concentration which would lower operating pressures without compromising CO_2 recovery and separation efficiency. From the results it was observed that hydrate formation rates are maximum at 1mol% THF over the range 0.5 to 1.5mol% THF studied. Thus 1mol% THF was chosen as the optimal concentration around which the conceptual process was designed. It is noted that the presence of THF achieves a reduction of compression costs from 75% to 53% of the power output of a 500MWe power plant. High CO_2 recoveries of 50% in the first two stages and 37% in the third hydrate stage were reported. It is also noted that the trend of reduced rate of gas consumption is also observed in this system with THF present. Finally, it is noted that improved gas-water contact is highly desirable for enhancement of the rate of hydrate formation and thus improvement of overall yield.

2.3.4 Significance of gas-water contact mode

It has been recognized by various workers [86-90] that hydrate crystallization is a heterogeneous process. The hydrate formation process itself is a complex combination of mass and energy transfer processes not fully understood. Englezos et al. [89] developed a mechanistic model based upon crystallization and mass transfer theories to describe the kinetics of hydrate formation. Their model assumes that particles may be located either in the bulk of the solution or in the liquid film at the gas–liquid interface and, in both cases, a stagnant liquid diffusion layer and an adsorption "reaction" layer surround the solid hydrate particle, as seen in Figure 2.6. The dissolved gas diffuses from the solution surrounding the stagnant diffusion layer to the hydrate–water interface and subsequently, by an adsorption process, the gas molecules are incorporated into the structured water framework [91].

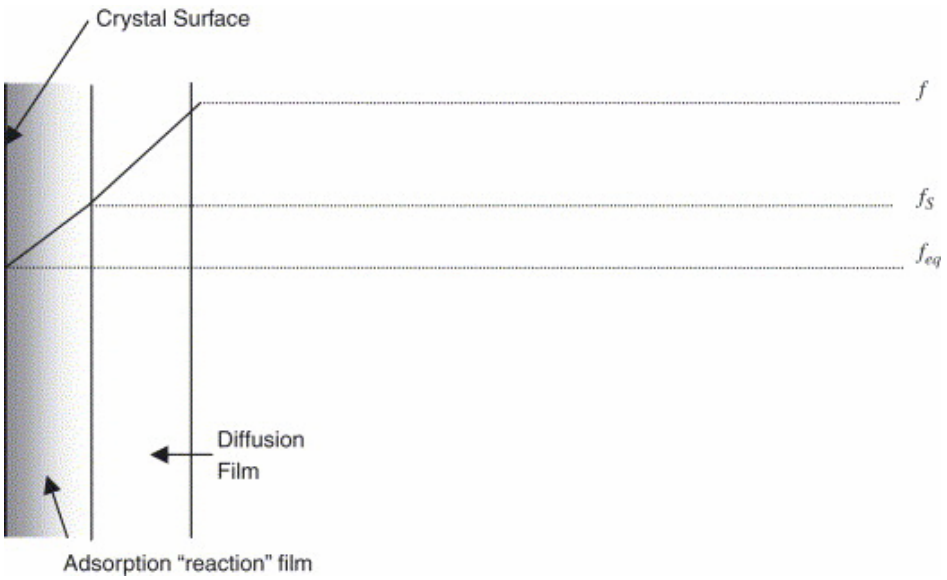

Figure 2.6 Fugacity gradients in the diffusion and adsorption "reaction" film around a growing hydrate particle. The fugacity is equal to f when the hydrate particle is located in the liquid-side film region of the gas–liquid interface and f_b when the hydrate particle's located in the bulk solution.

Hydrate formation studies have generally been conducted with a bulk water phase consisting of ice or liquid water [80-84, 86-90]. However, mass transfer limitations still exist in this system; hydrates form as a solid mass at the gas-water interface, this build up of solid serves as a barrier for gas diffusion to the water phase to form more hydrates, thus slowing down the rate of hydrate formation. [30]. Different methods have been proposed to resolve this mass transfer problem in hydrate forming systems. Stirred vessels fitted with baffles [29, 84-85] have been employed to counter this mass transfer limitation by continuously renewing the water-gas interface. Bubbling gas through the water to achieve improved hydrate formation rates has also been applied for storage and transport of methane in hydrates [92]. This area remains under active study because of the need to improve gas-water contact to achieve increased rates of hydrate formation.

.

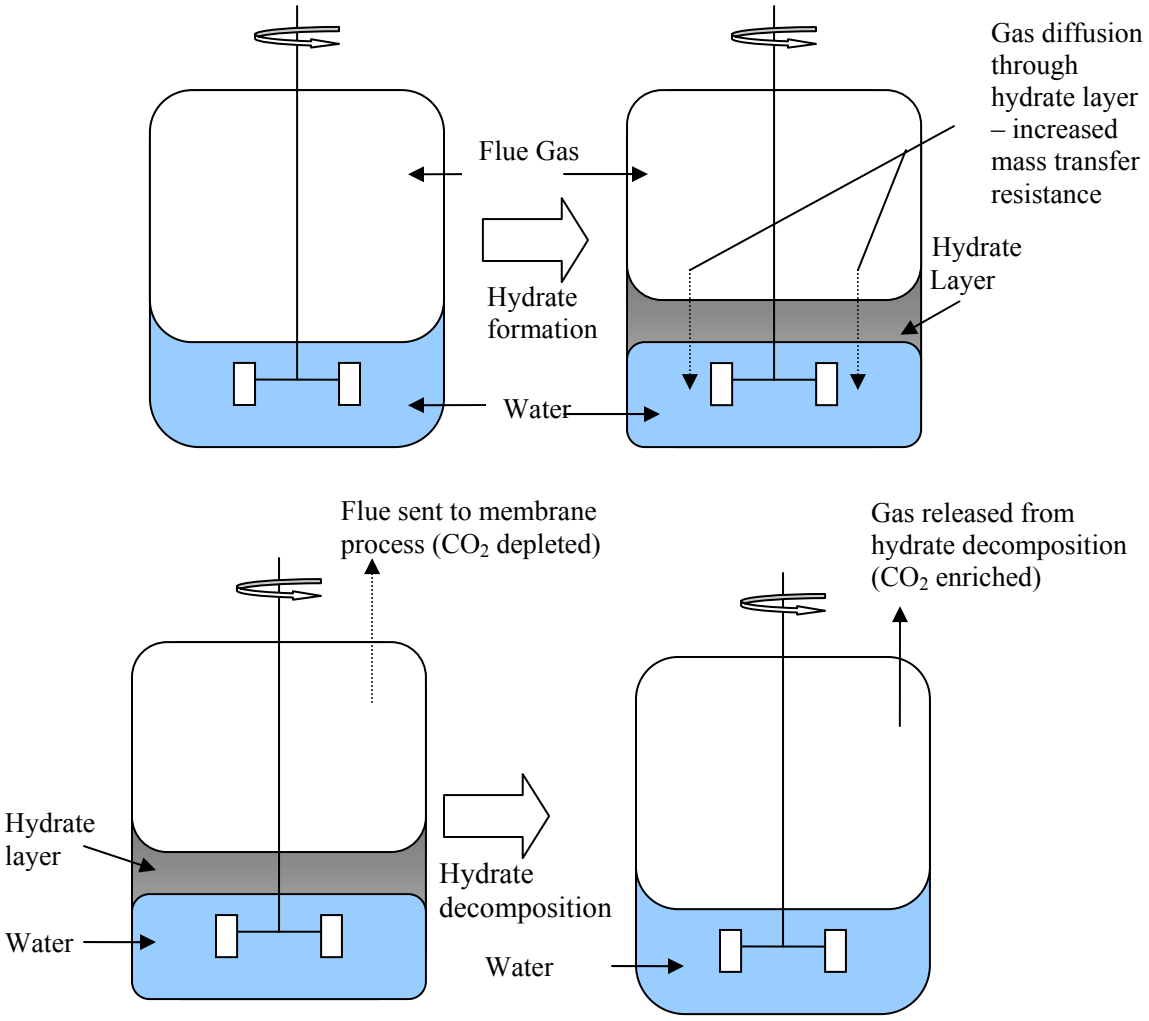

Figure 2.7 Single stage of hydrate formation/decomposition of a hydrate based process for post combustion CO_2 capture.

2.4 CO_2 capture via hydrate formation in silica gel pores

One of the methods that have been proposed for countering this gas-water contact limitation involves increasing the gas-water contact area by contacting the gas phase with water dispersed in the pores of silica gel. Porous materials such as silica gel possess useful properties high internal surface area in a small volume, which makes them suitable candidates for achieving greater contact area between the liquid and vapour phases for rapid hydrate formation. Silica gels have been widely used for exclusion and liquid chromatography, metal scavenging and other separation processes. It is also possible to incorporate bonded phases to the surface of the silica gel to achieve increased functionality for applications such as metal scavenging. [93].

2.4.1 Silica gel properties

Silica gel is a porous, amorphous form of silica (SiO_2). Due to its unique internal structure silica gel is radically different to other SiO_2-based materials. It is composed of a vast network of interconnected microscopic pores. As opposed to zeolites, silica gels have larger pores with a wide range of diameters – typically between 5 Å and 3000 Å, which enables them to be suitable for a number of different applications. It is possible to adjust the pore size range during the manufacturing process to suit various end uses. Silica gel can be broadly categorized into two groups based on pore size.

Silica gel is extremely pure by industrial standards due to the absence of noticeable concentrations of metallic compounds like aluminium, iron or heavy metals. Therefore pure silica gel is much less active as a catalyst than other adsorbents like

zeolites or aluminas, which means unwanted reactions like cracking reactions in hydrocarbon streams and resulting coke formation can be minimized. By varying the pore size distribution, silica gels can be produced that are well suited for adsorption of liquids or gases and vapours.

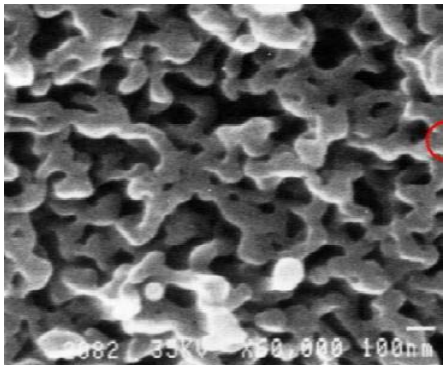

Figure 2.8 Scanning electron microscope (SEM) image of porous silica gel

There are two broad groups of silica gels – spherical silica gel and irregular silica gel, depending on the mode of production. Irregular silica gel is produced when the '*xerogel*' of polymerized silicic acid obtained during the manufacturing process is allowed to dry after which grinding is done with subsequent sieving to determine particle sizes. Spherical silica gels on the other hand are produced by spraying the neutralized silicate solution (the colloidal silica sol) into fine droplets prior to gelling, and subsequently drying the droplets with a stream of hot air.

Spherical silica gel consists of small spherical particles with diameters of a few microns, which, in turn, are made up of fused primary particles of silica a few Angstroms in diameter. These primary particles coalesced together by condensation during gel synthesis. It is on the surfaces of these primary particles that the adsorption of water takes

place. The matrix of the primary silica gel particle consists of a core of silicon atoms joined together with oxygen atoms by siloxane bonds (silicon-oxygen-silicon bonds). However on the surface of each primary particle some residual, uncondensed hydroxyl groups from the original polymeric silicic acid remain. It is these residual hydroxyl groups that confer on silica gel its polar properties and it is with these hydroxyl groups that the silane reagents react to form bonded phases as used in liquid chromatography (LC). The silica surface, however, does not simply consist of uncondensed hydroxyl groups. The silica surface can be quite complex and contain more than one type of hydroxyl group, strongly bound or 'chemically adsorbed' water and loosely bound or 'physically adsorbed' water depending on the history of the gel.

Theoretically, these hydroxyl groups can be one of three types. Firstly, it may be a single hydroxyl group that is attached to a silicon atom which has three siloxane bonds joining it to the gel matrix. Secondly it can be one of two hydroxyl groups attached to the same silicon atom which, in turn, is joined to the matrix by only two siloxane bonds. These are called Geminal hydroxyl groups. The third configuration involves one of three hydroxyl groups attached to a silicon atom which is now only joined to the silica matrix by a single siloxane bond. By using NMR techniques Sindorf and Maciel [94] have determined that the single hydroxyl group is likely to be the most prolific, and is generally assumed to be the only type present for simplicity.

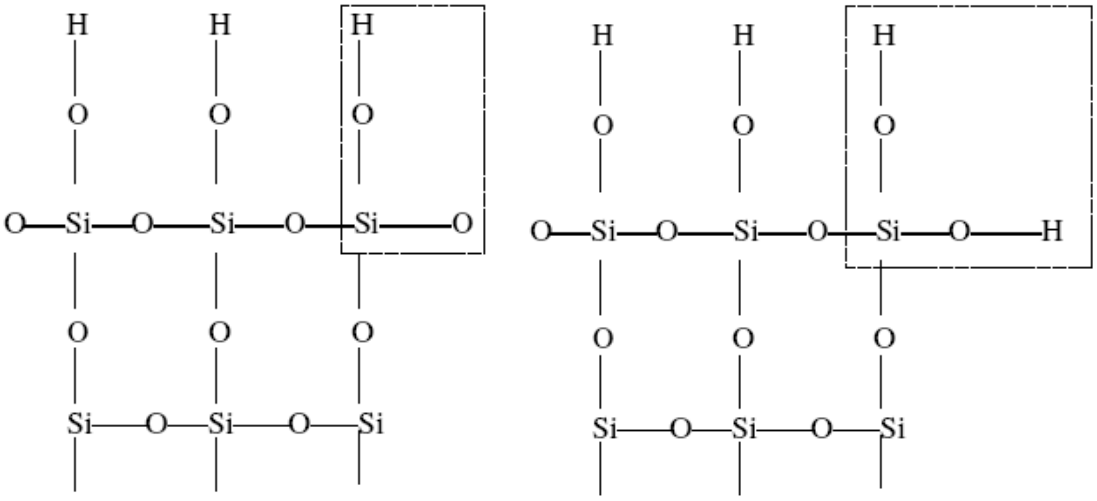

(a) (b)

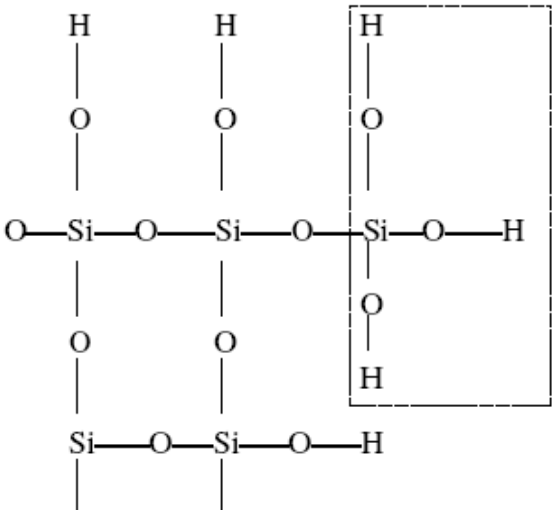

(c)

Figure 2.9 Different forms of Hydroxyl group that can occur on the surface of silica gel.

(a) The single hydroxyl group (one OH group on a single silicon atom)

(b) The double or *Geminal* hydroxyl group (two OH groups on a single silicon atom)

(c) The triple hydroxyl group (three OH groups on a single silicon atom)

2.4.2 Experimental studies for CO_2 capture

Recently, Seo et al. [30] presented hydrate phase equilibrium data for CO_2-N_2 mixtures varying from 10–50mol% CO_2 over a temperature range of 271–279 K in 30.0 nm pore size silica gel, which would be useful for designing a conceptual CO_2 capture process. 25cm^3 samples of water sorbed silica gel were used in the investigations, prepared by placing the dried silica gel in a desiccator till it became completely saturated. It is noted that C cross-polarization NMR spectral analysis and direct measurement of CO_2 content in the hydrate phase suggested that the mixed hydrate formed of more than 10mol% of CO_2 gas is structure I and the CO_2 molecules occupied mainly the more abundant $5^{12}6^2$ cages. From these measurements phase diagrams illustrating phase compositions were presented with a conceptual three-stage recovery process for CO_2 recovery included.

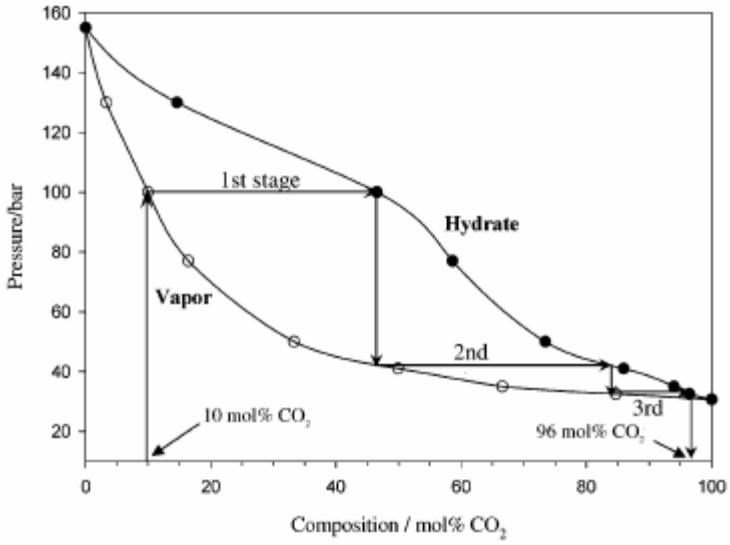

Figure 2.10 Pressure-composition diagram of the ternary N_2-CO_2-water system measured at 272.1 K

Kinetic studies with H NMR micro imaging showed that the dispersed water in the silica gel pore system reacts readily with the gas leading to increased hydrate formation rates. This rapid formation of hydrates obviates the need for a stirred type of reactor as is currently prevalent, thus making it a potential candidate for large scale CO_2 capture studies. In an test run performed to form pure CO_2 hydrates, 85% conversion to hydrate on water basis was achieved in 1 hour, with ~90% of this conversion achieved in 20 minutes. These results show that employing water dispersed in silica gel pores improves the rate of hydrate formation. Kinetic studies were not performed on CO_2-N_2 model flue gas mixtures, and it is noted that rates obtained when this mixture used may be different from those encountered in a pure CO_2 system. In addition, the process by which hydrates form in the pores is unclear, as well as any effects properties of the porous medium such as pore size, particle size and pore volume have on hydrate formation.

2.5 Motivation for research and research objectives

From the previous discussion, it is clear that devising optimal water-gas contact is essential for achieving higher rates of hydrate formation for CO_2 capture applications. A conceptual hydrate-based CO_2 process as developed by Linga et al. [29] achieves lower operating pressures without sacrificing separation efficiency by using THF as an additive, but improved contact modes are still needed to increase formation rates. Microscopic studies by Seo et al [30] indicate that dispersion of water in silica gel pores is a promising technique to achieve higher gas-water contact areas due to the high internal surface area of silica gels.

There is a need for additional investigations into the macroscopic rates and conversion levels that are obtainable in such a system. The effects of the silica gel properties such as pore size and particle size as well as operating (temperature-pressure) conditions require further study in order to determine optimal values needed to improve reaction and conversion rates. The hydrate formation kinetics of the CO_2-N_2 system in silica gel requires study, as well as mass and heat transfer characteristics of the system to give more information needed for process evaluation. The water layer next to the pore walls is generally considered as 'bound water' which does not undergo freeze transition and is unlikely to participate in hydrate formation [95]. It is therefore necessary to determine what portion of water present in the silica gels is available for hydrate formation in order to accurately measure water to hydrate conversion. Finally, the effect THF as an additive needs to be investigated with regard to reducing operating pressure

required for the process, thus lowering compression costs while maintaining separation efficiency.

Based on the foregoing, the goal of this thesis is to examine the capture of CO_2 from flue gas mixtures through hydrate formation in a silica gel column. The focus is to obtain kinetic data and study the process characteristics of a hydrate-based CO_2 capture process in silica gel pores.

More specifically, the main objectives are:

1. To study the macroscopic kinetics of hydrate formation from flue gases using water confined in the pores of a silica gel column.
2. To gain insight into the processes involved in the hydrate formation inside silica gel pores.
3. To determine process conditions required to achieve high CO_2 capture efficiency by examining
    a. silica gel properties
    b. operating temperature and pressure
4. To examine the effects of additives on hydrate formation in porous silica gel
5. To determine CO_2 separation efficiencies and conversion rates of the process

CHAPTER 3
MATERIALS AND METHODS

3.1 Apparatus

The experimental set up is designed to study the kinetics of hydrate formation/decomposition in a silica gel matrix. The main focus of the system is the hydrate reactor (HR) made of stainless steel with an internal volume of 227 cm^3 where the water-sorbed silica gel is contacted with the gas phase to form hydrates. An 8 cm length of coiled copper tubing with 0.95 cm diameter is located inside of the reactor through which circulating fluid flows in order to remove heat evolving from hydrate formation and ensure isothermal conditions. Four T-type thermocouples (Omega) are located within the reactor to monitor temperature changes during hydrate formation or decomposition at specific locations in the silica gel matrix as indicated in table 3.1. Gas is supplied to the reactor from the supply vessel (SV) connected to a gas cylinder. Both the supply vessel and the hydrate reactor are located inside the temperature controlled water bath (WB) in order to maintain the fresh gas supply at the same temperature as the reactor and maintain the isothermal state. A BROOKS 5860S/BC mass flow meter (FM1) calibrated for operation at three different inlet pressures is connected downstream of the supply vessel and upstream of the reactor to measure the quantity of gas supplied to the reactor. A pressure gauge is installed on the gas supply line to the reactor to ensure that the process is run at the desired operating pressure. A second BROOKS 5860S/BC mass flow meter (FM2) is connected downstream of the hydrate reactor to measure the quantity gas released from the hydrate during decomposition. Data from the flow meters

and thermocouples are collected by the data acquisition system on a personal computer for analysis. A sampling valve is located downstream of the reactor for collecting gas samples for analysis on a gas chromatograph. Water dispersed in the silica gel pore system reacts readily with the gas, thus obviating the need for stirring within the hydrate reactor. [30]

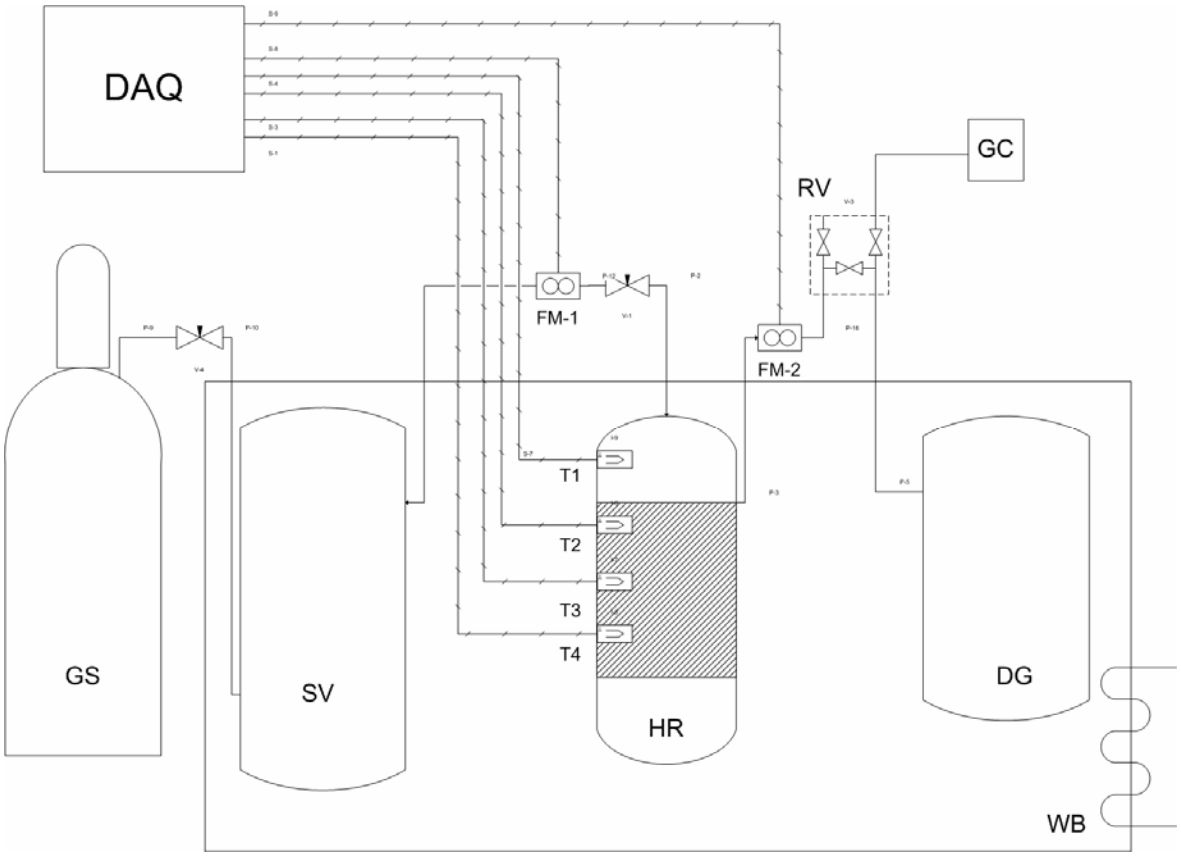

DAQ – Data Acquisition System	SV – Supply Vessel
FM – Gas Flow meter	GC – Gas Chromatograph
HR – Hydrate Reactor	DG – Decomposed Gas collection vessel
GS – Gas Supply Cylinder	WB – Temperature Controlled Water Bath
T1-T4 – Thermocouples	RV – Pressure Relief Valve

Figure 3.1 Experimental apparatus for investigating hydrate formation kinetics in a silica gel column

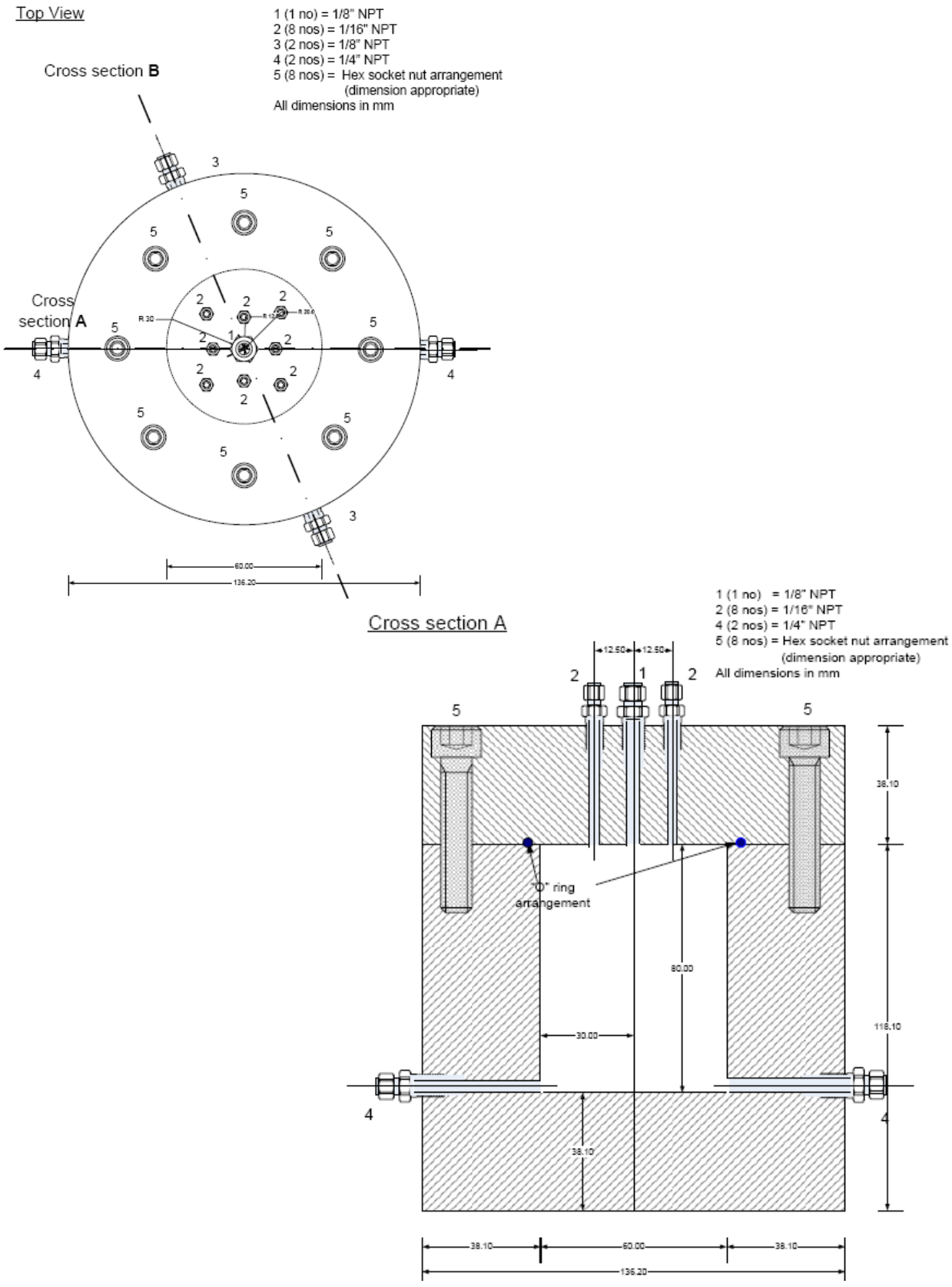

Figure 3.2 Hydrate Reactor (HR) cross section and dimensions

Table 3.1 Location of thermocouples within hydrate reactor

Thermocouple #	Location within column	Length within reactor[a] (cm)	Distance from axial center[b] (cm)
T1	Gas phase	3.2	4.0
T2	Gas-silica bed interface	5.3	2.0
T3	Within gel column	7.5	5.0
T4	Base of gel column	7.8	0.0

[a]Reactor height = 8cm. Lengths are measured from the top of the reactor

[b]Reactor radius = 6cm. Distances are measured from axial center, '0.0' indicates thermocouple is at axial center.

3.2 Materials

Three silica gel types with properties listed in table 3.2 were purchased from SiliCycle Inc. (Canada) with varying pore size, particle size distribution and surface area to study the effects of these properties on the CO_2 capture process. The gas mixtures used in the study were UHP grade and were supplied by Praxair Technology Inc. The gas compositions were chosen to represent power plant flue gas as well as the enriched product gas from the 'first stage' of a hydrate capture process. A typical conventional power plant emits a flue gas of composition 15–20% CO_2, 5– 9%O_2, and the rest N_2. Pre-treatment removes acid gases (H_2S, SO_2) and particulates. Thus, treated flue gas contains CO_2, N_2 and O_2. Since N_2 and O_2 form hydrate crystals at approximately the same conditions the treated flue gas is considered a CO_2/N_2 mixture. The dry molar (%) gas compositions of the binary gas mixtures were determined by gas chromatography and are as follows: CO_2 (17.0)/N_2 (83.0) for the model flue gas. THF used in the experimental

work was supplied by Fisher Scientific with 99% purity. Distilled and deionized water was used in all the experiments.

Table 3.2 Silica Gel Properties

Silica Gel #	Particle Size (μm)	Pore Diameter (nm)	Pore Volume (ml/g)	Surface Area (m^2/g)
1	40-75	30	0.81	100
2	40-75	100	0.81	50
3	75-200	100	0.83	50

3.3 Silica gel preparation and analysis

Silica gel analysis was performed on a Micromeritics ASAP 2010 pore size analyzer to confirm the properties of the gels as listed above. The silica gel was first dried at 373 K for 24 hours and then weighed to determine the dry weight of silica. Distilled water or THF solution equal to the pore volume of the silica gel determined during analysis was then added to the dried silica to obtain pore saturated silica gel. The gel was then placed in a Precision Durafuge® 100 centrifuge (Geneq Inc.) and spun at 3000 rpm for 3 minutes to aid the uniform dispersion of water. Visual observation and thermo-gravimetric analysis (TGA) were used to confirm that water was evenly dispersed in silica gel saturated in this manner.

3.3.1 Determination of free water content of water sorbed silica gel

The water layer next to the pore walls is generally classified as surface or 'chemically bound' water which does not undergo the usual freezing transition and is unlikely to participate in hydrate formation [95]. It is expected that the physically adsorbed water will be available for hydrate formation. Scott [93] studied water desorption from silica gels and concluded that physically adsorbed water is released from gels below 200^{o}C and water loss between 200^{o}C and 400^{o}C is due to either the loss of strongly bound water or condensation of Geminal silanol groups on the silica surface. Based on the foregoing, thermo-gravimetric analysis (TGA) will be performed on the water sorbed silica gel to determine the quantity of free water present in the gel.

A TA Instruments TGA 2050 Thermogravimetric Analyser was used to characterize the free water content of saturated silica gel. Sorbed silica gel (~10mg) is placed in the sample holder and heated from ambient conditions to 300^{o}C at a rate of 5^{o}C/min and weight loss due to water evaporation is recorded on a data acquisition system. The weight loss recorded below 200^{o}C gives the free water content of the gel.

3.3.2 Freezing point determination of water confined in silica gel pores

Water confined in silica gel pores is generally accepted to undergo freezing point depression due to reduction in water activity in the pores [95]. It has been reported in the literature that freezing point depression of water occurs within the range 0<T<-40^{o}C depending on the pore size [96]. Based on the work of Seo et al. [30] experiments will be carried out at 272.1K – below freezing point of water, thus it is important to determine

the freezing point of water adsorbed in the silica gel to confirm that gas-liquid water contact is indeed being achieved and not gas-ice contact.

A TA Instruments DSC 2920 Moulded Differential Scanning Calorimeter (DSC) with a sub-ambient liquid nitrogen cooling accessory allowing measurements to be made down to -150^{o}C was used to characterize the melting point of water in the silica gel. Sorbed silica gel (~10mg) was sealed in an aluminum pan under liquid nitrogen and placed in the DSC cell at -150°C. The sample was equilibrated at that temperature for ~10 minutes before heating to 30°C with the rate of 5°C/min. The thermal profile the sample was measured and recorded on the acquisition system, from which the melting point is determined.

3.4 Experimental Procedure

3.4.1 Hydrate Formation

The reactor is charged with ~100cm^3 of water saturated silica gel and placed in the water bath to attain thermal equilibrium at the desired temperature. Prior to commencing the kinetic experiment, two cycles of hydrate formation and decomposition are carried out. This ensured that the water in the gel matrix exhibited the 'memory' effect which is generally accepted to significantly shorten induction times [97, 98]. The reactor is then pressurized to the desired operating pressure and connected to the supply vessel as shown in the schematic. The regulator on the gas cylinder is set to the operating pressure and this serves as a constant pressure source for the system and is monitored via

the pressure gauge on the gas inlet supply line. As hydrate formation in the silica gel proceeds causing a pressure drop in the reactor, gas flows from the supply vessel through the mass flow meter (FM1) to maintain the pressure in the reactor. The flow meter accurately measures the gas uptake by the process and this can be used in subsequent material balances. Each experiment is run for a period of 4 hours after which final gas phase and hydrate phase compositions can be determined. During hydrate formation entire system is operated in a semi-batch mode under isothermal and isobaric conditions. A third kinetic experiment coupled with sampling is performed after two kinetic experiments with consistent results have been completed. 300 μL gas samples are taken at regular intervals for analysis on the GC to monitor the changes in gas composition during the reaction. Results for the two initial kinetic experiments without sampling are used in material balance calculations.

3.4.2 Operating conditions

The first task towards process development is to determine the operating temperature and the minimum hydrate formation pressure at the operating temperature for post combustion capture of CO_2 in a silica gel matrix. Seo and co workers [30] determined the equilibrium hydrate formation pressures at different temperatures for various CO_2+N_2+water mixtures in 30 nm silica gel pores as well as a pressure-composition (% CO_2) phase diagram measured at 272.1 K from which a conceptual CO_2 recovery process from hydrates was devised. Equilibrium pressure of ~7.0 MPa was reported for the 17% CO_2 83% N_2 gas model flue gas at 272.1 K.

Based on the foregoing, experiments were performed with distilled water at two operating pressures (P_{exp}) of 8.0 MPa and 9.0 MPa 17% CO_2 83% N_2 gas model at the selected operating temperature of 272.1 K with driving force of 1 MPa and 2 MPa respectively. Experiments involving THF solutions and the 17% CO_2 model flue gas were carried out at 5 MPa and 272.1 K and 274.1 K respectively to observe the effect of temperature on hydrate formation kinetics.

3.4.3 Hydrate dissociation

Dissociation is initiated by isolating the hydrate reactor (HR) from the supply vessel, then depressurizing to atmospheric pressure by opening the sampling valve and quickly closing it to allow the gas evolving from the decomposed hydrate to be collected in the decomposed gas reservoir (DG) via the outlet line from the reactor. The hydrates are allowed to dissociate completely, after which gas chromatography is used to determine the composition of the evolved gas. The composition of the evolved gas will be used to determine the feed gas into subsequent hydrate formation/dissociation stages required to achieve a 94-99% pure CO_2 stream suitable for sequestration.

3.5 Hydrate Analysis

The characterization of the solid hydrate phase is essential to determine hydrate properties prior to process scale up and to give insight into the crystal structure, crystal dimension/volume, and composition/occupancy values of the cages [97]. The hydrate samples were collected under liquid nitrogen temperature (82 K) at the end of the kinetic experiment to preserve the hydrates with the recovered hydrate samples stored in liquid

nitrogen for subsequent analysis. Raman Spectroscopy and Powder X-Ray Diffraction were applied to characterize the hydrate phase.

3.5.1 Structure Determination

Crystal structures and lattice constants were obtained from powder X-Ray Diffraction (PXRD) of the hydrate samples. The PXRD patterns were recorded at ~85K on a Rigaku Geigerflex diffractometer (λ=1.79021) in the $\theta/2\theta$ scan mode. The XRD experiments were carried out in step mode with a fixed time of 5 s and a step size of 0.05° for 2θ=5-50° with a total acquisition time of ~5 minutes for each hydrate sample.

3.5.2 Raman Spectroscopy

An Acton Raman spectrograph equipped with a 1200 grooves/mm grating and a CCD detector was used to collect Raman spectra on the hydrates. An Argon-ion laser was used as the excitation source emitting at 514.53 nm. The laser was focused on the sample using a 10cm focal length lens. The laser light was depolarized due to multiple reflections within the sample and the light scattered at 180^{o} was collected with an f/1.8 (50mm focal length) lens and focused through a polarization scrambler onto the entrance slits of an SPEX model 1403 double monochromator. The spectrograph was controlled with a computer and the spectra were recorded with a 1s integration time over 5 to 30 scans. All spectra were collected at liquid nitrogen temperature.

3.6 Gas phase analysis

An SRI 8610C (SRI Instruments) gas chromatograph (GC) with a thermal conductivity detector (TCD) and flame ionization detector was used. Ultra high purity Helium was used as carrier gas. Gas sampling was performed using a 1.8" stainless steel sample loop with internal volume of 300 μL. This small sample volume ensured that reactor conditions were not significantly altered during sampling as well as having a negligible effect on mass balance calculations. The sampling tube was flushed out three times with He before collecting a sample for analysis. Gas samples were injected into the GC via a two-port valve into a 100 μL sample loop.

3.7 Material balance calculations

In order to determine the performance characteristics of the CO_2 capture process, it is important to accurately determine the quantity of gas captured in the hydrate phase, thus necessitating setting up appropriate material balances on the system. At any given point in time, the total number of moles of gas ($n_{T,t}$) present in the system remains constant and equal to that at time zero ($n_{T,0}$). The system includes the hydrate reactor (HR), the supply vessel (SV) and the connecting tubing. The total number of moles at any given time is the sum of the number of moles (n_{SV}) in the supply vessel, the number of moles (n_G) in gas phase (G) of the crystallizer and the number of moles (n_H) consumed to form hydrate (H) or dissolved in water.

$$n_{G,0} + n_{SV,0} + n_{H,0} = n_{G,t} + n_{SV,t} + n_{H,t} \tag{3.1}$$

The number of moles of gas that have either dissolved in the water or been consumed for hydrate formation can then be calculated as follows:

$$n_{H,t} - n_{H,0} = n_{G,0} - n_{G,t} + n_{SV,0} - n_{SV,t} \tag{3.2}$$

Or

$$\Delta n_H = n_{H,t} - n_{H,0} = \left(\frac{PV}{zRT}\right)_{G,0} - \left(\frac{PV}{zRT}\right)_{G,t} + \left(\frac{PV}{zRT}\right)_{SV,0} - \left(\frac{PV}{zRT}\right)_{SV,t} \tag{3.3}$$

where z is the compressibility factor calculated by Pitzer's correlation [47].

During the kinetic experiment, the composition of the gas phase is determined by gas chromatography. At any given time by knowing the composition of the gas mixture in the crystallizer, the number of moles of the individual gas component consumed for hydrate formation can be calculated by the component mass balance:

$$\Delta n^i{}_H = n^i{}_{H,t} - n^i{}_{H,0} = \left(y^i \frac{PV}{zRT}\right)_{G,0} - \left(y^i \frac{PV}{zRT}\right)_{G,t} + \left(y^i \frac{PV}{zRT}\right)_{SV,0} - \left(y^i \frac{PV}{zRT}\right)_{SV,t} \tag{3.4}$$

$$= V_G\left[\left(y^i \frac{P}{zRT}\right)_{G,0} - \left(y^i \frac{P}{zRT}\right)_{G,t}\right] + y^i_{SV} V_G\left[\left(y^i \frac{P}{zRT}\right)_{SV,0} - \left(y^i \frac{P}{zRT}\right)_{SV,t}\right] \tag{3.5}$$

3.8 CO_2 recovery and efficiency

In addition to the information obtained from the material balance calculations, it is also desirable to assess the degree of separation obtained from the process as well the efficiency of the separation. Linga et al [84] defined two quantities for the performance of a hydrate based CO_2 capture system:

CO_2 Recovery

The CO_2 recovery or Split Fraction (Sp.Fr.) is defined as the fraction of CO_2 present in the system at the onset of the process or in the feed that is captured in the hydrate phase at the end of the experiment. It is calculated as follows

$$Sp.Fr. = \frac{n_{CO_2}^{H}}{n_{CO_2}^{Feed}} \tag{3.6}$$

where n^{Feed}_{CO2} is defined as number of moles of CO_2 in feed gas and n^{H}_{CO2} is the number of moles of CO_2 in hydrate phase at the end of the experiment.

Separation Factor

The Separation factor of the process (S.F.) is defined as the ratio of the split fraction for CO_2 to that of N_2. This quantity gives an indication as to how preferentially CO_2 is captured in the hydrate phase compared to N_2. It is calculated as follows

$$S.F. = \frac{n_{CO_2}^{H}}{n_{CO_2}^{Feed}} \times \frac{n_{N_2}^{Feed}}{n_{N_2}^{H}} \tag{3.7}$$

where n^{Feed}_{N2} is defined as number of moles of N_2 in feed gas and n^{H}_{N2} is the number of moles of N_2 in hydrate phase at the end of the experiment.

CHAPTER 4
RESULTS AND DISCUSSION

4.1 Freezing point depression and free water content of silica gel pores

The three silica gel types were subjected to DSC and TGA analysis as described in Chapter 3 in order to determine the free water content of the gel – i.e. water available for hydrate formation, as well as the freezing point of water confined in the silica gel pores to ascertain whether water exists as liquid or ice at 272.1 K in the gel. The melting point was determined from the crossing point between the baseline (horizontal) and the maximum inclination line of the endothermic reaction peak. Figure 4.1 displays the melting profile showing heat flow variation with temperature profile for the 30.0nm silica gel. Samples were cooled till liquid nitrogen temperature and then heating at a rate of 5^{o}C/min commenced. Melting was observed to begin from -5^{o}C and continued till 16^{o}C when no more exothermic heat flow was observed, yielding a melting point of -4^{o}C from the crossing point.. The results exhibit high reproducibility over multiple runs. Similar trends were observed for the 100 nm silica gels with a melting point of -2^{o}C observed. When runs were conducted with only pure water in the sample holders, the onset of melting occurred close to 0^{o}C indicating that a freezing/melting point depression is present in the gel and is consistent with literature values [95]. These results indicate that the water present in the silica gel pores exists as liquid water at the selected operating temperature of -1^{o}C and thus gas-liquid water contact will be achieved as desired.

Figure 4.2 shows the TGA weight loss variation with temperature profile for the 30 nm silica gel. In each sample prepared for TGA analysis, the silica was dried, and then weighed before and after water sorption in order to determine the quantity of water added to the gel before the onset of the analysis. Water sorbed samples contained 45$\pm$2% by weight of water and the balance silica gel. From figure 4.2 it can be clearly seen that all the sorbed water is released from the gel by ~90^{o}C, with no further water observed up to 300^{o}C. This analysis was repeated multiple times to confirm reproducibility. The final weight recorded on the instrument was in the range of 54-56% for all the runs conducted, which is within experimental error for the instrument. These results indicate that all the water added to the silica gel exists as free water and should therefore be available for hydrate formation. Based on these results it can be presumed 'bound water' was probably present with the silica gel as received, and is strongly held on the gel surface such that it is not released during the drying of the gel, and can be neglected in water conversion calculations.

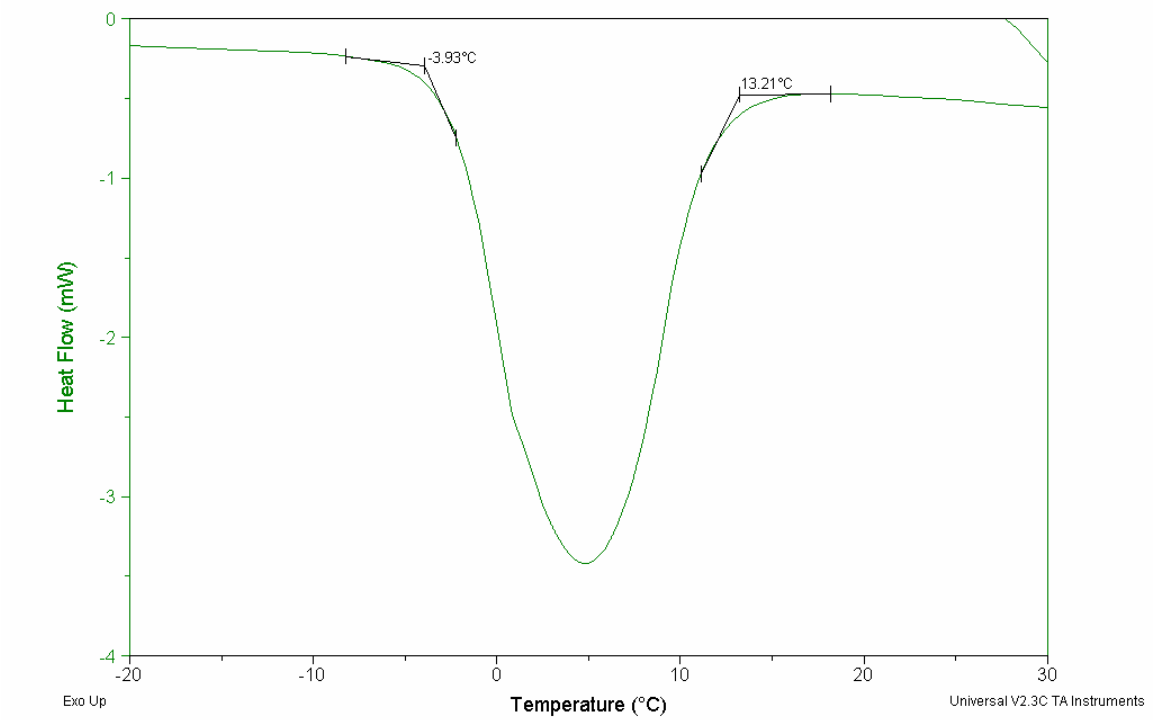

Figure 4.1 DSC spectra of water adsorbed in 30 nm pore size silica gel

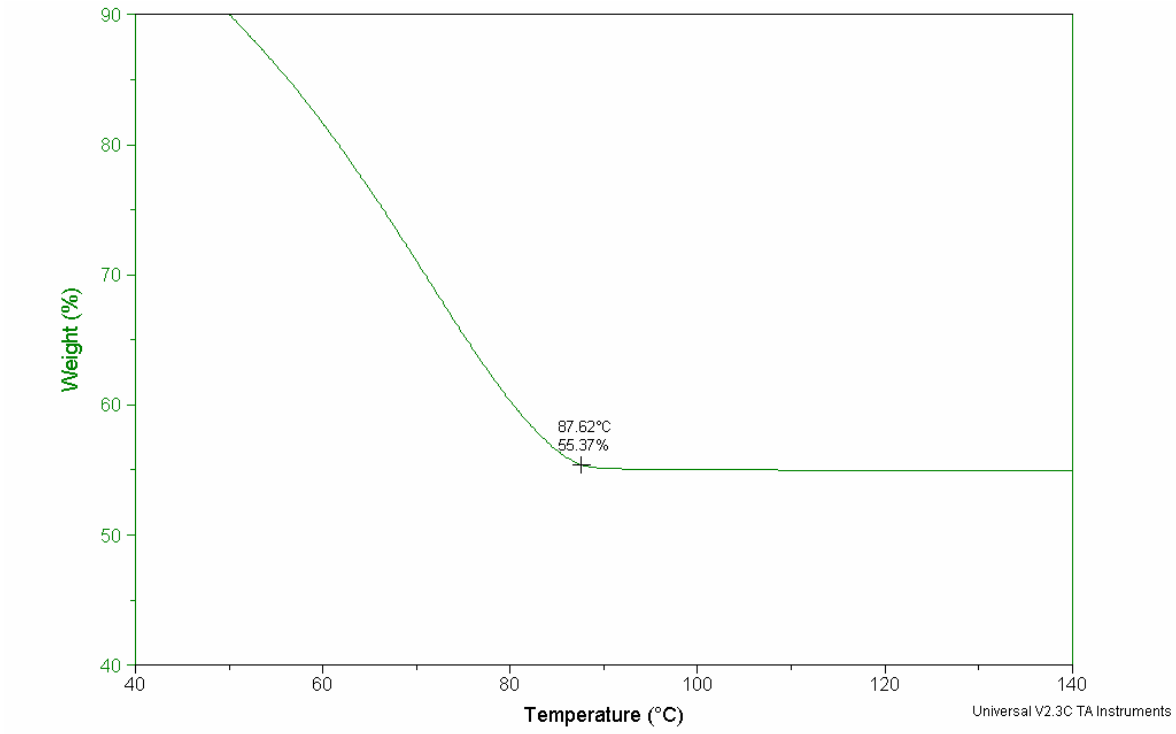

Figure 4.2 Thermo-gravimetric analysis results for water adsorbed in 30 nm silica gel

4.2 Gas uptake measurements

Figure 4.3 shows a typical gas uptake curve for a period of four hours. This curve represents the kinetics of hydrate growth for the indicated time duration. While the general shape of the curve agrees with the gas uptake curve described in detail by Bishnoi and Natarajan [99] and Lee et al. [97], the dispersed state of water in the silica gel pores likely prevents extensive agglomeration of the hydrates.

Temperature readings from thermocouples inserted in the silica gel column at different depths as described in Chapter 3 do not exhibit a distinctive temperature rise indicating hydrate nucleation; instead the trend observed is a slightly higher initial temperature, likely caused by the marginally increased temperature of the gas used to pressurize the reactor during its flow through piping and measuring instruments upstream of the reactor. Beyond this initial point all thermocouples record fluctuations in temperature over a small range as shown in figure 4.4. This indicates that due to the dispersed nature of the water, hydrate formation occurs at many different sites within the silica gel column thus there is no massive exothermic release at any single location within the column to cause a sharp rise in temperature. In addition, the presence of the internal cooling coil ensures that any exothermic energy release is quickly absorbed thus keeping the temperature profiles within the set range throughout the experiment. It should also be noted that because memory water is used in this study to simulate an actual process that would undergo many cycles of hydrate formation/decomposition, hydrate nucleation is expected to occur very quickly.

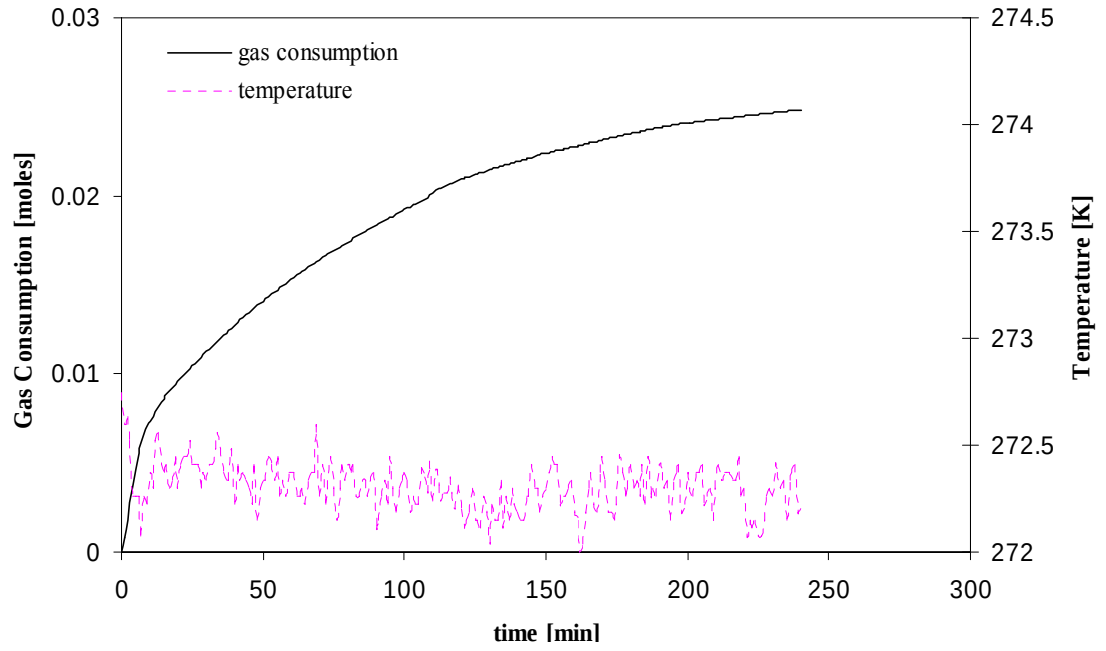

Figure 4.3 Gas uptake measurement curve for CO_2/N_2 hydrate in 30.0nm silica gel pores at 272.15 K and 8.0 MPa.

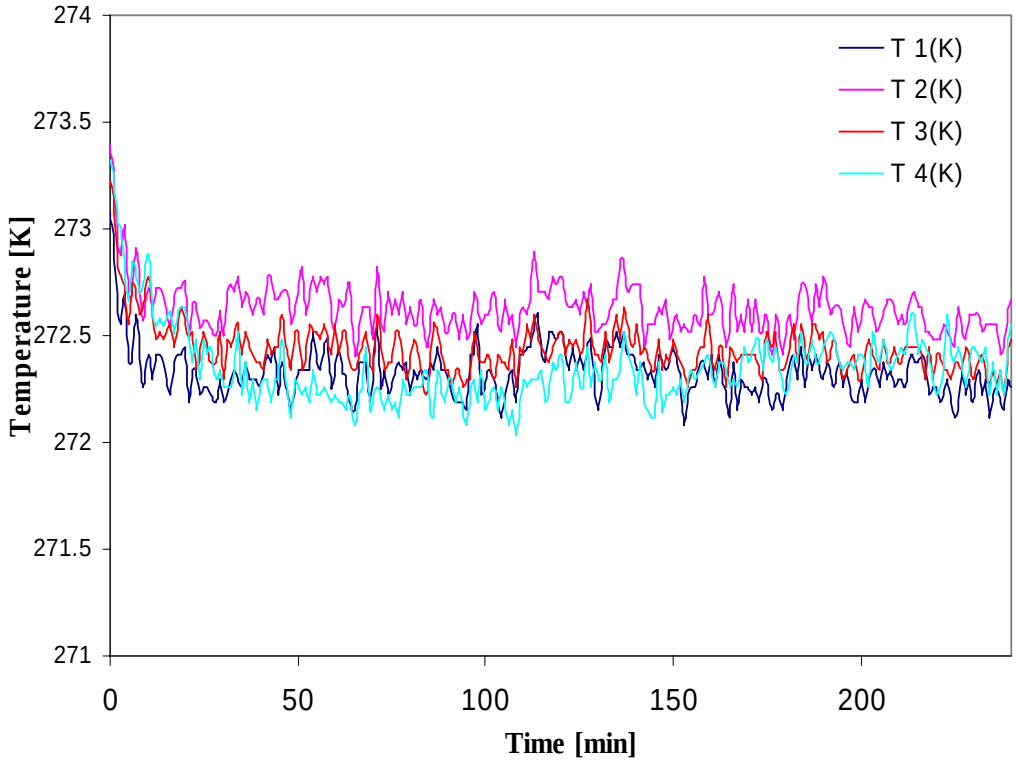

Figure 4.4 Temperature profiles for CO_2/N_2 hydrate formation in 30.0nm silica gel pores at 272.15 K and 8.0 MPa

4.3 Pore size effect on hydrate formation kinetics and CO_2 recovery efficiency

Figure 4.5 displays the gas uptake measurements for silica gel 1 and 2 at 8.0 MPa and 9.0 MPa respectively. These two silica gel types have the same particle size distribution and pore volume, but different pore diameters, in order to investigate the effect of the latter on hydrate formation kinetics. For the pore volume to remain the same for both gels, the larger pore of 100.0 nm diameter results in a lower internal surface area. The results show that remarkably higher gas consumption into the hydrate phase is obtained in the case of the 100.0 nm silica gel for both operating pressures. This indicates that though the internal surface area in the 100.0 nm gel is lower than that obtained in the 30.0 nm silica, the effect of the increased pore diameter is more favourable for increased hydrate formation as reflected by the increased gas uptake. It can also be seen that that the number of moles of gas consumed by hydrate formation increases with increasing driving force, thus making 9.0 MPa a preferable operating pressure.

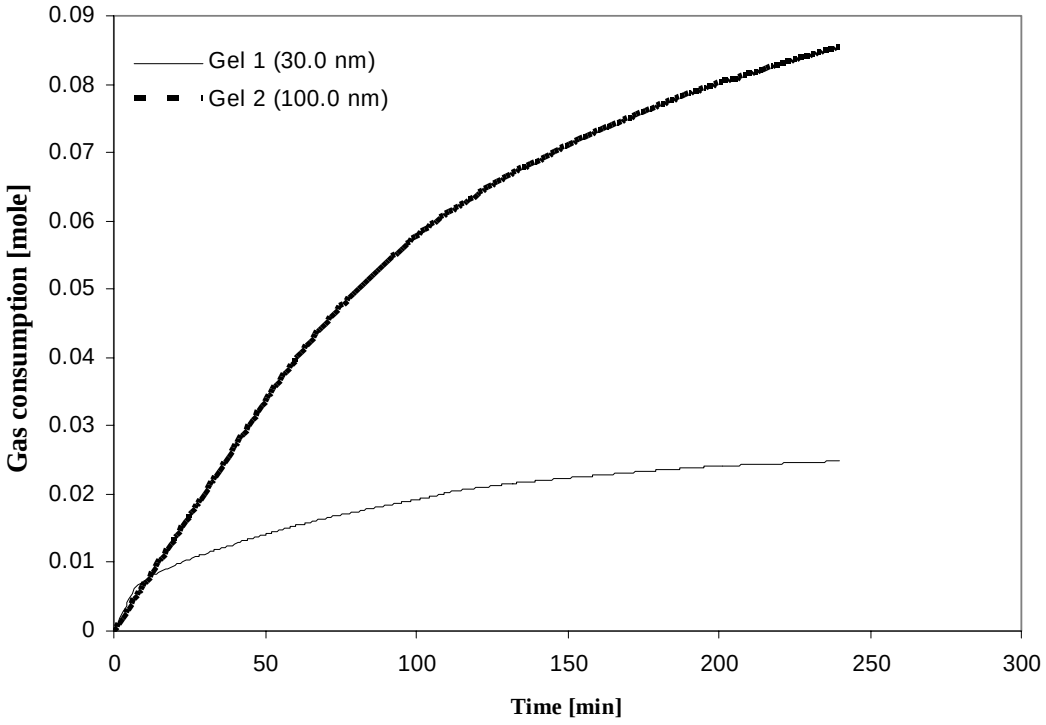

(a)

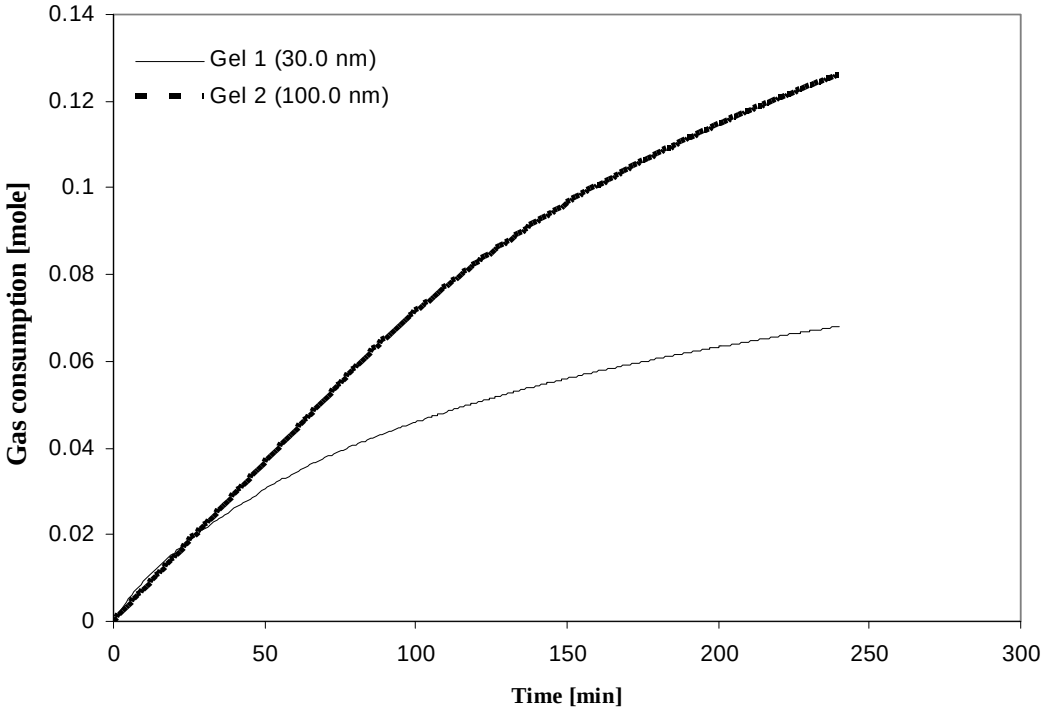

(b)

Figure 4.5 Gas uptake measurement curves for hydrate formation in 30.0 nm and 100nm silica gel pores at 272.15 K and 8.0 MPa (a) and 9.0 MPa (b).

Gas phase compositions were analysed by gas chromatography during the kinetic experiment at 30 minute intervals as shown in figure 4.6. At both pressures studied, little change is observed in CO_2 concentration over the first ~60 minutes of the reaction, likely indicating that both N_2 and CO_2 get incorporated into the hydrate at similar rates initially. As the experiment proceeds, the depletion of CO_2 in the gas phase becomes more pronounced, indicating that more CO_2 is being converted into hydrate than N_2. CO_2 concentration in the gas phase reduces from an initial value of 17% to 14.87% and 14.72% for the 8.0 and 9.0 MPa experiments respectively for the 30.0 nm gel. Gas phase composition measurements for the 100.0 nm show a similar progression as obtained in the 30.0 nm experiments. Gas phase CO_2 concentration reduces from an initial value of 17% to 11.27% and 12.02% for the 8.0 MPa and 9.0 MPa experiments respectively. These results show that a lower driving force achieves lower CO_2 concentration in the residual gas phase and is consistent with trends observed in the literature [29, 84]

At the end of the kinetic experiments, the residual gas phase analysed by gas chromatography after which the hydrates were decomposed as described in the experimental procedure. The gas released from hydrate decomposition was also analyzed by gas chromatography and the results for silica gel 1 and 2 are shown in figure 4.6 (a) and (b). At both operating pressures, the 100.0 nm silica gel achieves lower CO_2 residual gas phase content as well as increased CO_2 enrichment in the hydrate phase over the 30.0 nm gel. Hydrate phase compositions of 42.44% and 46.73% CO_2 were obtained at 8.0 MPa for gels 1 and 2 respectively, while the 9.0 MPa experiments yielded CO_2 compositions of 38.37% and 44.80% respectively. These results are in agreement with

the gas uptake measurements indicating that in addition to the increased hydrate formation obtained, the presence of a larger pore size also improves the preferential inclusion of CO_2 in the hydrate phase.

Rate of hydrate formation, R_f, was calculated for the 30.0 and 100.0 nm silica gels, based on the gas consumption during the first 20 minutes of hydrate formation. Since induction is expected to occur quickly, no induction point is determined from the data thus hydrate formation is viewed as beginning at time t=0. Initial hydrate formation rates of 0.00047 and 0.00066 mol/min were obtained at 8.0 MPa for the 30.0nm and 100.0 nm gels respectively, indicating an increased rate of hydrate formation in the larger pore size. However at 9.0 MPa the initial rates obtained were 0.00071 and 0.00073 mol/min for gel 1 and 2, which indicates that though initial rates may be similar, there is a limiting effect observed in the 30.0 nm gel that results in the lower final gas consumption value compared to the 100.0 nm gel.

Material balance calculations as previously described were used to calculate CO_2 recovery or split fraction (Sp.Fr.) and separation factor (S.F.) for gel 1 and 2 as shown in Table 4.1. The CO_2 recovery calculated for the 8.0 MPa experiments were higher than those obtained for the 9.0 MPa experiments in both cases, agreeing with the observations of Linga et al. [84] that a higher driving force reduces CO_2 inclusion in the hydrate phase. This is explained by the higher equilibrium formation pressure for pure N_2 compared to CO_2, indicating that at a higher pressure, the N_2 molecules compete more with CO_2 for cage occupancy thus lowering the CO_2 in the hydrate. As with the gas consumption and phase analysis results, the 100.0 nm gel also outperforms the 30.0 nm gel in CO_2 recovery, with a value 41% of CO_2 recovered for the 100.0 nm gel compared to 21% for the 30.0 nm gel.

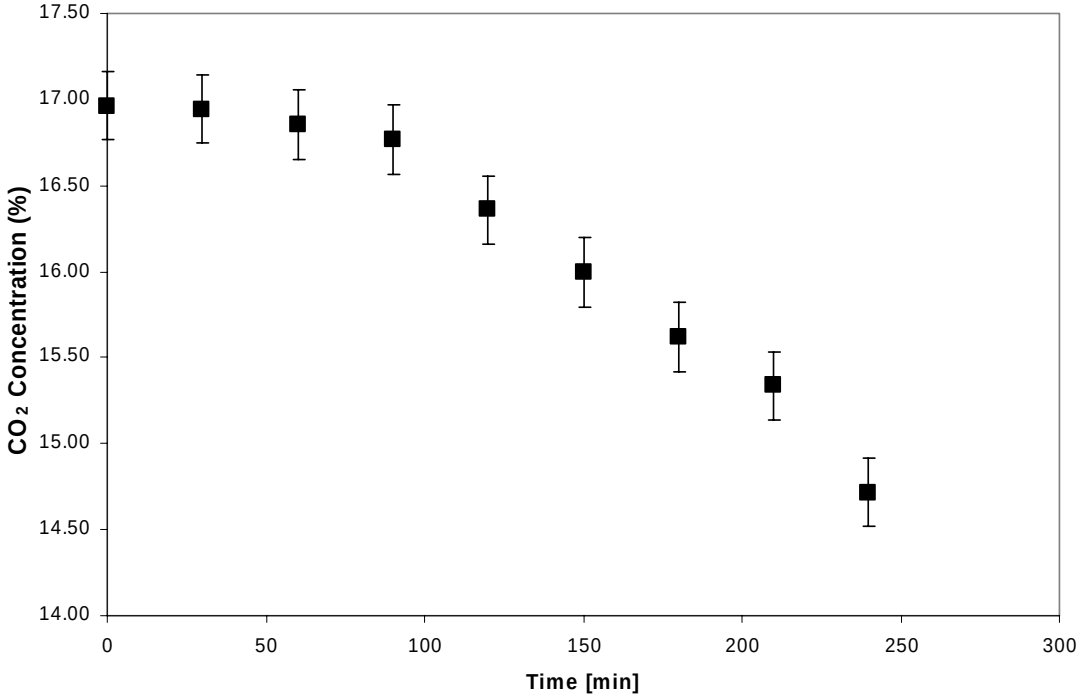

(a)

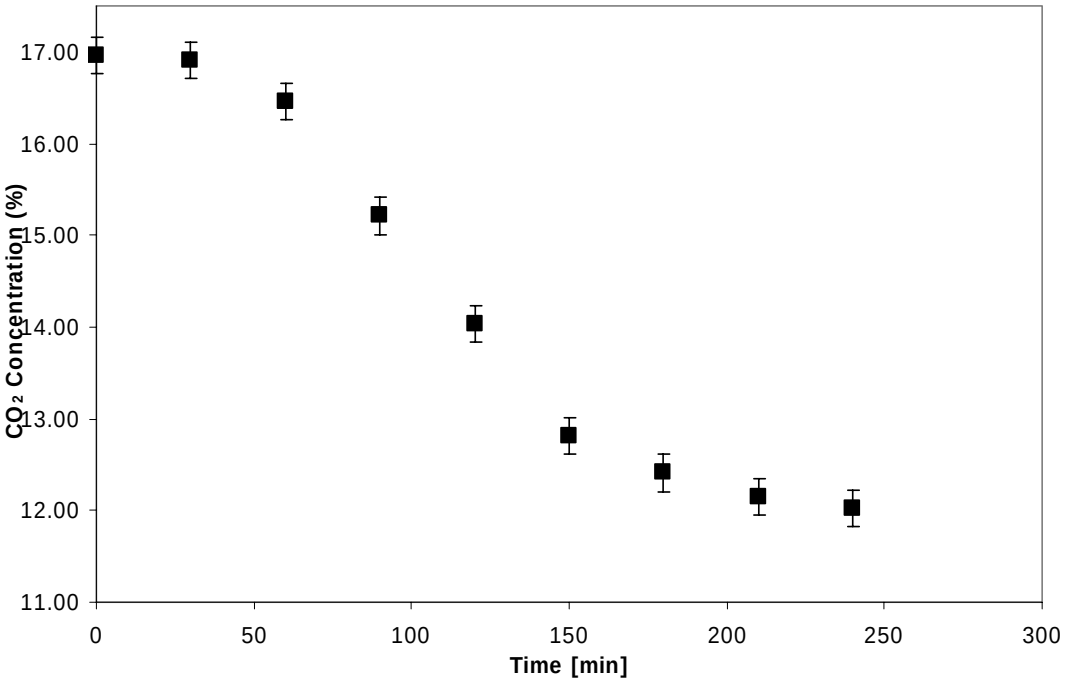

(b)

Figure 4.6 Gas phase CO_2 measurements during hydrate formation at 272.15 K and 9.0 MPa in 30.0 nm (a) and 100.0 nm (b) silica gel.

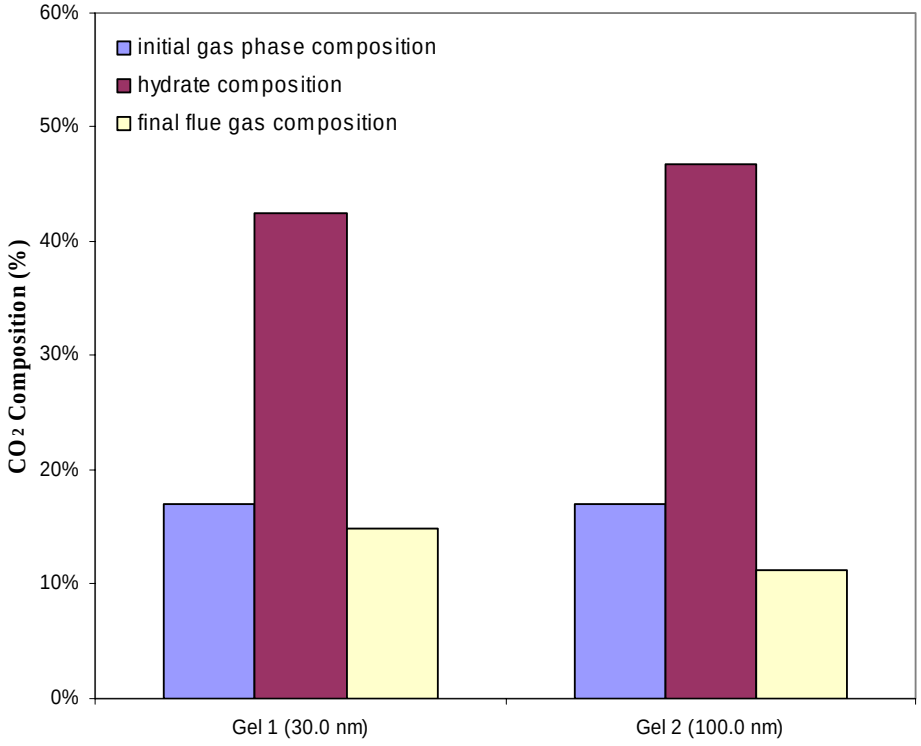

(a)

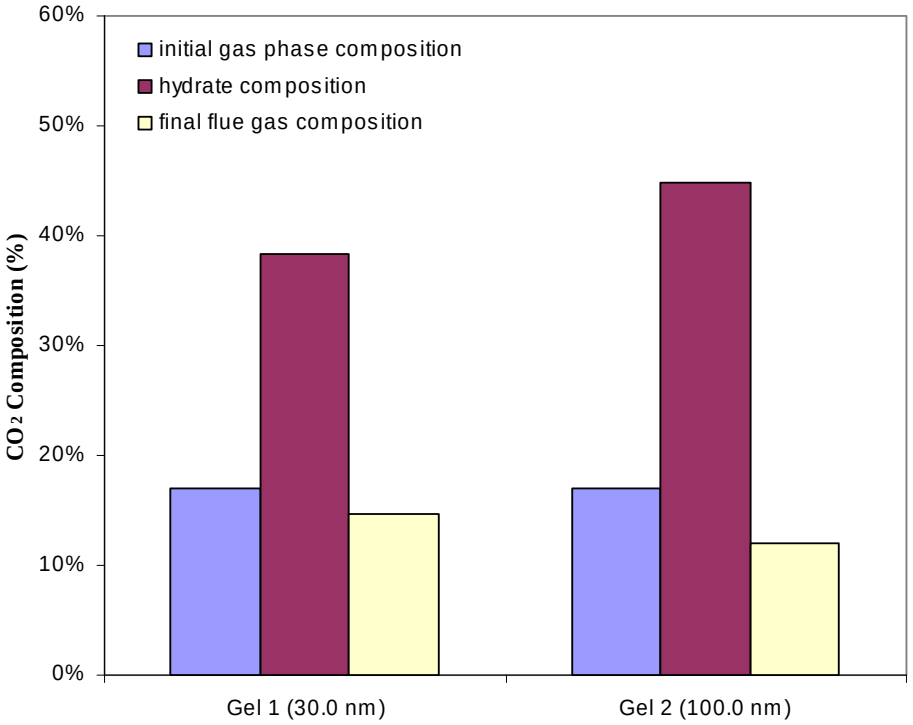

(b)

Figure 4.7 CO_2 content in the gas phase (initial composition), hydrate phase and residual gas phase (final composition) for CO_2/N_2 hydrate formation at 272.15 K and 8.0 MPa (a) and 9.0 MPa (b).

Table 4.1 CO_2 Recovery, Separation Factor and Hydrate Formation Rates for gel 1 and 2

	30.0 nm (40-75 μm)		100.0 nm (40-75 μm)	
	8.0 MPa	9.0 MPa	8.0 MPa	9.0 MPa
Split Fraction	0.16	0.21	0.42	0.41
Separation Factor	8.42	3.20	5.82	3.69
R_f^a *(mol/min)*	0.00047	0.00071	0.00066	0.00073

[a]Rate of hydrate growth (gas consumption rate for first 20 min)

The results from kinetic experiments on silica gel 1 and 2 show marked increases in gas uptake and final hydrate phase composition in the 100.0 nm gel compared to the 30.0 nm gel. The two silica gels have identical particle size distributions and pore volume, and were saturated with the same quantity of water. This indicates that the difference is between the two gels occurring as a result of the pore size difference between the gels. Though the process of hydrate formation in porous media like silica gel is not clearly understood, Seo et al. [30] postulated that CO_2 molecules are transported from the gas phase and are able to diffuse into the pores to participate in the formation of hydrate. Diffusion rates of gases through porous materials can be significantly lower than through air, and would depend on the properties of the medium such as porosity, pore sizes and pore connections [100]. Mu et al [101] describe diffusion of gases in porous materials mathematically by Fick's law. Considering the mass flux per unit volume ($gcm^{-1}s^{-1}$) in across a single pore as

$$m_{i,j} = D_{ij}(\rho_i - \rho_j) \tag{4.1}$$

where D_{ij} is the effective diffusion coefficient in cm^2s^{-1} of the pore connecting site i and site j, ρ_i and ρ_j are gas concentrations in g/cm^3 at site i and j respectively. The

diffusion coefficient essentially governs the rate at which gas diffuses from one site to the other, and this rate is usually expressed in the form diffusivity - ratio of the effective diffusion coefficient through the porous medium to the diffusion coefficient in ambient air. In mathematical terms the effective diffusion coefficient can be related to the corresponding coefficient through air by the porosity. By making simplified limiting case assumptions, such as no diffusion taking place through the solid portions of the porous material, the cross section area available for diffusion would be the average area of the pore space, that is εA, where A is the total area of the cross section [101]. The resulting expression is:

$$\frac{D_{eff}}{D_b} \equiv \varepsilon \tag{4.2}$$

where

D_{eff} = effective diffusion coefficient of the gas in the porous medium

D_b = bulk diffusion coefficient of the gas through air

ε = porosity of porous medium

Given this relationship between diffusivity and porosity, it is evident that the size of pores present in a porous material will have an effect on diffusion rates of gases within the material. Simulation studies on a 3-D bond pore network model were presented by Mu et al [101] to evaluate pore size effects on effective diffusion coefficient. Their results indicate that the diffusivity increases with mean pore diameter when the pore size < 1 μm as a result of the Knudsen effect, with a very strong dependence of effective diffusivity on pore size.

To estimate the pore size effect, D_{ij} in equation (4.2) was defined by Mu et al [101] as

$$\frac{1}{D_{ij}} = \frac{1}{D_b} + \frac{1}{D_k} \tag{4.3}$$

where $D_{i,j}$ is bulk diffusion coefficient in a single cylindrical pore, D_b is the bulk diffusion coefficient, and D_k is the Knudsen diffusion coefficient given by

$$D_k \approx 48.5 d_p \sqrt{\frac{T}{M}} \tag{4.4}$$

where d_p is the pore diameter, T is temperature and M is the molecular weight of the gas.

The equations as stated above describe the case of a gas diffusing through air as the bulk medium, but this study involves gas diffusion through water; assuming Knudsen diffusion is also important in water, pore size effect similar to that observed with in air can be expected while bulk diffusion coefficient D_b would be determined accordingly for water as the bulk medium. The pore sizes used in this current study lie within the stated < 1 μm range of pore size effects determined by Mu et al [8], thus it can be inferred from these results that the increased hydrate formation observed in the 100nm gel is likely as result of increased diffusion rates in the larger pore compared to the 30nm gel. As a result it will be favourable to carry out hydrate formation for CO_2 capture with the larger pore size gel.

4.4 Particle size effect on hydrate formation kinetics and CO_2 recovery efficiency

In light of the observed effects of pore size on hydrate formation kinetics and separation efficiency, further insight is needed into the effect of other silica gel properties such as particle size on the CO_2 capture process. Porosity of a porous material such as silica gel is a combination of the internal pore spaces, as well as the inter-particle spaces between individual silica gel spheres. Thus in order to investigate the effect variation in the inter-particle spaces on the kinetics and separation efficiency of hydrate formation, a third silica gel was studied. This silica gel has a 100.0 nm pore size, the same pore volume as the two gels previously studied (0.83ml/g) and a larger particle size distribution of 75 – 200 μm compared to the 45 – 75 μm used for gel 1 and 2. The effects of this property on the CO_2 capture process can thus be evaluated.

Gas uptake measurements for gels 2 and 3 are displayed in Figure 4.9. The figures show that the gas consumption values for hydrate formation as measured by the flow meters for both gels are quite similar, with a 2% difference in the number of moles at 8.0 MPa and 10% difference for the 9.0 MPa experiments. The initial hydrate formation rate, R_f, was calculated for the two experiments with values of 0.00066 and 0.00064 mol/min obtained at 8.0 MPa for gel 2 and 3 respectively, while a rate of 0.00073 mol/min was observed at 9.0 MPa in both cases. The experiments with the 75-200 μm gel in both cases show the larger consumption values, though the 2% difference obtained for the 8.0 MPa experiments can be said to be statistically insignificant. A larger increase in gas consumption for the larger particle size is observed in the 9.0 MPa experiments, but the other measures of process performance need to be evaluated to give further insight into the differences in the two experiments.

Gas composition measurements were taken during the kinetic experiment on gel 3 as previously described for gels 1 and 2, with a final CO_2 concentration of 10.20% and 10.83% for the 8.0 MPa and 9.0 MPa respectively. These values are less than 11.27% and 12.02% obtained under the same experimental conditions for gel 2 (100.0nm 40-75 μm). This indicates that though the gas consumption values from the flow meter readings are nearly equal, there is slightly higher CO_2 depletion in the 75-200 μm particle size gel. This is confirmed by the higher CO_2 hydrate composition obtained for the latter – 47.96% and 45.51% at 8.0 MPa and 9.0 MPa compared to 46.73% and 44.80% for the 40-75 μm gel.

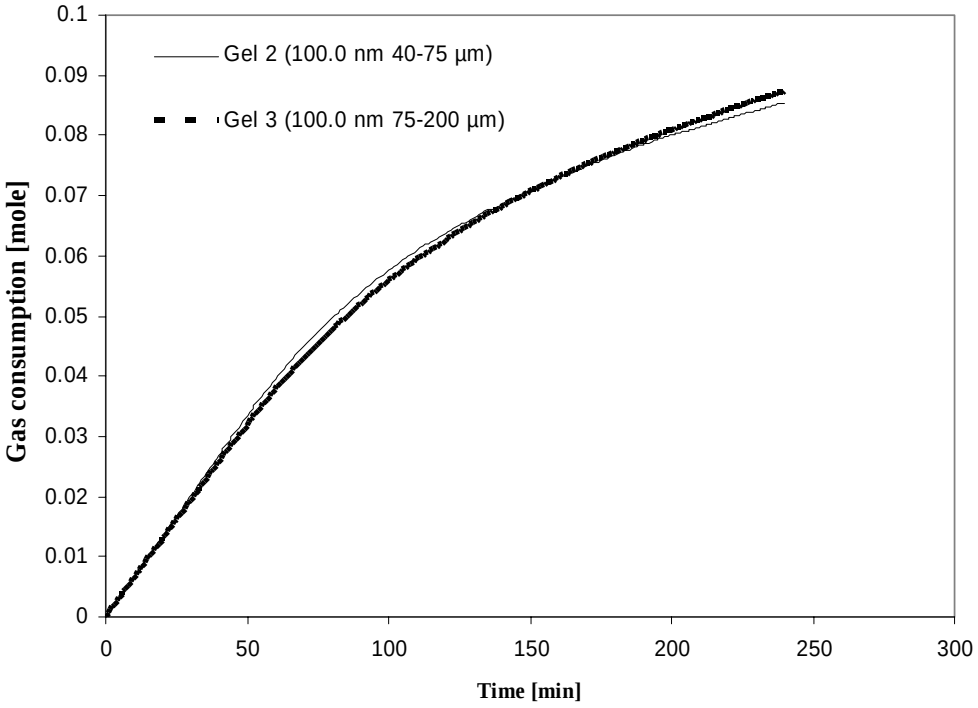

(a)

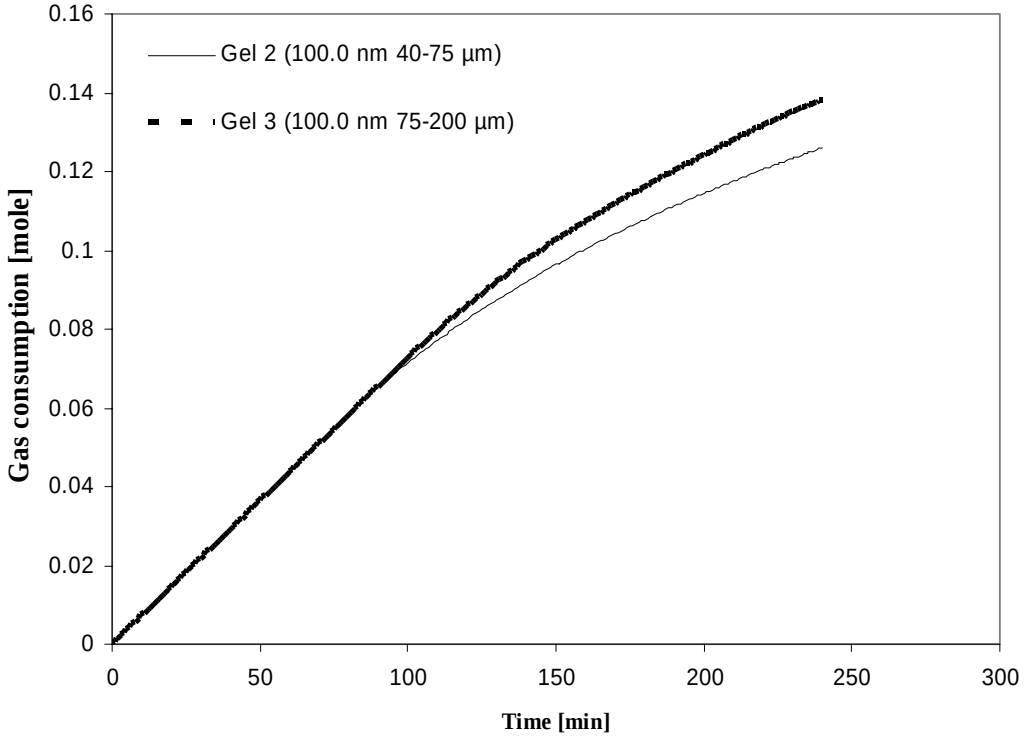

(b)

Figure 4.8 Gas uptake measurement curves for hydrate formation in two 100.0 nm silica gels with varying particle size at 272.15 K and 8.0 MPa (a) and 9.0 MPa (b).

Mass balance calculations for the three gels showing the split fraction/CO_2 recovery and separation factor results are displayed in Table 4.2. It can be seen from the figures that the 75-200 μm gel achieves higher CO_2 capture as shown by the split fraction results, with 51% of the CO_2 captured in the hydrate phase compared with 41% for the 40-75 μm gel at 9.0 MPa. This is in agreement with the earlier observations in phase measurements and gas uptake calculations. These results indicate that internal pore space is the dominant contributor to bed porosity with inter-particle spaces playing a lesser role.

It can thus be concluded that increased pore size achieves a large improvement on hydrate formation kinetics and CO_2 recovery from 30.0 to 100.0 nm. Increased particle size also produces some improvement in process performance as increased from 40-75 to the 75-200 range, albeit to a lesser extent.

Table 4.2 CO_2 Recovery, Separation Factor and Hydrate Formation Rates for gel 1, 2 and 3

	30nm (40-75 μm)		100nm (40-75 μm)		100nm (75-200 μm)	
	8.0 MPa	9.0 MPa	8.0 MPa	9.0 MPa	8.0 MPa	9.0 MPa
Split Fraction	0.16	0.21	0.42	0.41	0.45	0.51
Separation Factor	8.42	3.20	5.82	3.69	9.86	8.22
R_f^a *(mol/min)*	0.00047	0.00071	0.00066	0.00073	0.00064	0.00073

[a]Rate of hydrate growth (gas consumption rate for first 20 min)

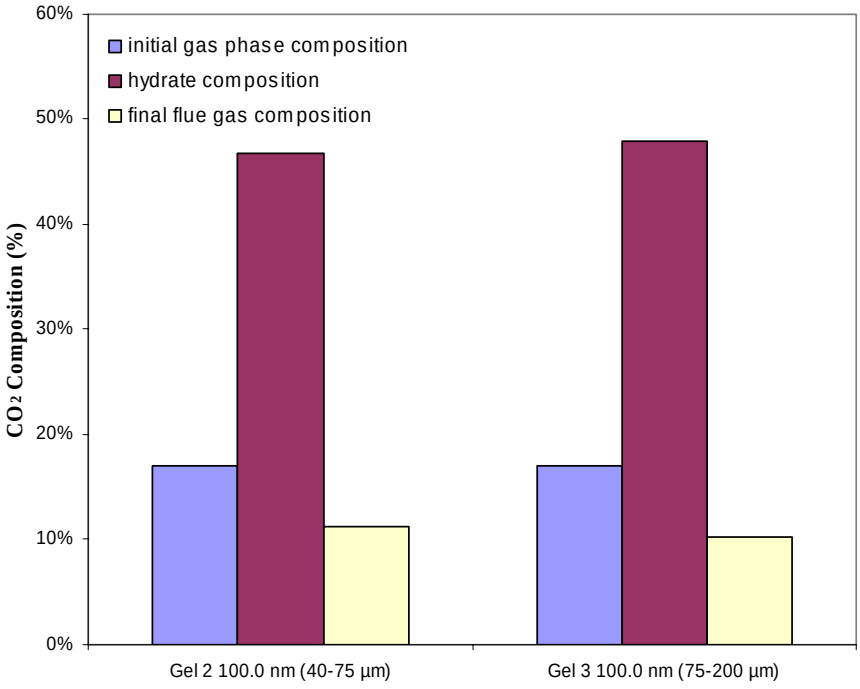

(a)

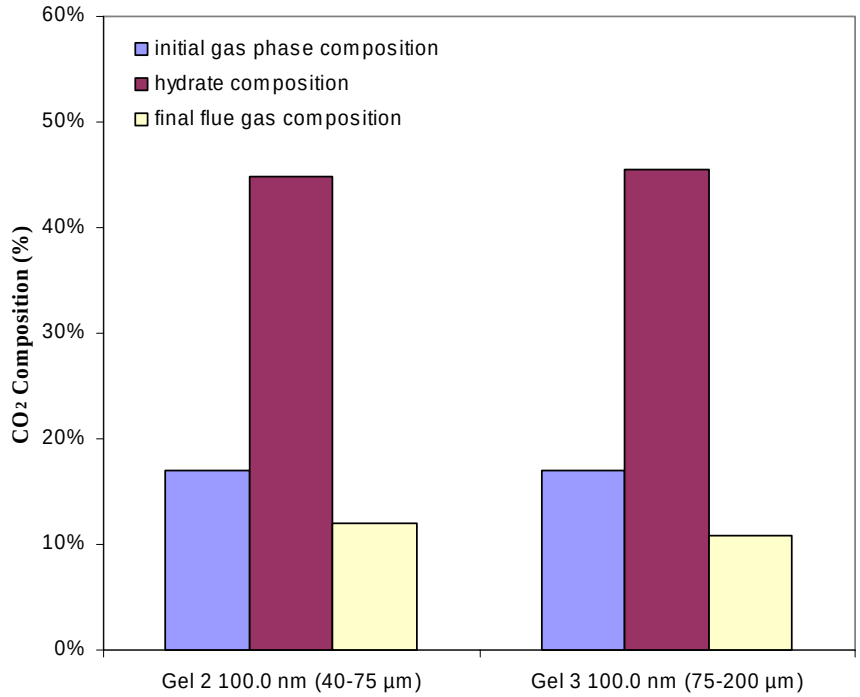

(b)

Figure 4.9 CO_2 content in the gas phase (initial composition), hydrate phase and residual gas phase (final composition) for CO_2/N_2 hydrate formation at 272.15 K and 8.0 MPa (a) and 9.0 MPa (b).

4.5 PXRD and Raman Analysis

Hydrate samples synthesized in each of the three silica gels were analyzed by PXRD first to confirm the presence of hydrate and to verify the crystal structure. A typical PXRD pattern of sI hydrate is shown in Figure 4.10. The pattern for hydrates formed from 17% CO_2/N_2/Water in silica gel was fitted to a standard sI hydrate. These structural results obtained for the hydrate samples are in agreement with results in the literature [51] indicating that the confined nature of these hydrates does not alter the crystal structure of the hydrates. Thus the hydrates confined in the silica pores can be considered to possess the same properties as bulk hydrate samples.

Hydrates formed from CO_2/N_2/THF/Water in silica gel were also analyzed by PXRD. The hydrates formed in this case were of sII crystal structure, as shown in Figure 4.10 below. THF forms sII hydrate as a single guest, with the CO_2/N_2/THF system reported to form sII as well. The presence of THF in the large $5^{12}6^4$ cages likely reduces the available cavities for CO_2 in the hydrate phase, and this leads lower CO_2 concentration in the decomposed gas from the hydrate compared to the previous results with no THF present.

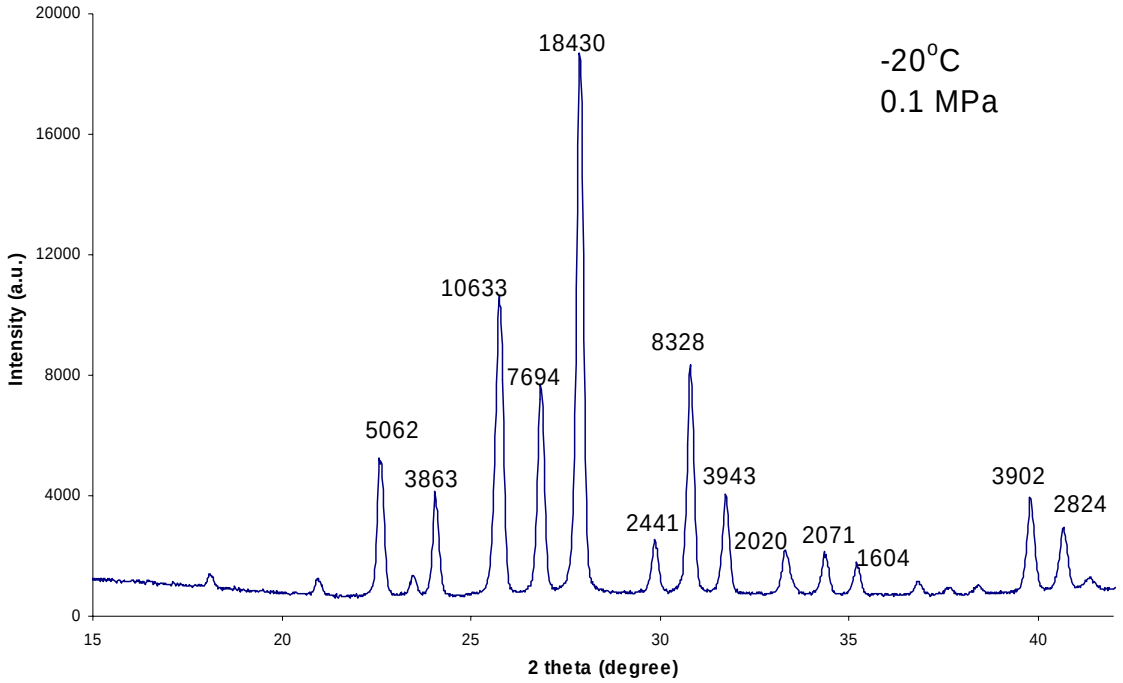

Figure 4.10 PXRD Pattern of CO_2/N_2/Water hydrate in 30.0nm silica gel forming sI hydrate

Hydrate samples were also analyzed with Raman spectroscopy to confirm the presence of hydrates in the three silica gel types. Distinct peaks from the symmetric stretching vibration bonds for CO_2 and N_2 molecules in the clathrate were obtained from the Raman spectra as shown in Figure 4.11. N_2 in hydrate produced a strong single peak of 2324.8 cm^{-1} while CO_2 yielded the combined Fermi diad peaks of 1279.53cm^{-1} and 1382.22cm^{-1}. Raman shift values obtained are in agreement with the results of Murphy and Roberts [102].

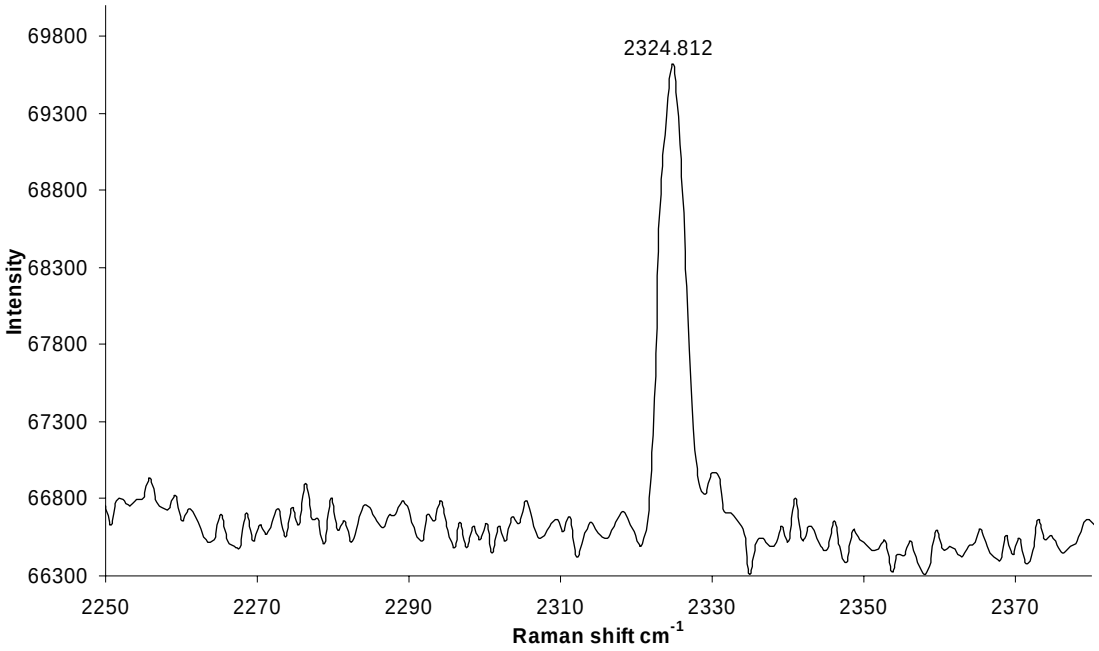

(a) Nitrogen

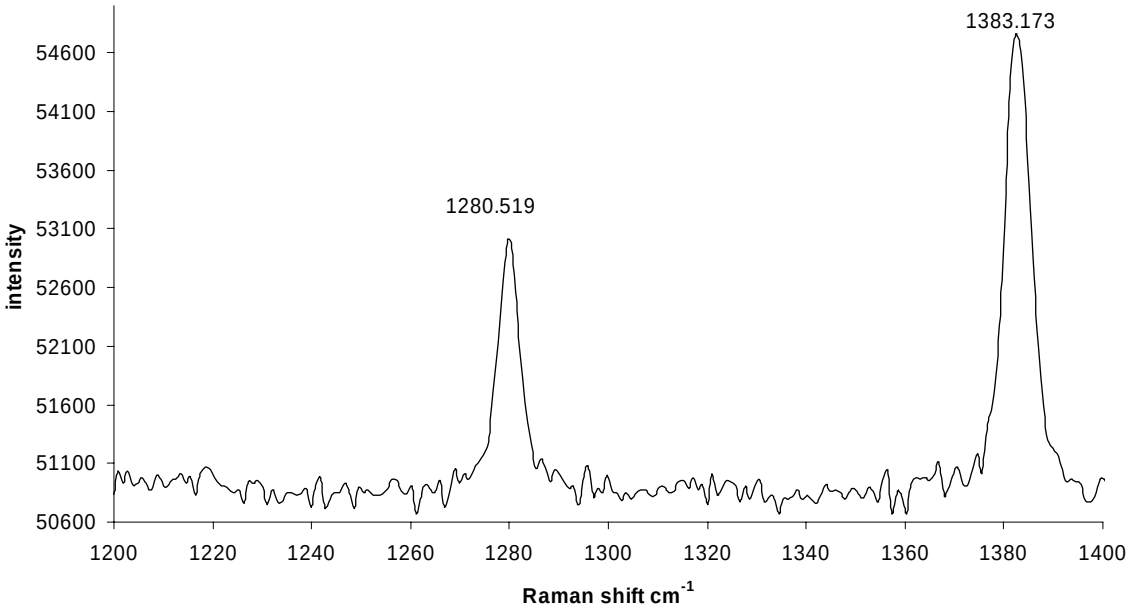

(b) Carbon dioxide

Figure 4.11 Raman spectra of 17% CO_2/N_2/1.0 mol% THF (sI) hydrate in 100.0 nm silica gel

4.6 CO_2/N_2/THF hydrate formation in silica gel pores

The results obtained so far have shown that high operating pressure remains a drawback of a hydrate-based CO_2 capture process as mentioned in previous studies [29, 84]. It is thus desirable to evaluate the CO_2 capture performance of hydrate formation in silica gel in the presence of THF as a pressure reducing additive. Kinetic experiments were carried out with a 17% CO_2/N_2 gas mixture with 1mol% THF solution in water, which is the optimal concentration determined by Linga et al [29] for hydrate formation. Based on the previous results, the experiments were performed with the 100.0 nm, 75-200 μm gel which gave optimum performance among the three gel types studied. The experiment was performed at 272.15 K and 5.0 MPa which is 4.0 MPa lower than the maximum operating pressure studied for the experiments without THF. This pressure was selected after a number of trials in order to achieve an appreciable rate of hydrate formation and CO_2 fractionation in the hydrate phase. The gas uptake measurements are shown in Figure 4.12 for the THF kinetic experiment, and it can be clearly seen that gas consumption tapers off at ~80 minutes with marginal incremental consumption observed beyond this point, compared to the experiment at 8.0 MPa where the gas consumption curve is still on an upward trend after 240 minutes. Initial rate of hydrate formation, R_f, calculated for the experiment with 1mol% THF 0.00087 mol/min. This initial rate is higher than the highest initial rate of 0.00073 mol/min observed in gel 3 without THF, indicating that the presence of THF improves initial rates of hydrate formation but reduces the total gas consumption. The decrease in gas consumption can be attributed to the presence of THF in the large cages of sII hydrate formed, thus reducing the available cavities for CO_2 and N_2.

Hydrate phase and residual gas phase analyses were performed for the THF kinetic experiment as shown in Figure 4.13. Gas phase CO_2 concentration reduced from 17% to 14.72%, while the evolved gas from hydrate composition contained 28.57% CO_2

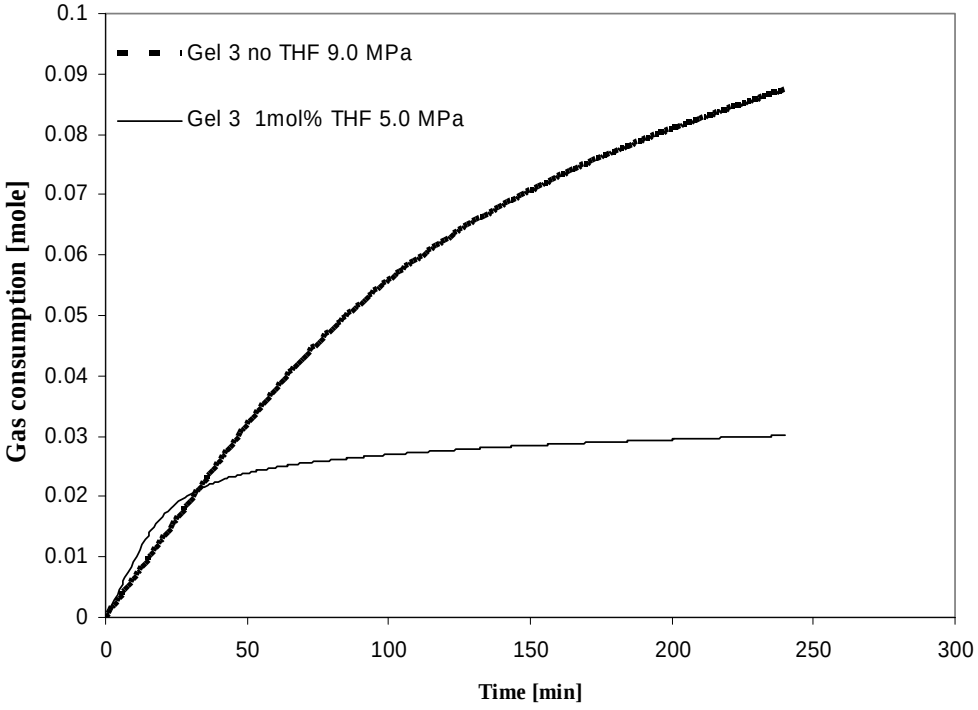

Figure 4.12 Gas uptake curves for CO_2/N_2 and CO_2/N_2/THF hydrate formation in 100.0 nm, 75-200 μm silica gel.

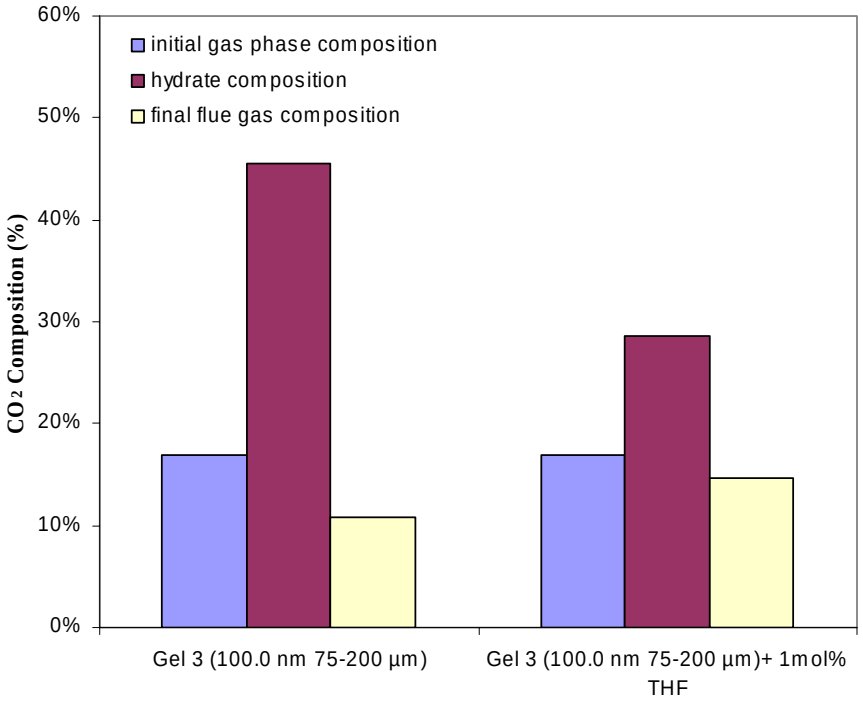

Figure 4.13 Comparison of CO_2 phase compositions from hydrate formation in THF solution and pure water systems.

4.7 Comparison between hydrate formation kinetics in bulk water systems and water dispersed in silica gel pores

One of the primary aims of utilising water dispersed in silica gel pores for hydrate formation is to investigate improvements in kinetics or conversion compared with bulk water systems. It is therefore necessary to compare the results obtained in this current study with bulk water experiments to ascertain any differences between the two systems. Linga et al. [84] reported CO_2 split fraction of 0.42 for hydrate formation with 16.9% CO2/N2 mixture at 0.6^{o}C and 10.0 MPa. The best case results in this study for silica gel 3 (100.0 nm 75-200 μm) give a split fraction of 0.51 at -1^{o}C and 9.0 MPa. In terms of hydrate phase and residual gas phase compositions, Linga et al. [84] report 57% and 9.7% CO_2 respectively at the aforementioned conditions, while results in this study on silica gel 3 give 45.51% and 10.83% CO_2 respectively.

These results indicate the bulk water system achieves a higher CO_2 concentration in the hydrate phase and a lower residual gas phase concentration, while higher CO_2 recovery is observed in the present study. It should be noted, however, that the bulk water experiments were carried out for 120 minutes while experiments in the current study were run for 240 minutes. The longer duration in the current study was used because significant gas consumption was still observed after 120 minutes; the experiments were not terminated till 240 minutes when hydrate formation as reflected by gas consumption had significantly reduced. In addition to this, the experimental pressure and temperature are not identical, but similar and this likely affects the results obtained.

A further important difference to note between the two studies is in the quantity of water charged to the system for hydrate formation. The Linga et al. [28, 84] studies use 140 ml of water, while 35 ml of water was used in this study. Thus in order to make a valid comparison in the gas uptake data, the variation of gas consumption/mole of water with time was determined from the previous study [28] and compared to this present work as displayed in Figure 4.14. It can clearly be seen that a far greater gas consumption/mole of water is recorded in the silica gel experiment compared to the bulk water system. While gas uptake from the bulk system has levelled off by 120 minutes, the rate of gas consumption is still sustained in the silica gel experiment. This confirms that dispersing water in silica gel pores increases the amount of hydrate formed dramatically over that obtained in a bulk water system. Thus it is highly beneficial to carry out CO_2 capture via hydrate formation with water confined in silica gel pores.

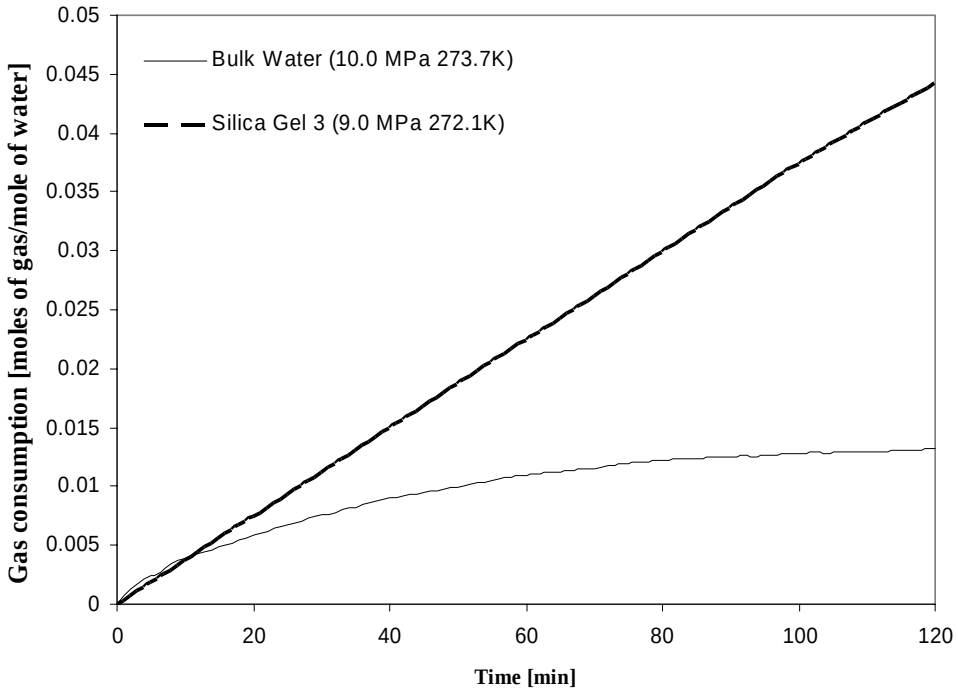

Figure 4.14 Comparison between gas uptake data of bulk water systems with pore confined water in silica gel for hydrate formation from 17% CO_2/N_2 mixture.

Figure 4.15 displays results in silica gel 3 compared with bulk water in a stirred reactor [28] with 1mol% THF used in both cases. This data is depicted in moles of gas consumed/mole of water. It should be noted that the experimental conditions for the two experiments differ: 2.6 MPa and 0.6^{o}C for the stirred reactor case and 5.0 MPa and -1^{o}C for the silica gel experiment. Increased gas consumption per mole of water is observed in the silica gel case over the bulk water experiment. A residual gas phase CO_2 concentration of 14.72% was obtained for the silica gel experiment, while the experiment in the bulk system yielded 11.23%. Hydrate phase analysis showed 28.57% CO_2 in the hydrate for the silica gel case and 37.21% CO_2 in the bulk water system. The bulk water experiment also yielded higher CO_2 recovery of 0.46 compared to 0.19 obtained in the current study.

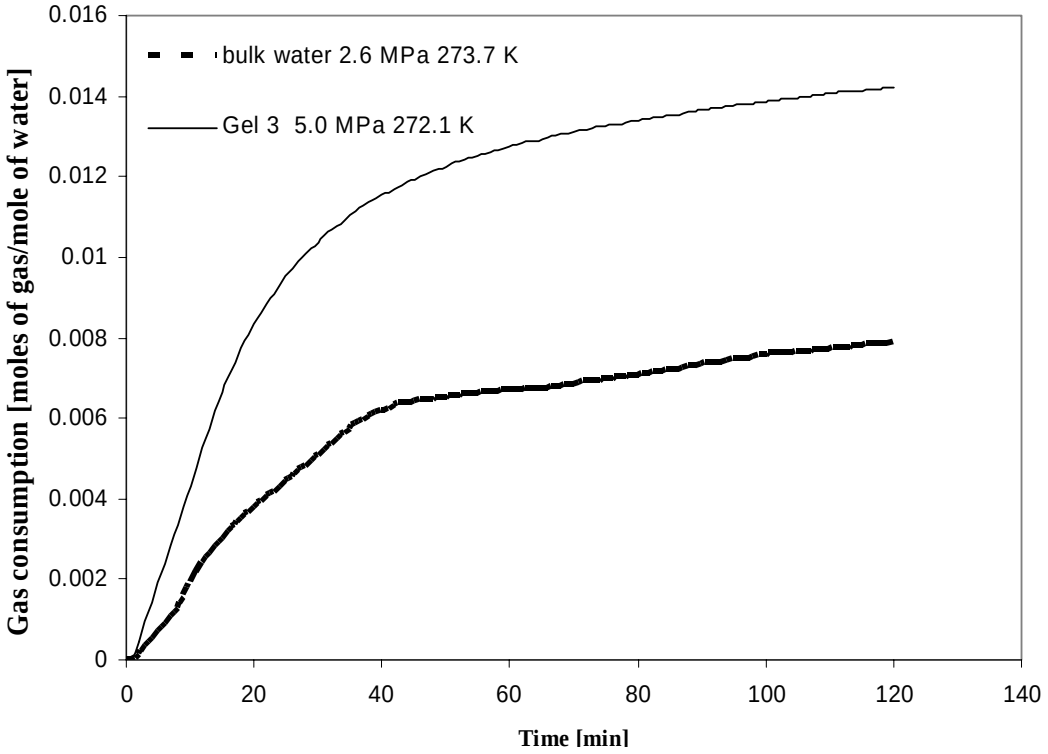

Figure 4.15 Comparison between gas uptake data of bulk systems with pore confined water in silica gel in the presence of 1mol% THF for hydrate formation from 17% CO_2/N_2 mixture

It is not clear why there is significantly poorer CO_2 inclusion in the hydrate phase for the silica gel experiment when compared to the stirred reactor case. 5.0 MPa was selected as an operating pressure for this study because appreciable hydrate formation was not obtained below this value in the porous silica gel. While there is an increase in gas consumption, CO_2 recovery is significantly lower in the silica gel case compared to bulk water. The hydrate phase composition is also reduced compared to the bulk water case, but this same trend was observed with the systems without THF as discussed previously. Linga et al [28, 84] report comparable CO_2 recovery of 0.42 and 0.46 for the

pure water and 1 mol% THF experiments respectively, while in this current study a reduction from 0.51 to 0.19 is observed. The interaction of silica gel with THF solution is not well known, and the inhibiting effect of confining the water in pores coupled with the presence of THF may be responsible for this reduced CO_2 recovery. It is also possible that due to differences in equilibrium conditions between bulk water systems and water confined in silica gel pores, 1 mol% THF may not be the optimal concentration for use in silica gel. Clearly this area requires more investigation and should serve as the basis for future studies.

CHAPTER 5
CONCLUSIONS AND RECOMMENDATIONS

5.1 Conclusions

Post combustion CO_2 capture through hydrate formation in a silica gel column has been investigated using different silica gel types, operating conditions and an additive. The following conclusions can be made from the results of this study.

1. Water confined in 30.0 nm and 100.0 nm silica gel pores exhibit freezing point depression such that gas-liquid contact is achieved during hydrate formation at 272.1 K. Water adsorbed on the silica gel surface is not chemically bound to the gel thus making it available for hydrate formation.

2. Higher pressures favour increased hydrate formation by achieving higher gas consumption into the hydrate phase. This results in a greater CO_2 capture by the process thus making it a suitable candidate for further study for industrial application.

3. Increasing pore size from 30.0 to 100.0 nm improves CO_2 capture by increased gas uptake and higher CO_2 recovery or split fraction. This effect arises from improved diffusion conditions in the larger pores for the gas molecules to form hydrates with the water confined in the silica gel pores.

4. Increasing silica gel particle size range from 40-75 μm to 75-200 μm improves the hydrate formation process in terms of increased gas uptake by the hydrate and higher CO_2 recovery. This improvement is not as large as is observed by increasing pore size, but is still significant since inter-particle spaces contribute to overall bed porosity thus contributing to improved gas diffusion through the silica gel column.

5. Gas uptake by hydrate formation (moles of gas/mole of water) is markedly improved when water dispersed in silica gel is used compared to bulk water. This results in energy savings by eliminating the need for mixers or agitators as well as achieving better conversion of water to hydrate.

6. The silica gel with 100.0 nm pore size and 75-200 μm particle size achieves higher CO_2 recovery than bulk water systems and can thus be used to evaluate process performance with additives.

7. The use of 1 mol% THF as an additive reduces the operating pressure required to achieve hydrate formation in silica gel pores and reduces the initial rate of hydrate formation over the experiments without THF. However hydrate phase CO_2 concentration is reduced due to the presence of THF in the hydrate phase.

8. CO_2 recovery when 1 mol% THF is used in silica gel was lower than results obtained in a stirred tank system, indicating that the optimum THF concentration for the silica gel system is different from that obtained in the bulk water case.

5.2 Recommendations

Significant insights into the effects of silica gel properties and the presence of THF on CO_2 capture through hydrate formation have been gained through this study. Based on the foregoing conclusions, a number of recommendations can be made as to how this work may be improved and extended in future investigation.

1. A conceptual process based on multiple hydrate formation stages in silica gel columns can be devised. This would involve determining the number of hydrate formation/decomposition stages needed to achieve a CO_2 stream of 95-99% purity suitable for sequestration/enhanced oil recovery uses, with the enriched gas from each stage serving as the feed gas for hydrate formation in the next stage.

2. More insight is required into the effects of THF on the hydrate formation kinetics in silica gel. A detailed study focusing on determining the optimum THF concentration for use in a silica gel system should be undertaken.

3. Particle sizes studied in this work involved one order of magnitude difference between the gels (40-75 and 75-200 μm). A wider study incorporating larger particles up to millimeter size should be studied to investigate any possible effects this would have on the hydrate formation kinetics.

4. Gas consumption/conversion into hydrate has received attention in this study; however accurate information is not available as to the quantity of water converted to hydrate. NMR micro-imaging and other microscopic techniques should be applied to give more insight into water conversion.

5. The current study employed a stationary silica gel column to form hydrates; alternative reactor designs such as fluidizing silica gel particles in the flue gas stream may be considered to improve kinetics.

6. For this process to be considered a valid alternative to the amine process and other technologies currently being promoted for CO_2 capture applications, process scale up and detailed economic analysis of the process should be carried out. This will facilitate a cost comparison between the silica gel process and other available technologies.

7. Hydrate formation in silica gel pores should be evaluated as a means of separating fuel gas produced from gasification - essentially CO_2/H_2 mixtures thus producing a pure H_2 feed to gas turbines in an integrated gasification combined cycle (IGCC) power plant.

REFERENCES

[1] Shindo, Y.; Lund, P.C.; Fujioka, Y.; Komiyama, H. *Int. J. Chem. Kinetics*. **1993**. *25*, 777-782.

[2] Davy, H. *Philos. Trans. R. Soc. London* **1811,** 101, 1–35.

[3] Makogon, Y**.** F.; Trebin, F. A.; Trofimuk, A. A.; Tsarev, V. P.; Chersky, N. V. *Dokl. Acad. Sci. USSR-Earth Sci. Sect* **1972,** 196, 197-200 **.**

[4] Hammerschmidt, E. G. *Ind. Eng. Chem***. 1934,** 26 (8), 851-855**.**

[5] Katz, D.L.; Cornell D.: Kobayashi R.; Poettmann, F. H.; Vary J. A.; Elenbaas, J.R.; Weinaug, C. F. *Handbook of Natural Gas Engineering*, McGraw Hill, New York 802, **1959.**

[6] von Stackelberg, M.; *Naturwiss* **1949**, 36, 359.

[7] Clennell, M.B.; Hovland, M.; Booth, J.S.; Henry, P.; Winters, W.J. *J. Geophysical research*, **1999**

[8] Ripmeester, J. A.; Tee, J. S.; Ratcliffe, C. I.; Powell, B. M. *Nature* **1987,** *325*, 136-136

[9] Koh, C. A.*Chem. Soc. Rev.* **2002,** 31, 157–167**.**

[10] Sloan, E. D.*Nature* **2003,** 426, 353-359**.**

[11] Kvenvolden, K. A.*Chem. Geol.* **1988a** 41-51**.**

[12] Dickens, G.; O'Neil, J.; Rea, D.; Owen, R.*Paleoceanography* **1995,** 10**,** 965–971.

[13] Dallimore, S. R.; Collett, T. S.; Uchida, T.; *GSC Bull.* **1999.** 544 1, 1–10**.**

[14] Englezos, P. Clathrate hydrates. *Ind. Eng. Chem. Res.* **1993,** *32***,** 1251–1274.

[15] Englezos, P.; Hatzikiriakos, S. G.; The Stability of Permafrost and Gas Hydrates Subject to Global Warming. *Proc. Third (1993) International Offshore and Polar Engineering Conference*, Singapore, June 1993**;** ISOPE: Golden, CO, **1993.**

[16] Dickens, G. R.; Castillo, M .M; Walker, J. C. G. *Geology* **1997,** 25**,** 259–262.

[17] Kennett, J. P.; Cannariato, G.; Hendy, I. L.; Behl, R. J. Methane Hydrates in Quaternary Climate Change: The Clathrate Gun Hypothesis *Am. Geophys. Union,* Washington DC **2003.**

[18] Gudmundsson, J. S.; Borrehaug, A. Frozen hydrate for transport of natural gas. *Proc. 2nd International Conference on Gas Hydrates,* Toulouse, France. **1996**

[19] World Energy Outlook 2007: China and India Insights. *International Energy Agency ISBN 978-92-64-02730-5.* **2007**

[20] IPCC, 2007: *Climate Change 2007: The Physical Science Basis. Contribution of Working Group I to the Fourth Assessment Report of the Intergovernmental Panel on Climate Change* [Solomon, S., D. Qin, M. Manning, Z. Chen, M. Marquis, K.B. Averyt, M. Tignor and H.L. Miller (eds.)]. Cambridge University Press, Cambridge, United Kingdom and New York, NY, USA, 996 pp. **2007**

[21] IPCC, 2007: *Climate Change 2007: Impacts, Adaptation and Vulnerability. Contribution of Working Group II to the Fourth Assessment Report of the Intergovernmental Panel on Climate Change,* [M.L. Parry, O.F. Canziani, J.P. Palutikof, P.J. van der Linden and C.E. Hanson, (eds.)], Cambridge University Press, Cambridge, UK, 976pp. **2007**

[22] IPCC, 2007: *Climate Change 2007: Mitigation. Contribution of Working Group III to the Fourth Assessment Report of the Intergovernmental Panel on Climate Change* [B. Metz, O.R. Davidson, P.R. Bosch, R. Dave, L.A. Meyer (eds.)], Cambridge University Press, Cambridge, United Kingdom and New York, NY, USA. **2007**

[23] IPCC, 2005: *IPCC Special Report on Carbon Dioxide Capture and Storage. Prepared by Working Group III of the Intergovernmental Panel on Climate Change* [Metz, B., O. Davidson, H. C. de Coninck, M. Loos, and L. A. Meyer (eds.)]. Cambridge University Press, Cambridge, United Kingdom and New York, NY, USA, 442 pp. **2005**

[24] Aaron, D.; Tsouris, C. *Separation Science and Technology* **2005,** 40, 321 – 348,

[25] Voormeij, D. A.; Simandl, G. L. *Geoscience Canada* **2004.** 31, 1, 11-22.

[26] Kang, S.-P.; Lee, H. *Environ Sci. Technol.* **2000,** 34, 4397-4400.

[27] McKee, B., Zero Emissions Technologies – Technology status Report, *OECD/IEA*, Paris, **2002**.

[28] Linga, P.; Kumar, R.; Englezos, P. *Chem. Eng. Sci.* **2007,** 32, 4268 – 4276.

[29] Linga, P.; Adeyemo, A.; Englezos, P. *Environ. Sci. Technol.* **2007**, *42*, 315-320

[30] Seo, Y.; Moudrakovski, I.; Ripmeester, J.; Lee, J.; Lee, H. *Environ Sci. Technol.*, **2005**, 39, 2315-2319

[31] Sloan, E. D. *Clathrate Hydrates of Natural Gas*, 2nd ed.; Marcel Dekker: New York, 1998.

[32] Kobayashi, R. *Vapor-Liquid Equilibrium in Binary Hydrocarbon-Water Systems* Ph.D Dissertation, U. Mich University microfilms No. 3521, Ann Arbor, MI 1951

[33] Bourrie, M. S.; Sloan, E. D. *Gas Proc. Assn. Res. Rpt. 100*. Tulsa, OK, **1986**

[34] Makogon, T.Y.; Mehta, A. P.; Sloan, E. D. *J. Chem. Eng. Data* **1996**, 41, 315.

[35] van der Waals; J. H.; Platteeuw, J. C. *Ad*v. *Chem. Phys*. **1959**, 2, 1.

[36] Handa, Y.P.; Stupin, D. *J. Phys. Chem.* **1992**, 96, 21

[37] Kleinberg, R. L.; Flaum, C.; Griffin, D. D.; Brewer, P. G.; Malby, G. E.; Peltzer, E. T.; Yesinowski, J. P. *J. Geophys. Res.*, **2003** 108, B10, 2508.

[38] Clennell, M.B.; Hovland, M.; Booth, J.S.; Henry, P.; Winters, W.J. *J. Geophys. Res*, **1999**

[39] Henry, P.; Thomas, M.; Clennell, M.B. *J. Geophys. Res*, **1999**, 104, B10, 23005-230022.

[40] Yousif, M.H.; Abass, H.H.; Selim, M.S.; Sloan, E.D. *SPE Reservoir Engineering,* **1991**, 69-76.

[41] Genov, G.; Kuhs, W. F.; Staykova, D. K.; Goreshnik E.; Salamatin, A. N. *American Mineralogist*, **2004**, *89*, 1228.

[42] Yousif, M. H.; Li, P. M.; Selim, M. S.; Sloan, E. D. *Journal of Inclusion Phenomena and Macrocyclic Chemistry*, **1990** 8, 71-88

[43] Yousif, M. H.; Sloan, E. D. *SPE Reservoir Engineering*, **1991** 6, 452–458.

[44] Kumar, A. *Experimental and Modeling Studies of Dissociation of Gas Hydrates in Porous Media.* M.A.Sc Thesis, University of Calgary. Calgary, Alberta. 2005

[45] Uchida, T.; Ebinuma, T.; Ishizaki, T. *J. Phys. Chem. B*, **1999**, 103, 3659-3662.

[46] Seshadri, K.; Wilder, J. W.; Smith D. H. *J. Phys. Chem.* **2001**, 105, 2627-2631.

[47] Smith, J.M.; Van Ness, H. C.; Abbott, M. M. *Introduction to Chemical Engineering Thermodynamics*, McGraw-Hill, New York 2001

[48] Seo, Y.; Lee, H., Uchida, Y. *Langmuir,* **2002,** 18, 9164-9170

[49] Uchida, T.; Ebinuma, T.; Takeya, S.; Nagao, J.; Narita H. *J. Phys. Chem. B*, **2002**, 106, 820-826

[50] Smith D. H.; Wilder J. W.; Seshadri, K. *AIChE Journal*, **2002**, 48, 10.

[51] Seo, Y., Lee, H. *J. Phys. Chem.* **2003**, 107, 889-894

[52] Aasberg-Petersen, K.; Stenby, E.; Fredenslund, A. *Ind. Eng. Chem. Res.* **1991**. 30, 2180-2185.

[53] Pitzer, K. S. *J. Phys. Chem.* **1973**, *77*, 268.

[54] Pitzer, K. S.; Mayorga, G. *J. Phys. Chem*. **1973**, *77*, 2300.

[55] Prausnitz, J. M.; de Azevedo, E. G.; Lichtenthaler, R. N. *Molecular Thermodynamics of Fluid-Phase Equilibria.* 3rd ed. East Rutherford, NJ: Prentice-Hall, **1999.**

[56] Paull, C. K.; Matsumoto, R.; Wallace, P. J. et al. Proc. ODP (Ocean Drilling Program), Initial Repts. *164*; College Station, TX, 1996; p 277.

[57] Wilder, J. W., Seshadri, K. and Smith, D. H.; *J. Phys. Chem. B* **2001,** *105,* 9970-9972

[58] Clarke, M.A., Darvish, M.P., Bishnoi, P.R., *Ind. Eng. Chem. Res.*, **1999**, 38, 2485-2490.

[59] Zhang, W.; Wilder, J. W.; Smith, D. H.; *AIChE. J.*,**2002** 48, 2324

[60] Herzog, H.; Drake, E.; Adams, E.; CO_2 Capture, Reuse, and Storage Technologies for Mitigating Global Climate Change, *DoE Report* (order No. DE-AF22-96PC01257), 1997.

[61] McKee, B.; Zero Emissions Technologies-Technology Status Report, OECD/IEA, Paris 2002.

[62] Chakravarti, S.;Gupta, A; Hunek, B.; Advanced Technology for the Capture of Carbon Dioxide from Flue Gases, *Proceeding of 1st National Conference on Carbon Sequestration, May 14-17, Washington DC*. 2001. http://www.netl.doe.gov/publications/proceedings/01/carbon_seq/carbon_seq01.html

[63] Klara, S. M.; Srivastava, R. D. *Environmental Progress*, **2002,** 21, 4, 247

[64] Deutch, J; Moniz, J. E. *The Future of Coal: An MIT Interdisciplinary Study* http://web.mit.edu/coal/

[65] Ripmeester, J. A.; Ratcliffe, C. I.; Klug, D. D.; Tse, J. S., Molecular perspectives on structure and dynamics in clathrate hydrates. *Annals of the New York Academy of Sciences -1994, 715 (Int. Conf. on Natural Gas Hydrates*, 1993), 161-176, 1994.

[66] Udachin, K.A.; Ratcliffe, C. I.; Ripmeester, J.A. *J. Phys. Chem. B*, **2001,** 105, 4200-4204**.**

[67] Deaton, W. M.; Frost, E. M. Jr., *U.S. Bur. Mines, Monograph* **1946,** 8, 101

[68] Larson, S.D., Phase Studies of the Two-component Carbon Dioxide - Water System, Involving the Carbon Dioxide Hydrate, *PhD thesis*, University of Illinois, 1955.

[69] Robinson, D. B.; Mehta, B. R. *J. Canad. Petrol. Technol*. **1971**10(1): 33-35.

[70] Miller, S. L.; Smythe, W. D. *Science*, **1970,**170, 531-533.

[71] Dholabhai, P.D.; Kalogerakis, N.; Bishnoi, P.R. *J. Chem. Eng. Data*, **1993** 38, 650-657.

[72] Englezos, P.; Hall, *S. Can. J. Chem. Eng.* **1994,** 72(5), 887-93.

[73] Breland, E.; Englezos, P. *Can. J. Chem. Eng. Data* **1996,** 41(1), 11-13.

[74] Fan, S.-S.; Chen, G.-J.; Ma, Q.-L.; Guo, T.-M. *Chem. Eng. J*., **2000**, 78,173-178.

[75] Davidson, D**.** W.; Handa, Y. P.; Ratcliffe, C. I.; Tee, J. S. *Nature* **1984**, *311*, 142-143.

[76] van Cleef, A.; Diepen, G.A.M. *Rec. Trav. Chim*. **1960**, *79*, 582.

[77] Marshall, D. R.; Saito, S.; Kobayashi, R. *AIChE Journal*, **1964,** *10*, 202-205.

[78] Sugahara, K.; Tanaka, Y.; Sugahara, T., Ohgaki, K. *Journal of Supramolecular Chemistry* **2002,** *2*, 365-368.

[79] Englezos, P.; Lee, J. D. *Korean Journal of Chemical Engineering* **2005**, *22*, 671-681.

[80] Kang, S.-P.; Lee, H. *Environ. Sci. Technol*. **2000**, *34*, 4397.

[81] Kang, S.-P.; Lee, H.; Ryu, B.-J.; *J. Chem. Thermodynamics.* **2001**, 53, 513.

[82] Kang, S.-P.; Lee, H.; Lee, C.-S.; Sung, W. M.; *Fluid Phase Equilibria*. **2001**, *185*, 101.

[83] Seo, Y.-T.; Lee, H., *J. Phys. Chem. B,* **2004**, *108*, 530

[84] Linga, P.; Kumar, R.; Englezos, P. *J. Hazard. Mater.* **2007**, *149*, 625–629

[85] Mooijer-van den Heuvel, M. M.; Witteman, R.; Peters, C. J. *Fluid Phase Equilibria* **2001**,*182*, 97-110.

[86] Vysniauskas, A.; Bishnoi, P.R. *Chem. Eng. Sci.* **1983** 38, 1061-1072.

[87] Vysniauskas, A; Bishnoi, P. R. Thermodynamics and Kinetics of Gas Hydrate Formation. *In Natural Gas Hydrates: Properties, Occurrence and Recovery*; Cox, J. L., Ed.; Butterworth: Woburn, MA, **1983b;** 35-48.

[88] Vysniauskas, A.; Bishnoi, P. R. *Chem. Eng. Sci.* **1985** 40, 2, 299–303

[89] P. Englezos, P.; Kalogerakis, P.; Dholabhai, P. D.; Bishnoi, P.R. *Chem. Eng. Sci.* **1987** 42, 2659–2666.

[90] Malegaonkar, M.B.; Dholabhai, P.D.; Bishnoi, P.R. *Canadian Journal of Chemical Engineering*, **1997**, 75, 1090-1099.

[91] Clarke, M. A.; Bishnoi, P. R. *Chem. Eng. Sci.* **2004** 59, 2983–2993.

[92] Takaoki T.; Hirai K.; Kamei M.; Kanda H. *In Proc. Fifth International Conference on Natural Gas Hydrates*, June 13-16. Trondheim, Norway. Paper 4021. **2005**.

[93] Scott, R. P. W. *Silica Gel and Bonded Phases. Their Production Properties and Use in LC.* John Wiley & Sons: West Sussex, England 1993

[94] Sindorf, D. W.; Maciel, G. E. *J. AM. Chem. Soc.* **1983**, 105, 1487

[95] Handa, Y. P.; Zakrzewski, M.; Fairbridge, C. *J. Phys. Chem.* **1992**, *96*, 8594.

[96] Wallace, S; Hench, L. L. *J. Sol-Gel Sci. Tech.* **1994**, 1, 153-168

[97] Lee, J. D.; Susilo, R.; Englezos, P. *Energy Fuel* **2005**, *19*, 1008–1015.

[98] Uchida, T.; Ebinuma, T.; Narita, H. *J. Cryst. Growth* **2000**, *217*, 189–200.

[99] Bishnoi, P. R.; Natarajan, V. *Fluid Phase Equilib.* **1996**, *117*, 168–177.

[100] Bear, J. *Dynamics of Fluids in Porous Media* Dover, New York **1990**.

[101] Mu, D.; Liu, Z.; Huang, C. *Microfluid. Nanofluid.* **2007** Short Comm.1613-4982

[102] Murphy, P. J.; Roberts, S. *Geochim. Cosmochim. Acta.* **1995**, 59, 4809-4824

APPENDIX

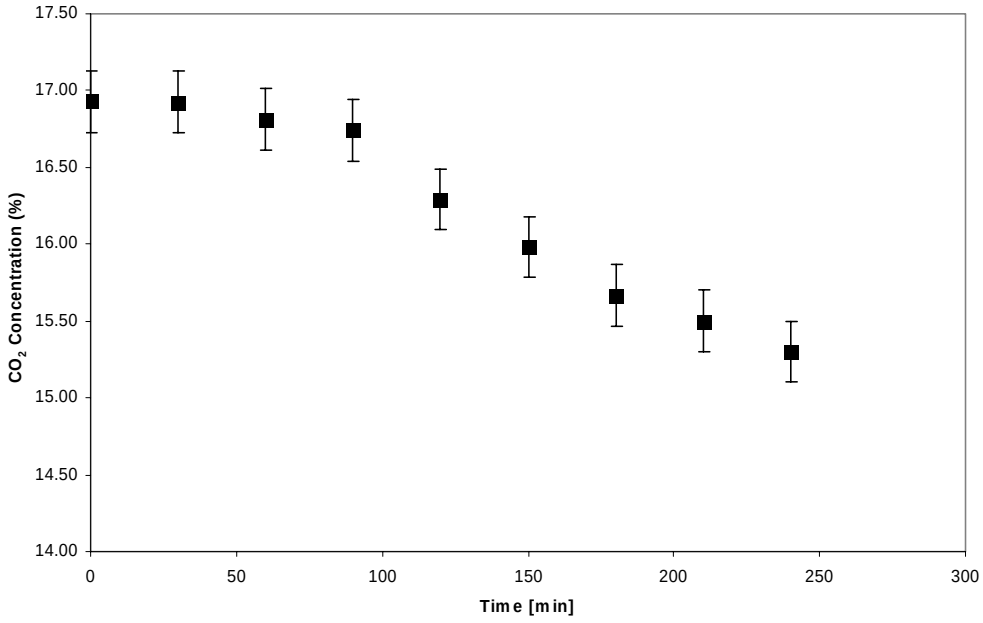

(a)

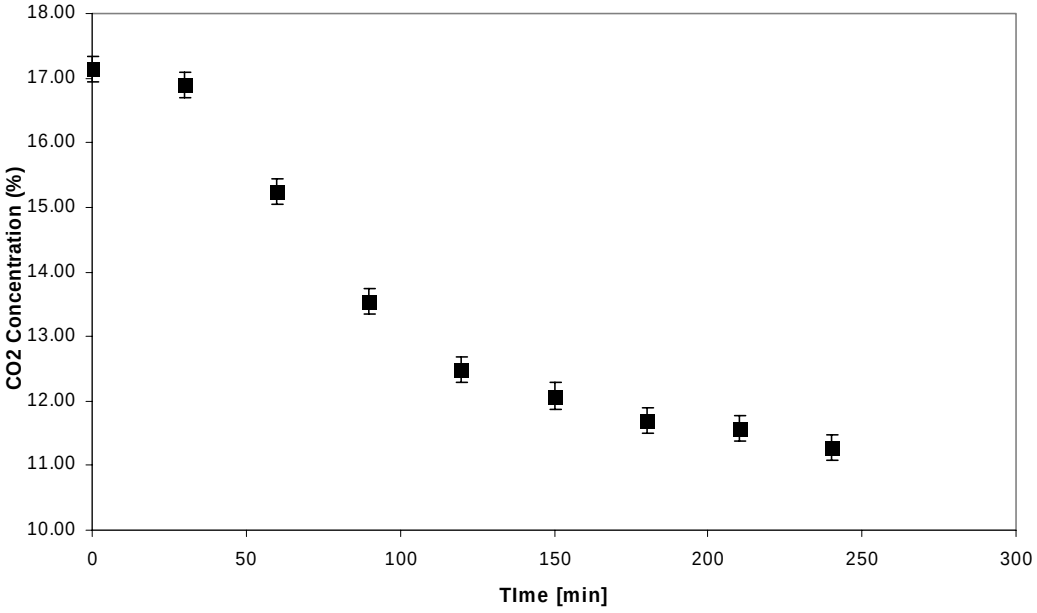

(b)

Figure A-1 Gas phase CO_2 measurements during hydrate formation at 272.15 K and 8.0 MPa in gel 1 (a) and gel 2 (b).

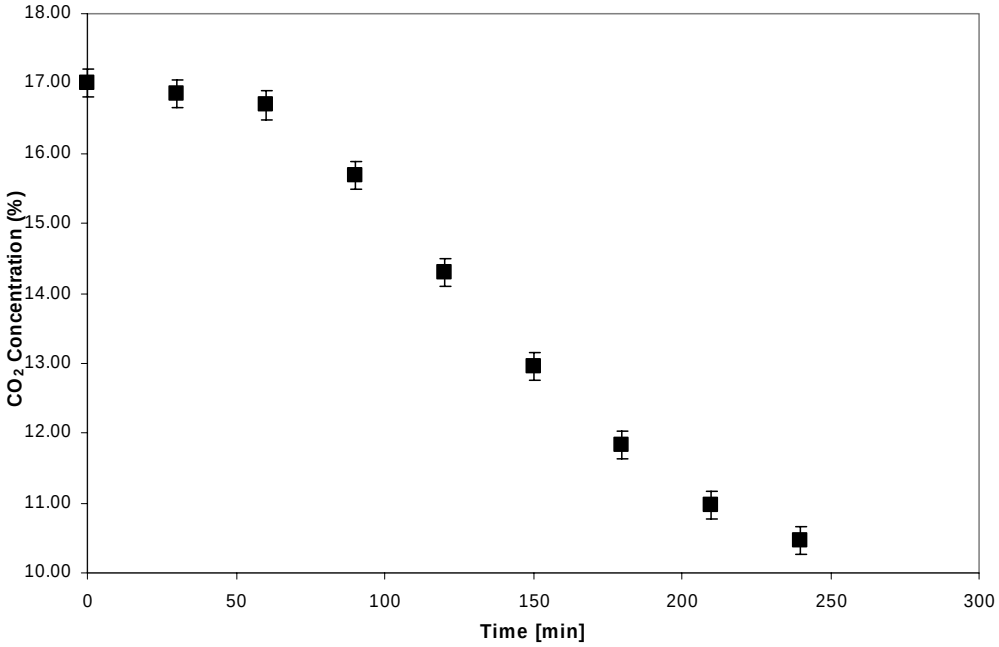

(a)

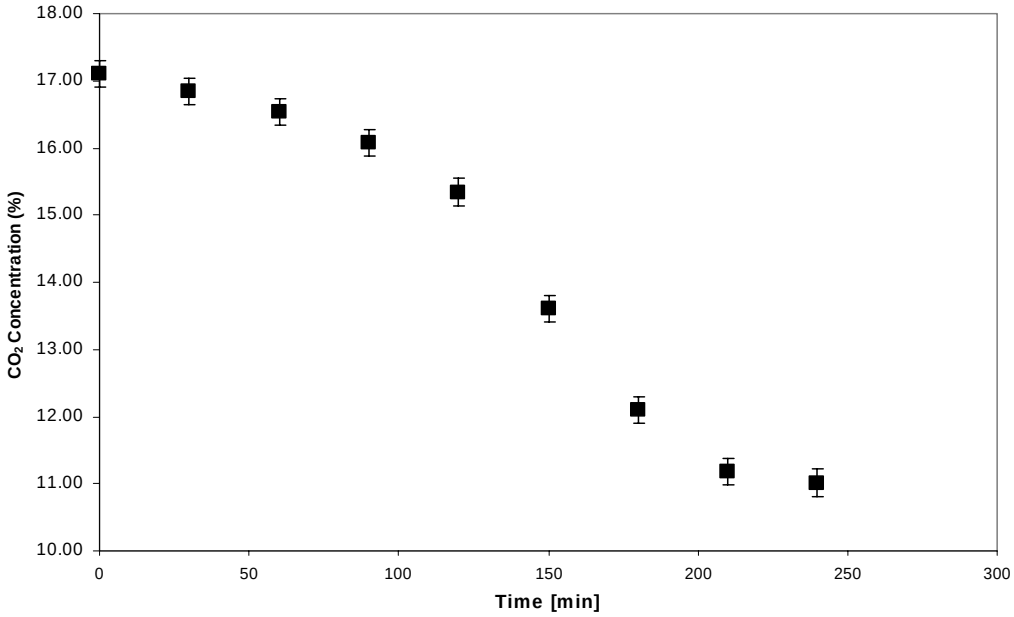

(b)

Figure A-2 Gas phase CO_2 measurements during hydrate formation in gel 3 at 272.15 K and pressure 9.0 MPa (a) and 8.0 MPa (b).

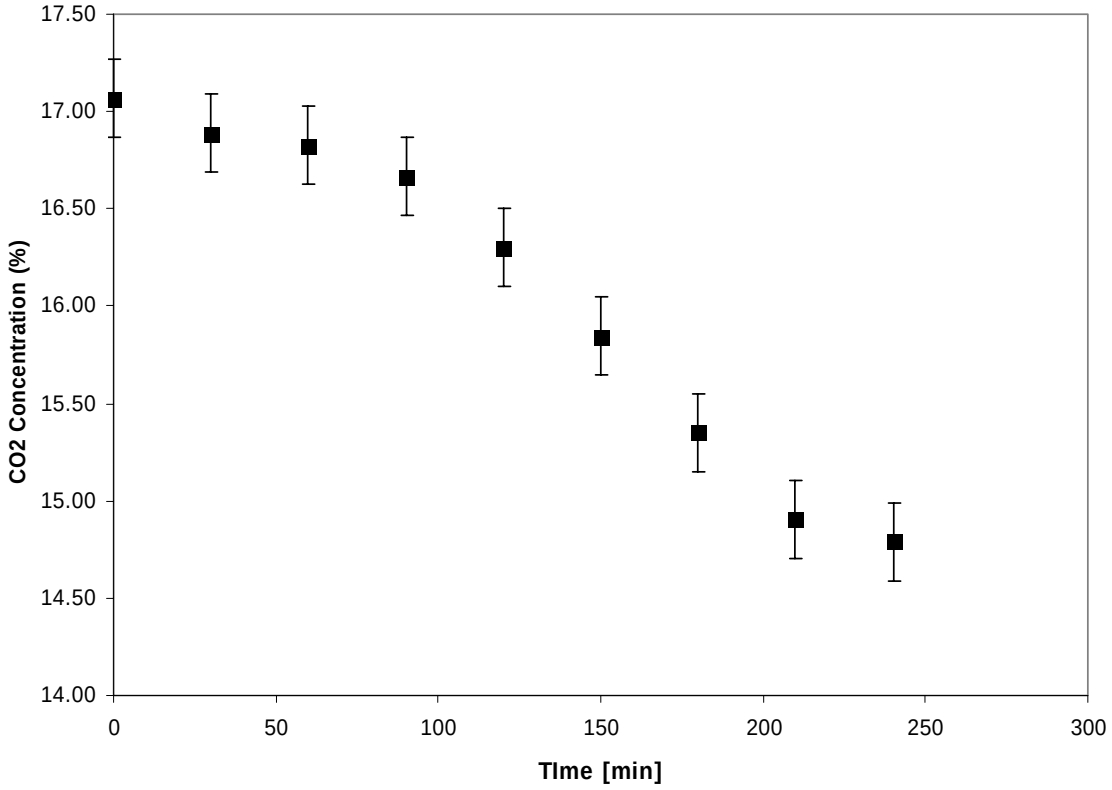

Figure A-3 Gas phase CO_2 measurements during hydrate formation at 272.15 K and 5.0 MPa 100.0 nm silica gel with 1 mol% THF.